Global fire activities and their impacts on the terrestrial carbon budget in context of multiple environmental changes

by

Jia Yang

A dissertation submitted to the Graduate Faculty of
Auburn University
in partial fulfillment of the
requirements for the Degree of
Doctor of Philosophy

Auburn, Alabama
August 1, 2015

Key words: Global Changes, Wildfire, Carbon fluxes,
Terrestrial ecosystem, process-based model, fire emissions

Approved by

Hanqin Tian, Chair, Solon Dixon Professor of School of Forestry and Wildlife Sciences
Lisa Samuelson, Dwain G. Luce Professor of School of Forestry and Wildlife Sciences
Latif Kalin, Professor of School of Forestry and Wildlife Sciences
Chandana Mitra, Assistant Professor of College of Sciences and Mathematics

Abstract

As one major disturbance in the earth system, fires modified vegetation structure and functioning, atmospheric composition, and climate conditions at both regional and global scales. Under the impacts of substantial changes in environmental factors (such as human activities, climate warming, and CO_2 concentration), global fire regimes present significant changes, and generate strong feedbacks to ecosystem and climate system. Our knowledge regarding fire disturbances have been substantially improved under the help of satellite observations. However, long-term fire history and fire impacts on ecosystem carbon budget were rarely investigated prior to satellite era due to the lack of available spatially-explicit, large-scale datasets. In this dissertation, multiple study approaches were used to investigate the changes in burned area, fire emissions, and fire impacts on the terrestrial carbon budget and storage in the Conterminous United States (CONUS), boreal North America (BONA), African continent, and the entire globe. Historical burned area datasets were collected from satellite observations, official fire records, and reconstructed based on fire model simulations. Burned area data were applied to drive the Dynamic Land Ecosystem Model (DLEM) to investigate fire emission and fire impacts on ecosystems. As indicated by the analysis, average area burned in the CONUS was 14,430.51 km^2 $year^{-1}$ and fire-induced carbon emissions were ~17.65 Tg C $year^{-1}$ during 1984-2012. Inter-annual variations of burned area and carbon consumption presented significant increasing trends in the CONUS. In the BONA, average fire-induced carbon emissions were 50.95 Tg C $year^{-1}$ during 1960-2010, with a significant increasing trend at

the rate of 1.08 Tg C $year^{-1}$. Over the period of 1901-2010, African burned area presented a significant declining trend at the rate of -0.77×10^4 km^2 $year^{-2}$ due to the intensified human activities across the African continent and climate changes in the South Hemisphere of the African continent (SHAF). In Africa, pyrogenic carbon emissions decreased at the rate of -1.6 Tg C $year^{-2}$ during 1901-2010, while the decline trend was not significant in the last five decade. During 1901-2007, average global burned area was $\sim442\times10^4$ km^2 $year^{-1}$. Our results suggest a notable declining rate of burned area globally (1.28×10^4 km^2 $year^{-2}$). From 1901 to 2010, global pyrogenic carbon emissions were estimated to be 2.43 Pg C $year^{-1}$, and global average combustion rate was 537.85 g C m^{-2} burned area. Due to fire impacts, global terrestrial net primary productivity and net carbon sink were reduced by 4.14 Pg C $year^{-1}$ and 0.57 Pg C $year^{-1}$, respectively. Results of this study suggest that, in the future, the more intensive human activities would continue to suppress fire activities in the tropics and subtropics, while burned area and fire-induced carbon emissions would increase substantially in the boreal regions under the impact of climate warming and more frequent droughts. In order to mitigate global fire emissions, special attention should be paid to fire activities in the peatlands and tropical rainforest ecosystems.

Acknowledgements

Completion of this dissertation has been supported by many people. My first gratitude goes to my supervisor, Dr. Hanqin Tian, for supporting me during these past five years. He is one of the smartest and most knowledgeable people I have ever met. He provided insightful advice and discussions about my research. His passion and scientific insight have inspired me, and will always benefit me in my future scientific career. I highly appreciate the support from my committee: Dr. Lisa Samuelson, Dr. Latif Kalin and Dr. Chandana Mitra. I learned a lot from my committee members in their classes and through conversations with them, which are invaluable in conducting my PhD projects. I also thank Dr. Ming-Kuo Lee for reviewing this dissertation.

Dr. Shufen Pan gave me substantial helps on both my research and daily life. I thank all of our previous group members: Dr. Mingliang Liu, Dr. Chi Zhang, Dr. Xiaofeng Xu, Dr. Guangsheng Chen, and Dr. Qichun Yang for their development of the Dynamic Land Ecosystem Model. Special thanks go to Dr. Wei Ren, Dr. Chaoqun Lu, Dr. Bo Tao, Mr. Kamaljit Banger, Ms. Bowen Zhang, and Mr. Shree Dangal. You are my teachers, friends, and family. None words can express how deep my gratitude is for you guys. The junior group members, Mr. YuanZhi Yao, Ms. Rongting Xu, Mr. Jingwei Wu, and Ms. Dan Liu, are all a fun bunch with enthusiasm and full of energy. I would appreciate the helps from Dr. John Kush. Furthermore, I thank Dr. Graeme Lockaby, Ms.

Patti Staudenmaier, Ms. Audrey Grindle, Ms. Pam Beasley, Mr. James Fukai, Mr. Kent Hanby, and all the faculty and staff members in the School of Forestry and Wildlife Sciences.

This work has been supported by NSF/USDA/DOE Decadal and Regional Climate Prediction using Earth System Models (NSF1243232, NSF1243220 and NIFC2013-35100-20516), USDA/USDI Joint Fire Science Program (JFSP 11172), NSF Dynamics of Coupled Natural and Human Systems (1210360), NSF Computer and Network Systems (CNS-1059376), NASA Carbon Monitoring System Program (NNX14AO73G), and NASA Interdisciplinary Science Program (NNX10AU06G, NNX11AD47G).

Last, yet the most important, I am deeply grateful to my parents, parents-in-law, sister, and nephews for their unconditional and endless love. My wife, Ms. Liu Shi, and my daughter, Ms. Kaitlyn Yang, are always the sources of happiness and the most precious gifts in my life.

Table of Contents

List of Tables

List of Figures

Chapter 1. Introduction

Fire is of vital importance for the global climate system (Bowman *et al.*, 2009, Randerson *et al.*, 2006a, Rogers *et al.*, 2013, Ward *et al.*, 2012b). During fires, large amounts of greenhouse gases (GHG, such as CO_2 and methane) and aerosols are ejected into the atmosphere, and then modify the atmosphere components and radiation budget (Kaiser *et al.*, 2012b, Langmann *et al.*, 2009, van der Werf *et al.*, 2010b, Wiedinmyer *et al.*, 2011a). The inter-annual variations in global fire emissions have been acknowledged as one of the major factors in controlling atmospheric CO_2 and CH_4 growth rate (Bousquet *et al.*, 2006, Van Der Werf *et al.*, 2004). Moreover, fire could affect land surface albedo and energy partitioning, and cause feedbacks to climate system (Jin *et al.*, 2012, Lyons *et al.*, 2008). The post-fire recovery processes is composed of numerous physiological, biophysical and biochemical processes, and may persist for months, years, decades, or even centuries.

Global vegetation distribution can be substantially shaped by fire activities. Field experiments indicated that fire exclusion strategies substantially enhanced the fraction of forest and ecosystem carbon storage (Bowman & Panton, 1995, Moreira, 2000, Tilman *et al.*, 2000). Simulations by the Dynamic Global Vegetation Model (DGVM) (Bond & Keeley, 2005) indicated that the global forest coverage may increase from 27% to 56% if global fires were suppressed. Fire intensity and frequency also determine the distribution of tree species. According to their relationship to fires, tree species can be classified into “fire embracer”, “fire resister”, and “fire avoider” (Rogers *et al.*, 2015).

Fires are strongly influenced by climate conditions and human activities (Bowman *et al.*, 2009, Rogers *et al.*, 2015, van der Werf *et al.*, 2008a, van der Werf *et al.*, 2008b, Westerling *et al.*, 2006b). It has been recognized that precipitation amount is negatively correlated with fire activities in regions with abundant fuels, while in arid regions with lower fuel loading, higher precipitation during vegetation growing season could stimulate fire activities in the following fire season (van der Werf *et al.*, 2008a). The impact of human activities on fire could be either positive or negative. On the one hand, human activities provide ignition sources and increase the probability of fire ignition through camping, logging, and arson, etc. (Nepstad *et al.*, 1999, Turetsky *et al.*, 2015); on the other hand, human-induced cropland expansion break fuel continuity, and fire suppression activities reduce the fire spread and duration (Archibald *et al.*, 2012, Marlon *et al.*, 2008b).

Fires at global level are largely unknown until the emergence of satellite observations in the 1980s (Seiler & Crutzen, 1980). In the 2000s, satellite-observed burned area and fire emissions products have been developed based on multiple satellite sensors, including single-year fire products, such as GBA2000 (Grégoire *et al.*, 2003) and GlobScar (Simon *et al.*, 2004), and multiple-year fire products, such as L3JRC (Tansey *et al.*, 2008a), GLOBCARBON (Plummer *et al.*, 2006), MCD45A1 (Roy *et al.*, 2008b) , and GFED4 (Giglio *et al.*, 2013a). Although these fire products have been validated across various regions, significant differences among them are still found by intercomparison (Chang & Song, 2009, Giglio *et al.*, 2010b, Korontzi *et al.*, 2004, Roy & Boschetti, 2009). Small fires with low radiative power were often neglected and account for approximately 26% of total burned area globally (Randerson *et al.*, 2012). Satellite-derived global burned area products were often coupled into terrestrial ecosystem model to estimate global fire emissions (Hoelzemann *et al.*, 2004, Ito & Penner, 2004b, Jain *et al.*, 2006, Knorr *et al.*, 2012, van der Werf *et al.*, 2010a, van der Werf *et al.*,

2006b). However, the divergences in the satellite-observed burned area lead to large uncertainties in the estimations of fire emissions and the evaluations of fire impact on ecosystems. For example, Knorr et al. (2012) used three burned area products as input to drive LPJ-GUESS model and found that L3JRC leads much higher carbon emission than GFED and MCD45A1; Poulter et al., (2015) reported that simulations driven by different satellite burned area products can lead to large variations in global aboveground carbon stocks, and woody coverage. Moreover, biomass burning can also be estimated directly through fire radiative power (FRP) and biomass combustion rate (Kaiser *et al.*, 2012a, Wooster *et al.*, 2005, Zhang *et al.*, 2014).

Fire models are an important tool to study fire activities and the underlying mechanisms, and can be classified into statistical fire models and process-based fire models. The statistical fire model is usually reconstructed based on regression model by using the observed climate-fire relationship e.g. (Balshi *et al.*, 2009c, Westerling *et al.*, 2011); while process-based fire model considers the complex mechanisms of fire event as influenced by weather, fuel, and topography (Thonicke *et al.*, 2010). Process-based fire modeling has provided an effective tool to estimate large-scale fire patterns. It simulates fire activities (e.g. ignition, spread and extinguishment) while considering critical environmental factors such as climate, land cover, and land management practices (Pechony & Shindell, 2009). Process-based fire models have been applied in reconstructing global fire history and investigating fire impacts on ecosystems. These models include MC-FIRE [*Lenihan et al.*, 1998], Glob-FIRM (Thonicke *et al.*, 2001), Reg-FIRM (Thonicke *et al.*, 2010), SPITFIRE (Thonicke *et al.*, 2010), CLM-Fire (Li *et al.*, 2012), and CTEM-FIRE (Arora & Boer, 2005). Model simulated fire patterns are not often consistent with each other. For example, *Kloster et al*. (2010) estimated global fire patterns based on the modified CTEM-Fire model and found a declining trend in burned areas from the 1900s to the

1960s and an increasing trend from the 1970s to the 1990s. However, the estimation by *Li et al.* (2013) based on CLM-Fire model presented a continuous declining trend from the 1870s to the 1990s.

As projected by General Circulation Models (GCM), global climate will experience substantial changes in the future, which could influence fire patterns in many regions of the world. For example, Pechony and Shindell (2010) investigated future fire under three SRES scenarios (A2, A1B, and B1), and found that global fire activities would increase a lot under the impacts of climate warming. Balshi et al., (2009) reported that fire-induced carbon emissions in boreal North America could increase by 2.5-4.4 times at the end of the 21st century. In the recent years, a new set of Representative Concentration Pathways (RCP) have been developed for modeling experiments, with the increased radiative forcing value in 2100 ranging from 2.6 to 8.5 W m^{-2} (Van Vuuren *et al.*, 2011). As indicated by the RCP8.5 scenario, atmospheric CO_2 concentration will reach 930 ppmv (http://www.pik-potsdam.de/~mmalte/rcps/index.htm), and temperature will increase by more than 4 °C relative to 1986-2005 at the end of the 21st century (Knutti & Sedláček, 2013). The understanding of historical fire regimes and fire-induced terrestrial carbon balance can shed light on the changes in fire activities in the future.

In order to investigate historical changes in fire regimes and fire impacts on the terrestrial ecosystems, we collected burned area dataset from satellite observation and inventory-based reconstruction, and simulated burned area by using a process-based ecosystem model. The burned area datasets are then coupled into the ecosystem model to estimate the fire-induced carbon emissions and the impacts of fires on the terrestrial carbon budget at both global and regions levels.

1. Objectives

The overall goal of this study is to examine the long-term changes of fire activities at both regional and global scales, and investigate the underlying mechanisms controlling the changing trends. It is hypothesized that climate, ecosystem, and human activities are the three most important factors in controlling fire regimes; meanwhile, ecosystem properties, such as vegetation carbon storage and carbon budget, are substantially modified by fires.

Question 1: What were the changing trends of burned area?

Hypothesis: As global warming and frequent droughts increase, fire activities will become more frequent, and burned area will become larger across the globe.

Question2: What is the magnitude of fire-induced carbon emissions? How did the fire emissions change in the past century?

Hypothesis: The magnitude of fire-induced carbon emissions can be estimated by the fuel loading, burned area, and combustion completeness. The changes in fire emissions follow the changes in burned area.

Question 3: How much do global fires affect the terrestrial carbon budget?

Hypothesis: Global fires could reduce terrestrial carbon budget through fire-induced carbon emissions and the reductions in forest coverage, vegetation carbon storage, and soil fertility.

Our strategies to answer these questions include the following tasks:

I. Examine the changes in burned area by collecting data from satellite observations and inventory-based reconstruction, and reconstructing burned area data according to fire model.

II. Investigate fire-induced carbon emissions and terrestrial carbon budgets.

III. Conduct factorial numerical experiments to quantifying the contribution of the changes in multiple environmental factors, including climate change, human activities, CO_2 concentration, and nitrogen deposition.

2. Approaches

• Data collection:

(1) Burned area dataset from satellite observations and inventory-based reconstructions.

(2) Model input datasets, such as, climate, atmospheric CO_2 concentration, nitrogen deposition, land use and land cover, and topography, etc.

(3) Benchmark datasets to validate model simulations.

• Model development:

(1) Improve the DLEM by coupling a process-based fire model, which is capable of simulating burned area, fire emissions, and fire-induced mortality.

(2) Improve the DLEM by optimize the post-fire regrowth processes.

(3) Calibrate and validate the model.

• Model application:

(1) Regional-scale evaluations of fire emissions and fire impacts of regional carbon budget in the Conterminous United States, boreal North America, and African continent.

(2) The reconstruction of century-long burned area dataset by the DLEM-fire model

(3) Assess the fire-induced changes in carbon budget at global scale in the context of multiple environmental changes.

3. Dissertation Structure

This Dissertation is organized according to the structure as below (Figure 1-1),

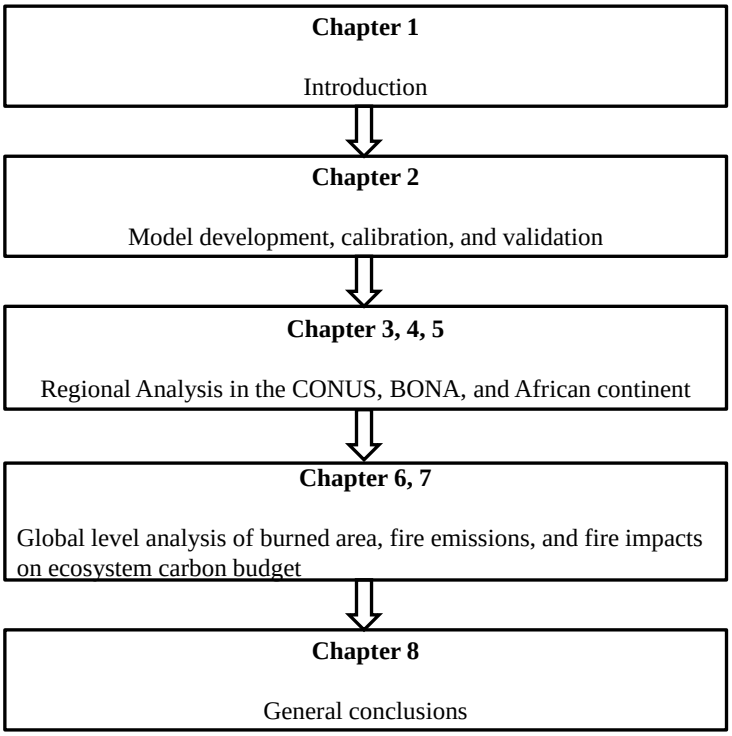

Figure 1-1. The structure of this dissertation.

Chapter 1 presents a brief introduction of background, previous fire-related works, research questions, specific objectives and tasks, and approaches to solve these questions.

Chapter 2 describes the detailed processes regarding the DLEM fire module, including the processes to estimate burned area, fire emissions, and fire impacts on carbon cycles. The DLEM-simulated carbon fluxes, burned area, and fire emissions are validated according to benchmark datasets at both regional and global levels.

Chapter 3-5 investigate burned area, fire emissions, and fire impacts on carbon budget at regional scales in the CONUS, BONA, and African continent. All the three regional studies investigated the changing trends in burned area. Study in the CONUS highlights the importance of mega-fires in the recent three decades; study in the BONA highlights fire impacts on terrestrial carbon budget and storage; while study in the African continent highlights the contributions of multiple environmental factors to the century-scale fire activities.

Chapter 6-7 describe the reconstruction of century-scale global burned area by applying the DLEM model. Then, the reconstructed burned area data is used to study fire-induced changes in terrestrial carbon fluxes and budget at global level from 1901 to 2010. .

Chapter 8 summarizes the major findings of this study and discusses the possible improvement needs for future work.

Chapter 2. The description of the DLEM Fire module

The DLEM is an integrated process-based biosphere model, which mainly simulates the carbon/nitrogen/water storages in the terrestrial ecosystem and their fluxes across the land-atmosphere interface under the influences of multiple environmental factors, including climate, atmospheric components, land use/cover changes, and various disturbances (Chen *et al.*, 2013, Chen *et al.*, 2012, Liu *et al.*, 2013a, Lu & Tian, 2013, Pan *et al.*, 2014, Ren *et al.*, 2011, Tao *et al.*, 2014, Tian *et al.*, 2014, Tian *et al.*, 2011, Yang *et al.*, 2014a, Yang *et al.*, 2014c). It is mainly composed of five components, namely biophysics, plant physiology, soil biogeochemistry, dynamic vegetation, and disturbances (Figure 2-1). The detailed processes can be referred in Figure S1 in Appendix I.

The biophysics component simulates the latent and sensible heat fluxes, soil water content and soil temperature in different soil layers, runoff and drainage. The plant physiology component simulates major physiological processes, including photosynthesis, vegetation respiration, carbon allocation to different tissues, nitrogen uptake and allocation, tissue turnover, transpiration, and phenology. The component of soil biogeochemistry simulates mineralization, nitrification/denitrification, decomposition and fermentation. The dynamic vegetation component simulates the biogeography redistribution of plant functional types under environmental changes, and plant competition and succession during vegetation recovery after disturbances (Tian *et al.*, 2011). DLEM builds on the concept of plant functional types (PFT) to simulate vegetation distributions.

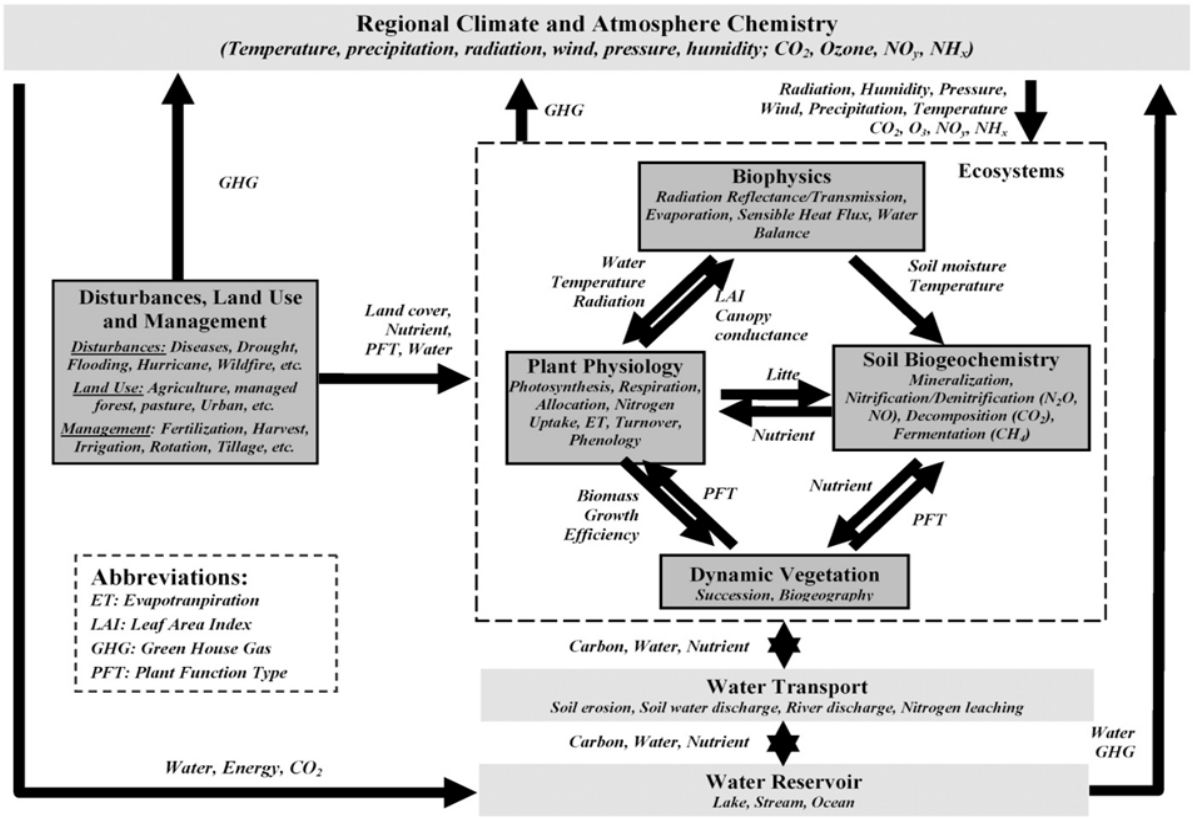

Figure 2-1. Framework of the Dynamic Land Ecosystem Model (Tian *et al.*, 2010a).

1. The development of the DLEM Fire module

The DLEM-Fire is a process-based fire module built on DLEM. It is capable of estimating burned area, fire emissions and fire impacts on ecosystem function and structure by simulating fuel characteristics, number of fires, and fire behavior (Figure 2-2).

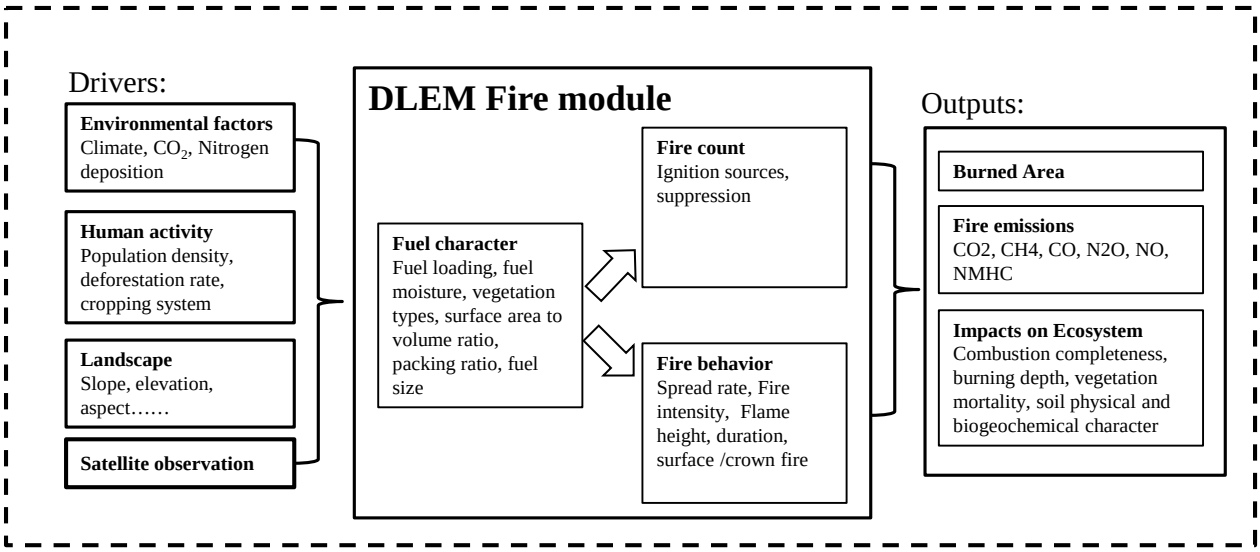

Figure 2-2. Conceptual diagram presenting inputs, outputs, and the major processes of DLEM-Fire.

1.1 Burned area

For each grid, the daily burned fraction BF, is calculated as:

$$BF = BF' \times v = ({BF_{wd}}' + {BF_{def}}' + {BF_{ag}}') \times v$$

where BF' is DLEM simulated burned fraction prior to coupling with satellite information, which is equal to the sum of DLEM simulated wildfire burned fraction (${BF_{wd}}'$), deforestation fire burned fraction (${BF_{def}}'$), and agricultural fire burned fraction (${BF_{ag}}'$); v is the grid-based satellite-adjusted scalar to regulate the magnitude and spatial distribution of fires, and is calculated as the quotient of satellite-observed fire climatology and DLEM-simulated fire climatology prior to coupling with satellite information.

The following briefly describes the wildfire, agricultural fire, and deforestation fire schemes adapted from previous fire models (Arora & Boer, 2005, Li *et al.*, 2013, Li *et al.*, 2012, Pechony & Shindell, 2009)

Daily burned fraction in each grid as a result of wildfire, $BF_{wd}{}'$ (day^{-1}), is calculated as a function of the number of daily fire events, N_f (count day^{-1}), average burned area of each fire event, A_f (km^2 count^{-1}), and grid area, A_{grid} (km^2):

$$BF_{wd}{}' = N_f A_f / A_{grid}$$

The number of daily fire events, N_f (count day^{-1}), is expressed as:

$$N_f = (I_a + I_n)(1 - f_s)(1 - f_{crop}) P_m P_b A_{grid}$$

where I_a and I_n are the anthropogenic and natural ignition (count km^{-2} day^{-1}), respectively; f_s is the fraction of suppressed fires; f_{crop} is the fraction of cropland; P_m is reduction factor on ignition probability caused by fuel moisture; P_b is the reduction factor on ignition probability caused by the insufficient fuel loading.

At the global level, cloud-to-ground lightning is the major natural fire ignition source. The natural ignition, I_n (count km^{-2} day^{-1}), is estimated through the frequency of lightning flashes, I_l (flash km^{-2} day^{-1}), and latitude, λ (Prentice & Mackerras, 1977):

$$I_n = I_l [5.16 + 2.16 \cos(3\lambda)]^{-1}$$

Anthropogenic ignition, I_a (count km^{-2} day^{-1}), is parameterized as:

$$I_a = P_D \alpha k(P_D)$$

where P_D is population density (person km^{-2}); α is the daily potential anthropogenic ignitions (1.3×10^{-4}, count person^{-1} day^{-1}); $k(P_D)$ is a population density related parameter for adjusting anthropogenic ignition potential ($= 6.8{P_D}^{-0.6}$) (Venevsky *et al.*, 2002).

Fire suppression, f_s, is estimated as a function of population density (Pechony & Shindell, 2009):

$$f_s = 0.99 - 0.98\exp(-0.025P_D)$$

The reduction factor, P_m, is calculated as a function of the available soil water (Li *et al.*, 2012):

$$P_m = \begin{cases} 1, & \theta < \theta_{wp} \\ \exp[-\pi(\theta - \theta_{wp})^2/(\theta_{fc} - \theta_{wp})^2], & \theta \geq \theta_{wp} \end{cases}$$

where θ is the volumetric soil water content in the top 20 cm; θ_{wp} and θ_{fc} are the volumetric soil water content at wilting point and field capacity, respectively.

The reduction factor, P_b, is determined by the abundance of fuel loading and calculated as a function of aboveground biomass (Arora & Boer, 2005):

$$P_b = \begin{cases} 1, & b_{ag} > b_{up} \\ (b_{ag} - b_{low})/(b_{up} - b_{low}), & b_{low} \leq b_{ag} \leq b_{up} \\ 0, & b_{ag} < b_{low} \end{cases}$$

where b_{ag} is the aboveground biomass (gC m^{-2}), including leaf, stem, woody debris, and litter; b_{up} is the upper limit of aboveground biomass (1000 gC m^{-2}) where fuel load is not a limiting factor; b_{low} is the lower limit of aboveground biomass (150 gC m^{-2}), below which ignition probability is 0.

The post-fire area, i.e. fire spread from starting point, is postulated to be elliptical in shape. The equation to calculate burned area of single fire event is:

$$A_f = 0.25\pi {u_{down}}^2 \tau^2 (1 + 1/H_B)^2 / L_B$$

where u_{down} is fire spread rate in downwind direction (km hr^{-1}); τ is the fire duration (hr); L_B and H_B are the length-to-breadth ratio and head-to-back ratio of the post-fire area, respectively. Fire spread rate, u_{down} (km hr^{-1}), is computed as:

$$u_{down} = u_{max} f_m f_{vpd} f_w$$

where u_{max} is the maximum spread rate in optimum condition (0.6 km hr^{-1}); f_m, f_{vpd}, f_w are the limiting scalars of fuel moisture, vapor pressure deficit (VPD), and wind speed to adjust spread rate, respectively. The fuel moisture scalar, f_m, is estimated as:

$$f_m = \begin{cases} 1, & \theta < \theta_{wp} \\ (\theta_{sat} - \theta)^2 / (\theta_{sat} - \theta_{wp})^2, & \theta \geq \theta_{wp} \end{cases}$$

VPD scalar, f_{vpd}, is calculated as (Pechony & Shindell, 2009):

$$f_{vpd} = 20 \times 10^Z (1 - RH/100)$$

and

$$Z = -7.90298(T_s/T - 1) + 5.02808 \cdot \log(T_s/T) - 1.3816 \times 10^{-7}\left(10^{11.344(1-T_s/T)} - 1\right) + 8.1328 \times 10^{-3}(10^{-3.49149(1-T_s/T)} - 1)$$

where RH is relative humidity (%), T is air temperature (K), T_s is water boiling point temperature (373.15 K).

Wind speed scalar, f_w, is parameterized as (Li *et al.*, 2012):

$$f_w = 0.1L_B/(1 + 1/H_B)$$

Fire duration, τ (hr), is the time that each fire lasts, which is estimated as a function of the global average fire persistence τ_{ave} (24 hr) and the slope of landscape (γ):

$$\tau = \begin{cases} \tau_{ave}, & \gamma < \gamma_{min} \\ \tau_{ave}(\gamma_{max} - \gamma)/(\gamma_{max} - \gamma_{min}), & \gamma_{min} \le \gamma \le \gamma_{max} \\ 0, & \gamma > \gamma_{max} \end{cases}$$

where $\gamma_{min}(2^{\circ})$ and γ_{max} (10°) are the lower and upper limits of the slope effect on fire duration, respectively. Terrain with steep slopes indicates more watercourse or rocks, which could break down fuel continuity and reduce fire persistence time (Pfeiffer & Kaplan, 2012).

Length-to-breadth ratio (L_B) and head-to-back ratio (H_B) are computed according to wind speed, w (m/s):

$$L_B = 1 + 10[1 - \exp(-0.06w)]$$

$$H_B = [L_B + \left({L_B}^2 - 1\right)^{0.5}]/[L_B - \left({L_B}^2 - 1\right)^{0.5}]$$

The burned area of agricultural fire, ${BF_{ag}}'$ (month^{-1}), is calculated as:

$${BF_{ag}}' = 0.2f_{crop}f_{harv}P_b f_{GDP}$$

where f_{crop} is the fraction of cropland, f_{harv} is the monthly harvest index (1 means harvest happens, and 0 stands for no harvest happens), P_b is the reduction factor of fuel loading which is the same as that used for wildfire, f_{GDP} is the socioeconomic factor indicated by gross domestic production (GDP), which is set as by *Li et al*., (2013).

The burned area of deforestation fire, $BF_{def}{}'$ (month^{-1}), is calculated as:

$$BF_{def}{}' = f_{def} P_b f_{dry}$$

where f_{def} is the annual deforestation fraction of tropical forests, P_b is the same reduction factor of fuel loading as used for wildfires, f_{dry} is monthly dryness function indicating the influence of dry season, which is computed by the ratio of monthly precipitation to potential evapotranspiration (P/PET):

$$f_{dry} = \max(0, 1 - P/PET)$$

1.2 Fire emissions and fire mortality

In the DLEM, available fuels include vegetation biomass (leaf, stem, and root), litter, coarse woody debris, and soil organic carbon. The carbon emissions during biomass burning (C_{bt}, g C m^{-2}) at grid level are estimated as,

$$C_{bt} = \sum_{ipft=1}^{4} \sum_{ifuel=1}^{5} (C_{ipft,ifuel}\, CC_{ipft,ifuel} BF_{ipft} f_{ipft}) + f_{peatfire} Depth_{fire} Dens_{peat}$$

where $ipft$ is the index of natural vegetation types within one model grid (DLEM allows a maximum of four biome types coexisting in the same grid); $ifuel$ is the index of fuel types (1- leaf, 2- stem, 3- root, 4- litter, 5- coarse woody debris); BF_{ipft} is the monthly burned fraction of each natural vegetation type (%), which is assumed to be equal to the burned fraction at grid level; f_{ipft} is the fraction of biome in the grid (%); $C_{ipft,ifuel}$ is the DLEM simulated fuel loading of each fuel types (g C m^{-2}); $CC_{ipft,ifuel}$ is the combustion completeness (%), which could be retrieved from the vegetation specific parameter table (Table 2-1).

Table 2-1. The parameter table of combustion completeness and tree mortality used in this study[a]

Vegetation types	Combustion completeness (%)					Tree mortality (%)
	leaf	stem	root	litter	coarse woody debris	
BBDF	80	30	5	95	30	70
BNEF	80	30	5	95	30	70
BNDF	80	30	5	95	30	70
TBDF	80	30	5	95	30	70
TBEF	80	30	5	95	30	70
TNEF	80	30	5	95	30	70
TNDF	80	30	5	95	30	70
TrBDF	50	20	5	95	30	60
TrBEF	80	30	5	95	30	70
Shrub	90	30	5	95	30	50
C3 grass	95	-	5	95	-	-
C4 grass	95	-	5	95	-	-

Note: BBDF stands for Boreal Broadleaf Deciduous Forest; BNEF stands for Boreal Needleleaf Evergreen Forest; BNDF stands for Boreal Needleleaf Deciduous Forest; TBDF stands for Temperate Broadleaf Deciduous Forest; TBEF stands for Temperate Broadleaf Evergreen Forest; TNEF stands for the Temperate Needleleaf Evergreen Forest; TNDF stands for the Temperate Needleleaf Deciduous Forest; TrBDF stands for Tropical Broadleaf Deciduous Forest; TrBEF stands for the Tropical Broadleaf Evergreen Forest.

$CC_{ipft,ifuel}$ can also be estimated according to the satellite-observed burned severity, in form of the percentage of fire pixels in "Unburn to Low", "Low", "Moderate", and "High" burn severity within one model grid (f_{ibseve}, %) and burn severity corresponded combustion completeness ($CC_{ipft,ifuel,ibseve}$, %) (Table 2-2),

$$CC_{ipft,ifuel} = \sum_{ibseve=1}^{4} (f_{ibseve} CC_{ipft,ifuel,ibseve})$$

where $ibseve$ is the index of four burn severity levels. When calculating f_{ibseve}, satellite pixels labeled by "Increased Greenness" were merged into "Unburn to Low" severity group, and the pixels labeled by "Non-processing area mask" were excluded in the calculation. Parameters of burn severity corresponded combustion completeness (%) in Table 2-2 were compiled from

recently published literature studying burn severity in the US and across the globe (Campbell *et al.*, 2007, Ghimire *et al.*, 2012, Meigs *et al.*, 2009, van Leeuwen *et al.*, 2014a)

Table 2-2. Parameters of combustion completeness ($\boldsymbol{CC_{ipft,ifuel,ibseve}}$, %) under differing levels of burn severity.

Vegetation	Burn severity	Leaf	Stem	Litter	Coarse Woody Debris
Forest	Unburnt to Low	3	1	57	26
	Low	31	10	64	35
	Moderate	54.5	45	64	42
	High	80	70	99	55
Shrub	Unburn to Low	20	20	57	26
	Low	25	25	64	35
	Moderate	50	50	64	42
	High	95	95	99	55
Grass	Unburn to Low	70	-	57	-
	Low	75	-	64	-
	Moderate	76	-	64	-
	High	100	-	99	-

The peatland with high water table depth is resistant to fire disturbance. However, in the recent decades, climate warming and more frequent human activities dried up the peatland and promoted the frequency and extent of peat fires (Turetsky *et al.*, 2015). Forest plantation drains the water in peatland. Due to the small area of forest plantations prior to the year 1985 (Hooijer *et al.*, 2010), we assumed no peat fires occurred in tropical regions. For the fires in peatland, burned depth ($Depth_{fire}$, cm) is estimated separately for tropical peatland and boreal peatland. In the tropical peatlands, the $Depth_{fire}$ is estimated according to soil water content, with a maximum of 51 cm when soil water is lower than wilting point and a minimum of 15 cm when soil moisture is higher than the field capacity; and carbon density ($Dens_{peat}$) is set to be 570 g C m^{-2} cm^{-1}, which is similar to the field measurements of Southeast Asian peat fires in 1997 (Page

et al., 2002). For the boreal peatlands, $Depth_{fire}$ set to be 13.1 cm, and the $Dens_{peat}$ is set to be 269.3 g C m^{-2} cm^{-1}, which are estimated based on the measurements in *Turetsky et al.* (2011). Here, we assume no vertical variations in the peatland carbon density. The peatland area used in the current study is estimated as the overlapped area of peatland in *Yu et al.*, (2010) and the wetland in the Global Lakes and Wetlands Database (GLWD) (Lehner & Döll, 2004). The burned fraction in peatland at grid level ($f_{peatfire}$) is set to be the minima of grid burned fraction and peatland fraction.

Fire-induced tree mortality is explicitly considered by the DLEM. After the fire events, a fraction of the trees are killed and the dead plant tissues return back to their corresponding dead carbon pools (litter or woody debris).

$$Cmort_{ipft,leaf\rightarrow agl} = BF_{ipft}C_{ipft,leaf}(1 - CC_{ipft,leaf})Mort_{ipft}$$

$$Cmort_{ipft,stem\rightarrow agCWD} = BF_{ipft}C_{ipft,stem}(1 - CC_{ipft,stem})Mort_{ipft}$$

$$Cmort_{ipft,froot\rightarrow bgl} = BF_{ipft}C_{ipft,froot}(1 - CC_{ipft,root})Mort_{ipft}$$

$$Cmort_{ipft,croot\rightarrow bgCWD} = BF_{ipft}C_{ipft,croot}(1 - CC_{ipft,root})Mort_{ipft}$$

where $Cmort$ is the carbon density (g C m^{-2}) of living biomass killed by fires; $leaf \rightarrow agl$, $stem \rightarrow agCWD$, $froot \rightarrow bgl$, and $croot \rightarrow bgCWD$ denote that killed leaf returns to aboveground litter pool, killed stem returns to aboveground coarse woody debris pool, killed fine root returns to belowground litter pool, and killed coarse root returns to belowground coarse woody debris pool; $Mort_{ipft}$ is the fire-induced tree mortality rate (%). Similar to the combustion completeness, fire mortality in the DLEM can be either derived from satellite-based

burn severity index when satellite information is available (Yang *et al.*, 2015), or derived from the vegetation specific parameter table (Table 2-1).

2. The comparison between the DLEM simulations with benchmark datasets

2.1 Global-level comparison

2.1.1 Carbon flux and carbon storage

The DLEM-estimated gross primary productivity (GPP), net primary productivity (NPP), vegetation carbon, and pyrogenic carbon emissions were evaluated against benchmark datasets (Table 2-3). The spatial distribution of model-simulated GPP was compared with the global GPP estimates of Moderate Resolution Imaging Spectroradiometer (MODIS) (Zhao *et al.*, 2005) and empirical-based upscaling product from Multi-Tree Ensemble (MTE) (Jung *et al.*, 2011); the DLEM-estimated NPP was compared with MODIS and Advanced Very High Resolution Radiometer (AVHRR) NPP products (Nemani *et al.*, 2003, Zhao & Running, 2010); the vegetation carbon storage was compared with the Intergovernmental Panel on Climate Change (IPCC) Tier-1 Global Biomass Carbon Map (Ruesch & Gibbs, 2008); the pyrogenic carbon emissions were compared with the estimations of GFED3.1 (van der Werf *et al.*, 2010b) and Global Fire Assimilation System (GFAS) (Kaiser *et al.*, 2012b).

The DLEM-estimated GPP and NPP are close to the benchmark datasets. The global GPP simulated by the DLEM is 2.7% lower than MODIS estimates and 11.7% lower than MTE estimates. The DLEM-estimated global NPP is 3% higher than that of MODIS, and 3.1% lower than AVHRR estimation. The DLEM-estimated global pyrogenic carbon emissions are 21.5% and 17.1% higher than the GFED3.1 and GFAS estimates, respectively. In some regions, such as, the continental US (Zhang *et al.*, 2014) and Russia (Konovalov *et al.*, 2011), the GFED3.1

estimated fire emissions have been recognized to be underestimated. In the year 2000, the DLEM-simulated global vegetation carbon storage is 471.8 Pg C, which is 5.9% lower than the IPCC Tier1 result. In general, the CO_2 uptake by terrestrial ecosystem, pyrogenic carbon emissions, and vegetation carbon storage estimated by the DLEM fall into the reasonable range. In term of spatial distributions, carbon fluxes and vegetation carbon storage simulated by the DLEM are highly correlated with the benchmark datasets (Table 2-3 and Figure 2-3, 2-4, 2-5, 2-6).

Table 2-3. The comparison of the DLEM-simulated carbon fluxes and vegetation carbon storage with benchmark datasets.

	Period	**DLEM estimates**	**Benchmark datasets estimates**	**Spatial pattern correlation coefficient**
GPP	2000-2009	108.6 Pg C $year^{-1}$	MODIS: 111.58 Pg C $year^{-1}$ (Zhao et al., 2005)	0.836
	1982-2008	105.1 Pg C $year^{-1}$	MTE: 119 Pg C $year^{-1}$ (Jung et al., 2011)	0.829
NPP	2000-2009	55.1 Pg C $year^{-1}$	MODIS: 53.5 Pg C $year^{-1}$ (Zhao and Running, 2010)	0.784
	1982-1999	52.8 Pg C $year^{-1}$	AVHRR: 54.5 Pg C $year^{-1}$ (Nemani et al., 2003)	-
Pyrogenic carbon emissions	1997-2009	2.43 Pg C $year^{-1}$	GFED3.1: 2.0 Pg C $year^{-1}$ (van der Wrf et al., 2010)	0.686
	2003-2008	2.46 Pg C $year^{-1}$	GFAS: 2.1 Pg C $year^{-1}$ (Kaiser et al., 2012)	0.607
Vegetation carbon	2000	471.8 Pg C	IPCC Tier-1: 501.6 Pg C (Ruesch and Gibbs, 2008)	0.783

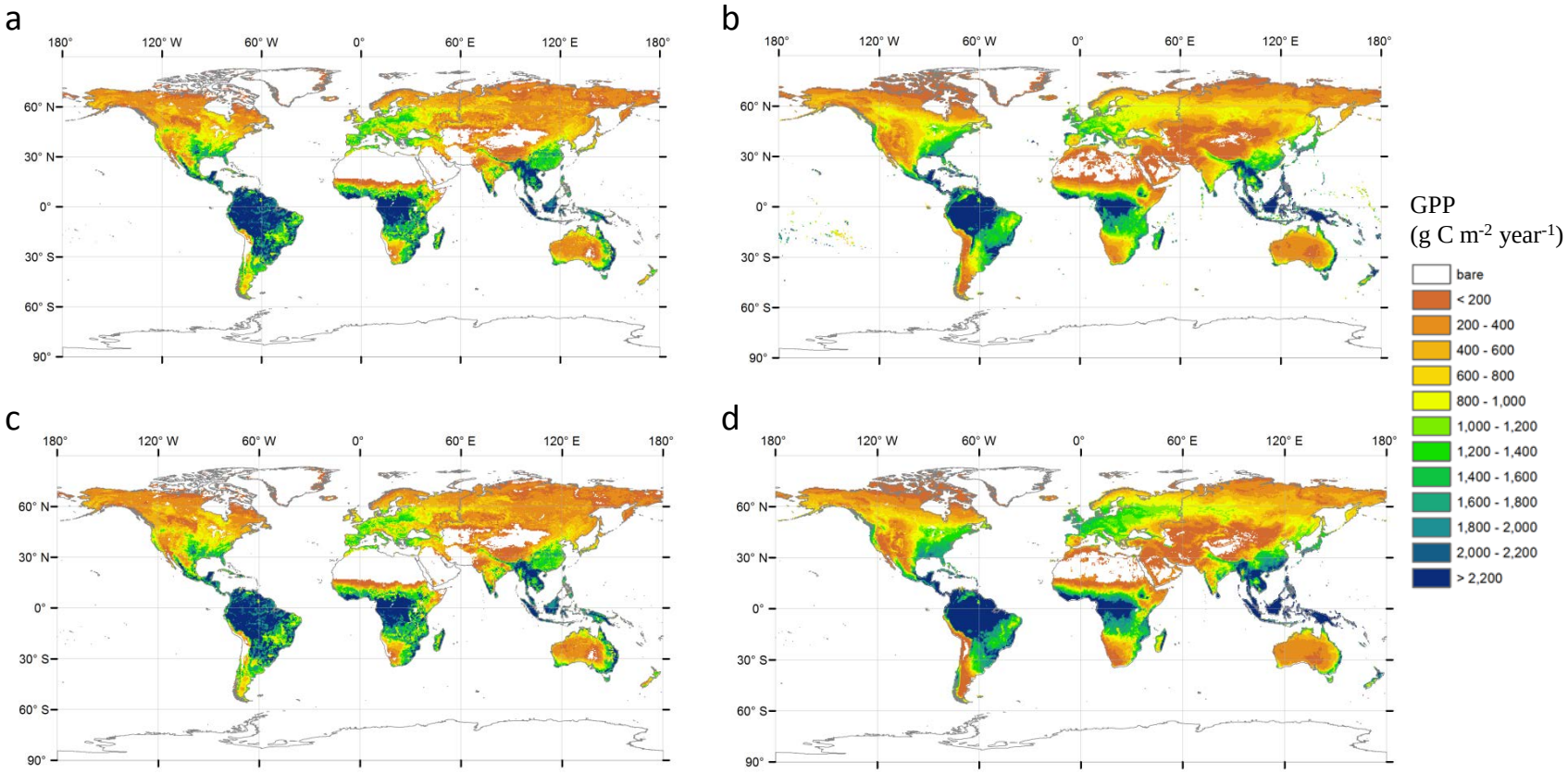

Figure 2-3. The comparison of global GPP between DLEM estimates and benchmark datasets. (a) DLEM-estimated GPP during 2000-2009, (b) MODIS-estimated GPP during 2000-2009, (c) DLEM-estimated GPP during 1982-2008, and (d) MTE-estimated GPP during 1982-2008.

Figure 2-4. The comparison of global NPP between (a) DLEM estimates and (b) MODIS estimates during 2000-2009.

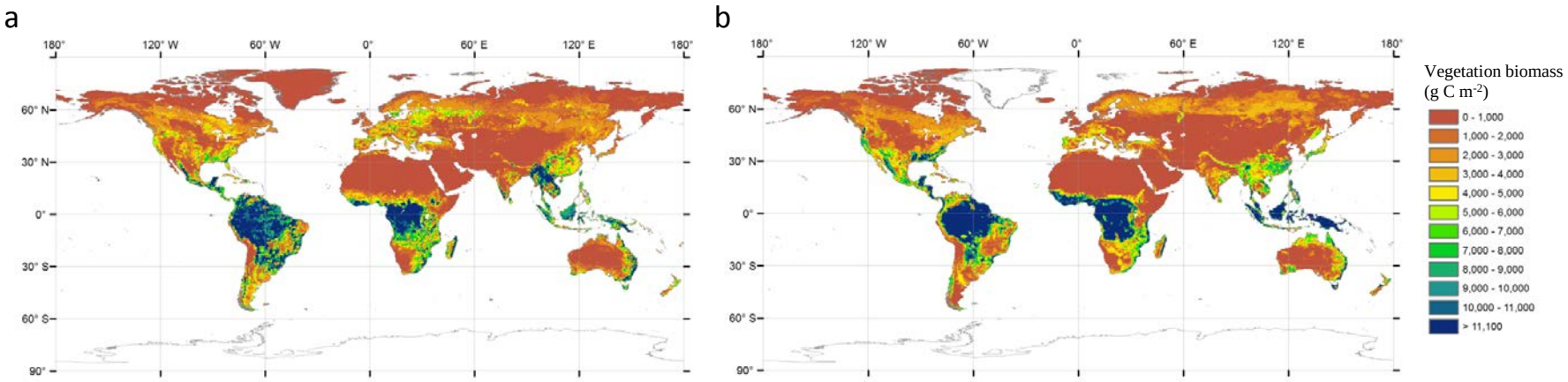

Figure 2-5. The comparison of global vegetation biomass between (a) DLEM estimates and (b) IPCC Tier1 estimates in year 2000.

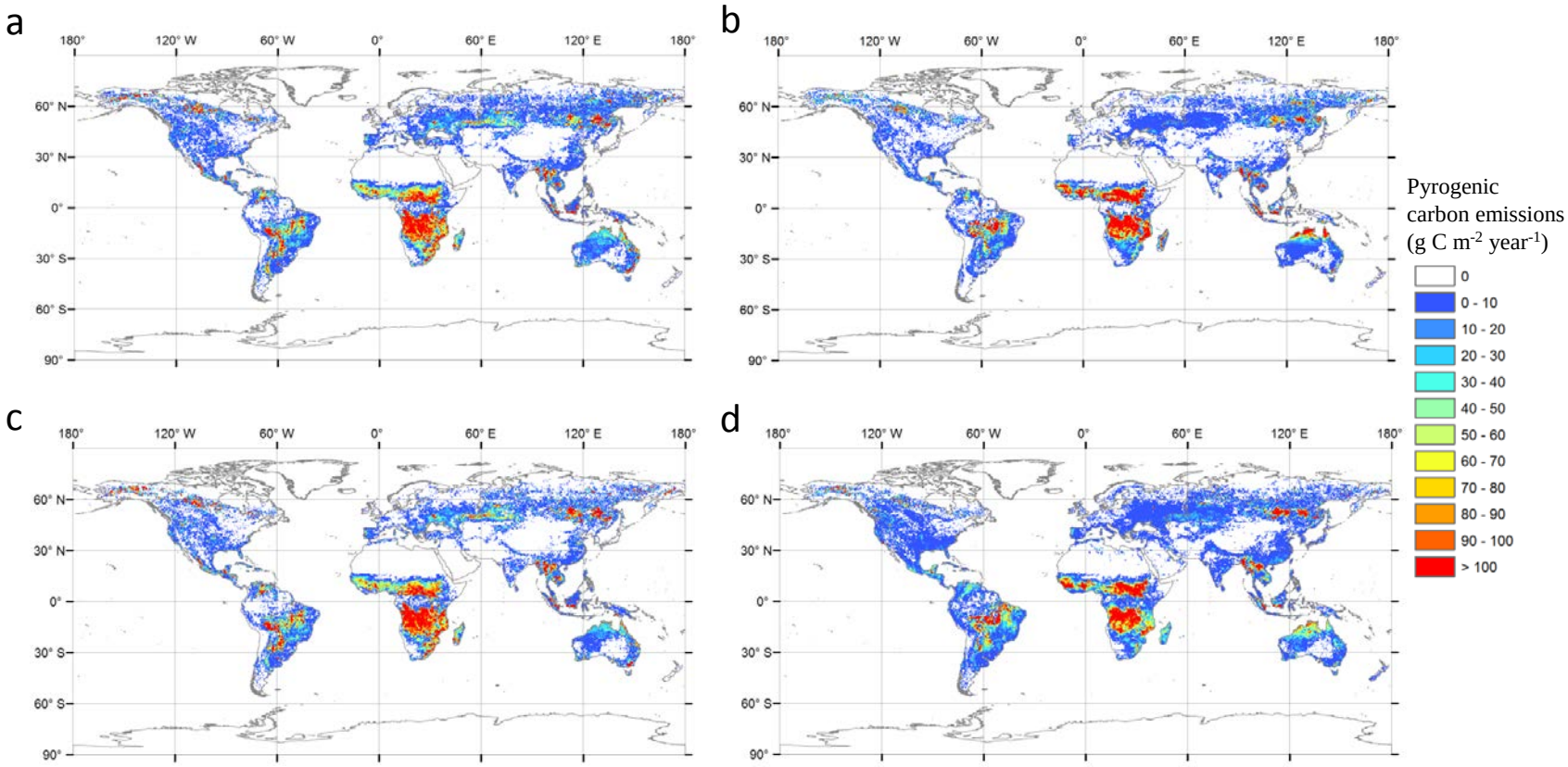

Figure 2-6. The comparison of global pyrogenic carbon emissions between DLEM estimates and benchmark datasets. (a) DLEM-estimated pyrogenic carbon emissions during 1997-2009, (b) GFED3.1 pyrogenic carbon emissions during 1997-2009, (c) DLEM-estimated pyrogenic carbon emissions during 2003-2008, and (d) GFAS pyrogenic carbon emissions during 2003-2008.

2.1.2 Burned area

The cross-validation scheme was used to evaluate DLEM-Fire simulated global fire patterns according to two satellite-based global fire products (GFED3 and MCD45A1). The DLEM-Fire simulation and GFED3 have 11-years overlap from 1997 to 2007. In the evaluation, 10 years from 11 overlapped years are selected to construct the satellite-adjusted scalar (v). And then, the scalar was applied to estimate burned area of the left year to compare with GFED3 observation. This procedure was rotated 11 times to make every overlapped year to be selected.

2.1.2.1. Evaluation of global fire distribution

The global fire distribution simulated by DLEM-Fire was compared with GFED3 and MCD45A1 data (Figure 2-7). The DLEM-Fire simulated tropical burned area was ~2% higher than GFED3 and ~4% higher than MCD45A1; DLEM-Fire simulated burned area in northern high latitudes was ~24.9% lower than GFED3 and ~11.7% higher than MCD45A1; DLEM-Fire simulated burned area in northern extratropics was ~9.5% lower than GFED3 and ~24.4% lower than MCD45A1; DLEM-Fire simulated burned area in southern extratropics was ~17.2% higher than GFED3 and ~68.1% higher than MCD45A1. Spatial correlations of the 6-year average burned area from 2002 to 2007 between our study and the two satellite products were 0.96 and 0.91, respectively. The result indicated the spatial patterns of DLEM-Fire simulation agreed with GFED3 and MCD45A1. *Li et al*. (2013) tested three fire schemes coupled in the Community Land Model (CLM) and reported the spatial correlations between three simulated global burned areas and GFED3 were 0.23, 0.44, and 0.69, respectively. The higher spatial correlations in this

study suggested that our method by incorporating remote sensing data could substantially improve the accuracy of simulated fire spatial pattern.

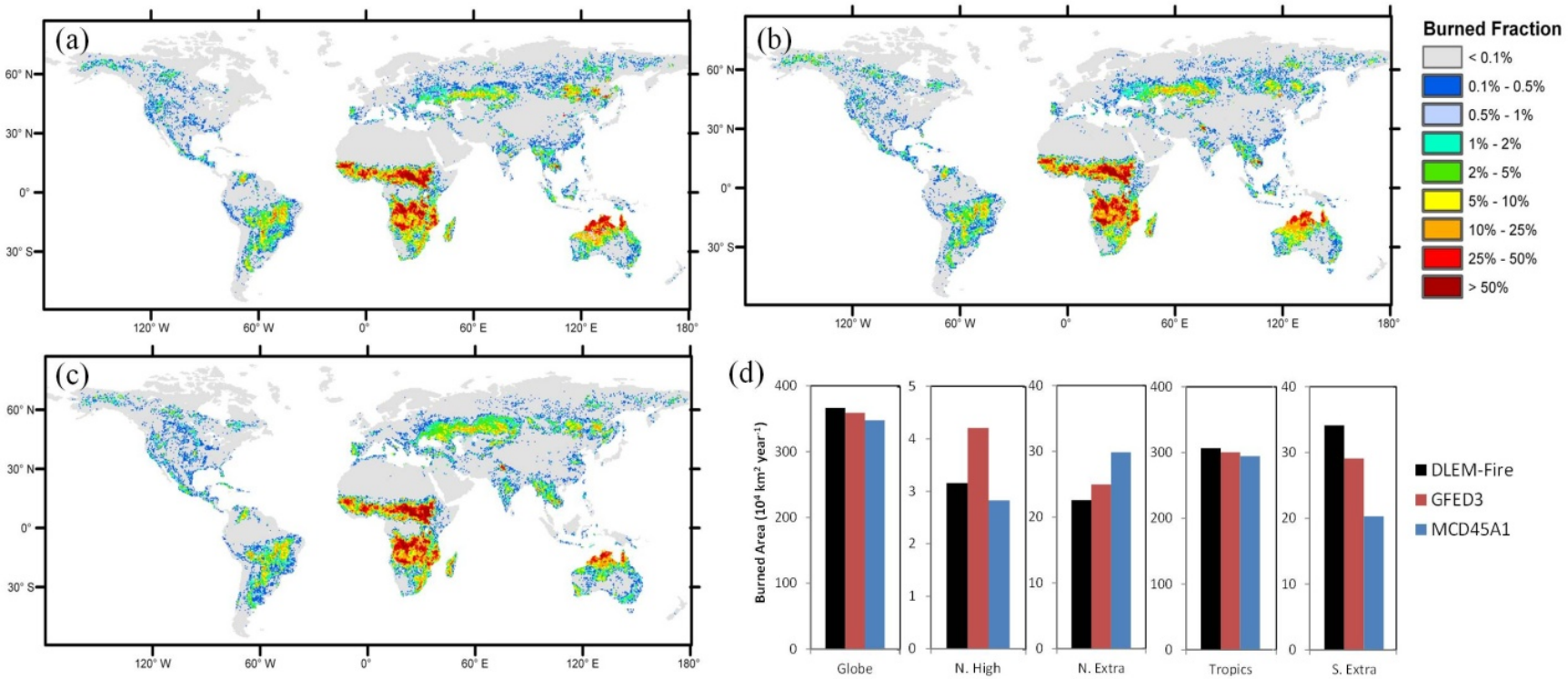

Figure 2-7. 6-year average of global burned fraction from 2002 to 2007 estimated by (a) DLEM-Fire, (b) GFED3, and (c) MCD45A1, and (d) the comparison of global and regional burned area in N. High, Northern high latitudes (>55° N); N. Extra, Northern extratropics (55° N to 30° N); Tropics (30° N to 20° S); S. Extra, Southern extratropics (>20° S)

2.1.2.2. Evaluation of inter-annual variation

Inter-annual variation from 1997 to 2007 of the global burned area from the DLEM-Fire simulation was compared with GFED3, MCD45A1, and *Mouillot and Field* (2005) (Figure 2-8). DLEM-Fire estimated global burned area as 369.4×10^4 km^2 year^{-1} compared to 374.9×10^4 km^2 year^{-1} estimated by GFED3. During 2002-2007, MCD45A1 estimated an area of 347.9×10^4 km^2 year^{-1}, while we estimated 366.6×10^4 km^2 year^{-1}. In terms of inter-annual variation, our estimation also presented a similar pattern as GFED3 and MCD45A1. From 1997 to 2000, the annual mean global burned area estimated by *Mouillot and Field* (2005) was 602×10^4 km^2 year^{-1}. Their estimate was 61% higher than our estimation and 51.3% higher than GFED3. This comparison with satellite products demonstrated our estimates for the global burned area and temporal patterns were close to satellite observations.

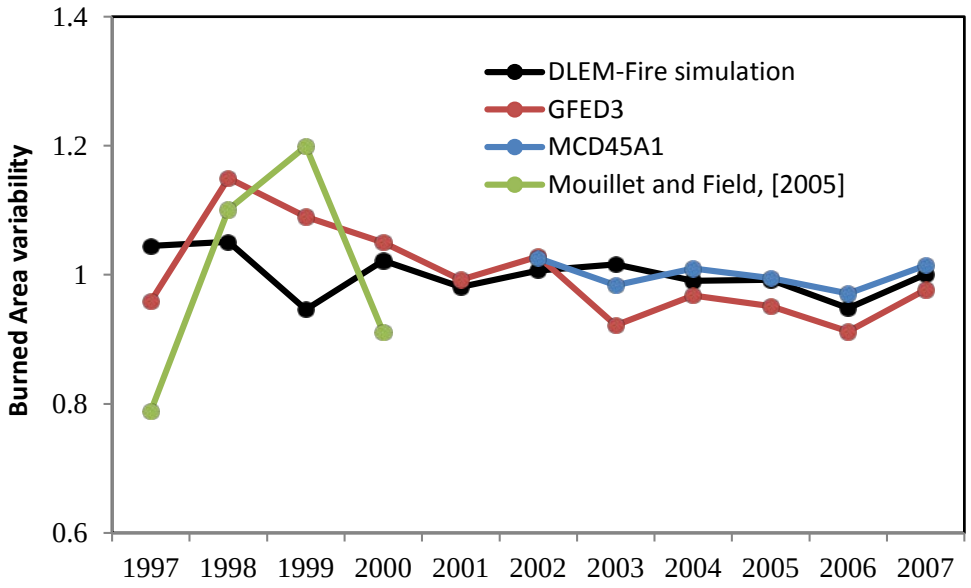

Figure 2-8. Annual variations of global burned area (annual burned area normalized by mean) estimated from multiple global burned area products.

2.1.2.3. Evaluation of fire seasonality

Fire seasonality simulated by DLEM-Fire from 2002 to 2007 was compared with GFED3 and MCD45A1 products along latitude (Figure 2-9). All datasets demonstrated evident seasonal fire variation. At middle and high latitudes, 40° N to 70° N, GFED3 and MCD45A1 revealed fires were likely to happen from June to September. Our simulated fire season was similar to GFED3 and MCD45A1, which also spanned from June to September. The fire season in summer was probably caused by the relatively warm climate, which dried up fuel moisture and increased fire danger potential. From 15° N to 40° N, GFED3 and MCD45A1 displayed fire season lasted from February to June, and the peak fire month shifted gradually from summer to spring toward the equator, roughly at a rate of 3.6 days per latitude degree. Our simulation also showed spring fire season shifting from June to February as it moved toward the equator. Overall, all datasets indicated fires were scarce in summer, which could be attributed to summer precipitation dampening fuel and reducing fire risk. From 15° N to the equator, satellite products revealed the fire season lasted from November to January, while the fire season of DLEM-Fire simulation was from December to March. In southern hemisphere from equator to 10° S, high fire activities in June and July were detected by all the datasets. From 10° S to 30° S, GFED3 and DLEM-Fire simulation demonstrated a fire peak from September to November, while MCD45A1 indicated fires were more active in August and September. From 30° S to 50° S, the fires estimated by GFED3, MCD45A1 and DLEM-Fire simulation were concentrated in December, January and February. In general, our estimated seasonal variation was similar to GFED3 and MCD45A1.

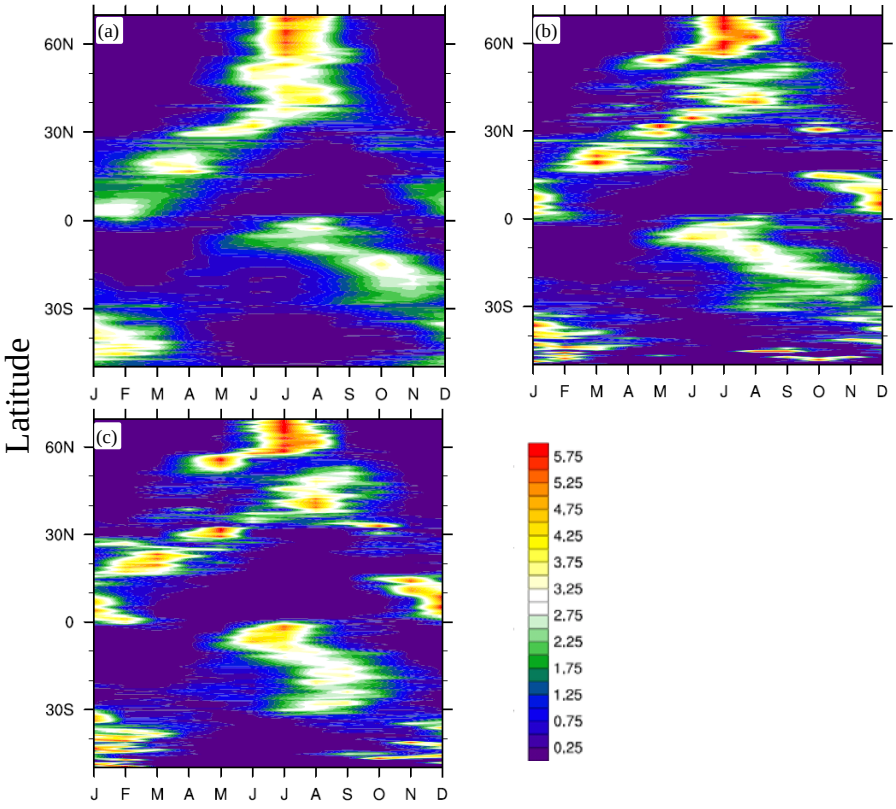

Figure 2-9. The zonal mean of monthly burned area of 6-year average (2002-2007), as normalized by the monthly average burned area of that latitude. (a) DLEM-Fire simulation, (b) GFED3, (c) MCD45A1.

2.2 Comparisons in Boreal North America

We collected several benchmark datasets to evaluate the DLEM-simulated GPP and pyrogenic carbon emissions in the Boreal North America (BONA) (Figure 2-10). GPP benchmark datasets were collected from the Moderate Resolution Imaging Spectroradiometer (MODIS) GPP product (satellite-based) (Zhao *et al.*, 2005) and two empirical-upscaling GPP products of model tree ensembles (MTE) (Jung *et al.*, 2011) and EC-MOD (Xiao *et al.*, 2014). The benchmark datasets of pyrogenic carbon emissions were collected from the Global Fire Emission Database version 3 (GFED3) (van der Werf *et al.*, 2010b) and Global Fire Assimilation System (GFAS) (Kaiser *et al.*, 2012b). Pyrogenic carbon emissions of GFED3 were developed

based on the CASA model driven by satellite-observed burned area (Giglio *et al.*, 2010a), while pyrogenic carbon emissions of GFAS were developed based on the satellite-observed Fire Radiative Power (FRP).

In the overlapped 10 years (2001 - 2010) of the four GPP estimates, DLEM-simulated GPP is 5206.6 Tg C $year^{-1}$, which is between the estimates of the other three benchmark datasets (MODIS: 5556.3 Tg C $year^{-1}$; EC-MOD: 4773.9 Tg C $year^{-1}$; MTE: 5320.9 Tg C $year^{-1}$); the inter-annual variations of DLEM-simulated GPP are significantly correlated with each benchmark dataset (P-value < 0.05). From 2001 to 2010, inter-annual variations of DLEM-simulated pyrogenic carbon emissions are highly correlated with GFED3 and GFAS estimations (P-value < 0.001), while DLEM estimation (67.8 Tg C $year^{-1}$) is slightly higher than GFED3 estimation (60.9 Tg C $year^{-1}$) and GFAS estimation (65.4 Tg C $year^{-1}$). In general, DLEM-simulated GPP and pyrogenic carbon emissions agree well with these benchmarks in terms of both magnitude and inter-annual variations.

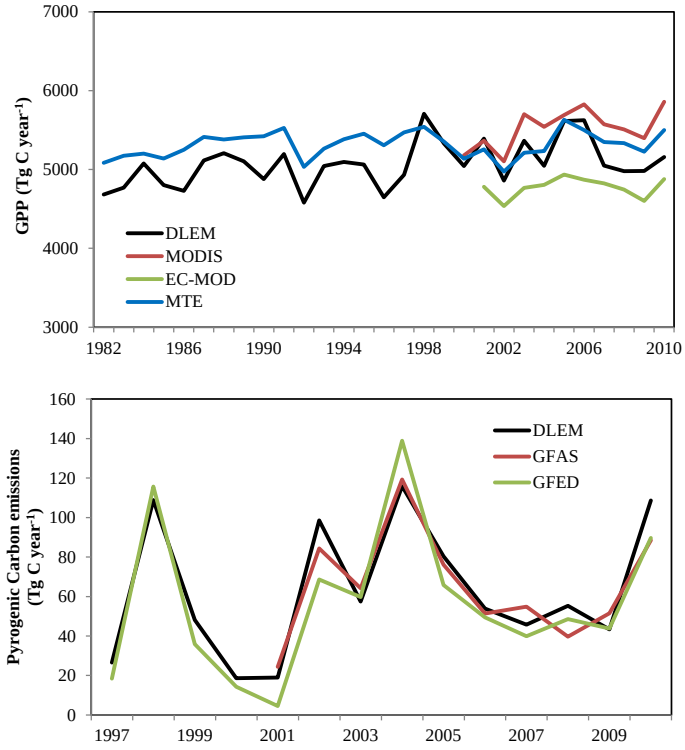

Figure 2- 10. Evaluation of DLEM-simulated gross primary productivity and pyrogenic carbon emissions against benchmark datasets.

2.3 Comparisons in Africa

DLEM-simulated burned area and pyrogenic carbon emissions were compared with the global fire emissions datasets version 3.1 (GFED3.1) (van der Werf *et al.*, 2010b) during 1997-2010 (Figure 2-11, Figure 2-12, Figure 2-13, and Figure 2-14). In the 14 years, DLEM-simulated African burned area was 232.4 Mha year^{-1}, with 48.3% occurred in the NHAF and 51.7% in the SHAF. DLEM-simulated burned area was 8% lower than that of GFED3.1. The trends of DLEM-simulated burned area in Africa, NHAF, and SHAF were -2.8 Mha year^{-2}, -2.9 Mha year^{-2} Mha year^{-2}, and 0.1 Mha year^{-2}, compared to -2.9 Mha year^{-2}, -3.5 Mha year^{-2}, and 0.6 Mha year^{-2} as estimated by GFED3.1. Inter-annual variations of DLEM-simulated burned areas in both NHAF and SHAF were significantly correlated with GFED3.1 estimates (p-value < 0.05).

DLEM-simulated pyrogenic carbon emissions were 0.85 Pg C year^{-1}, which were 17% lower than GFED3.1 estimates. DLEM-simulated pyrogenic carbon emissions were similar to GFED3.1 estimates in the SHAF, but 35% lower than GFED3.1 estimates in the NHAF. Inter-annual variations of DLEM-simulated pyrogenic carbon emissions were significantly correlated with GFED3.1 estimates (p-value < 0.05). In general, the DLEM captured the magnitude, inter-annual variations, and trends in both burned area and pyrogenic carbon emissions in Africa from 1997 to 2010.

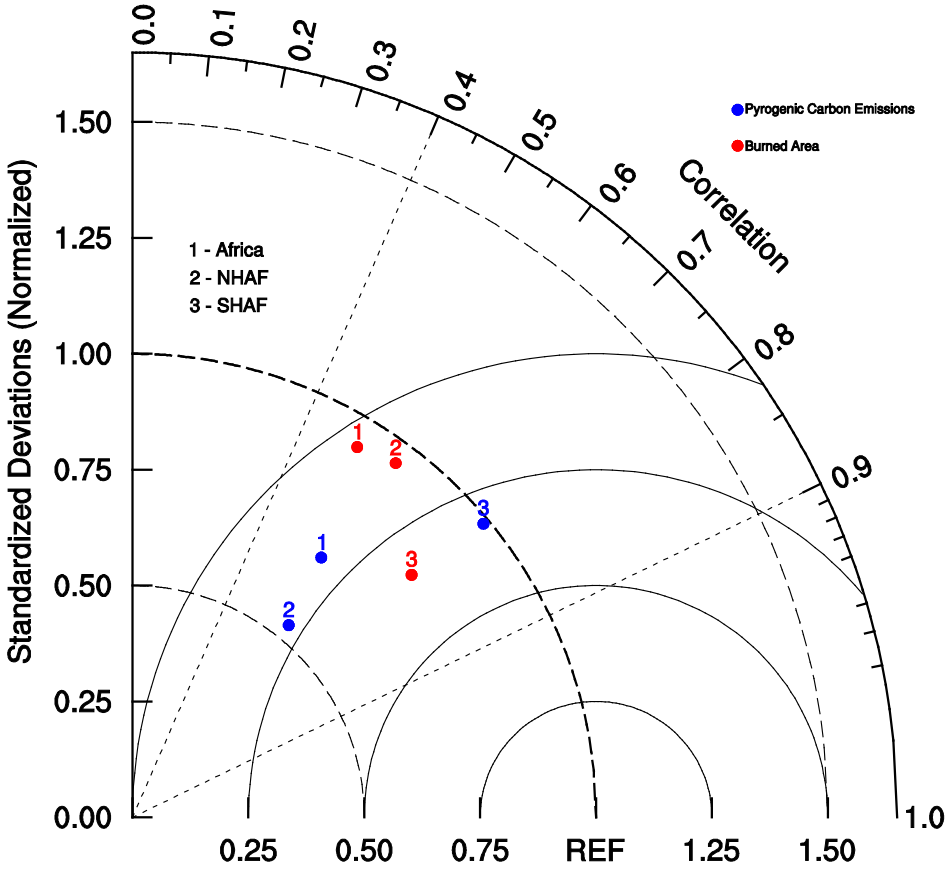

Figure 2-11. Taylor diagram presenting comparisons of DLEM-simulated inter-annual variations in burned area and pyrogenic carbon emissions against GFED3.1 estimates during 1997-2010.

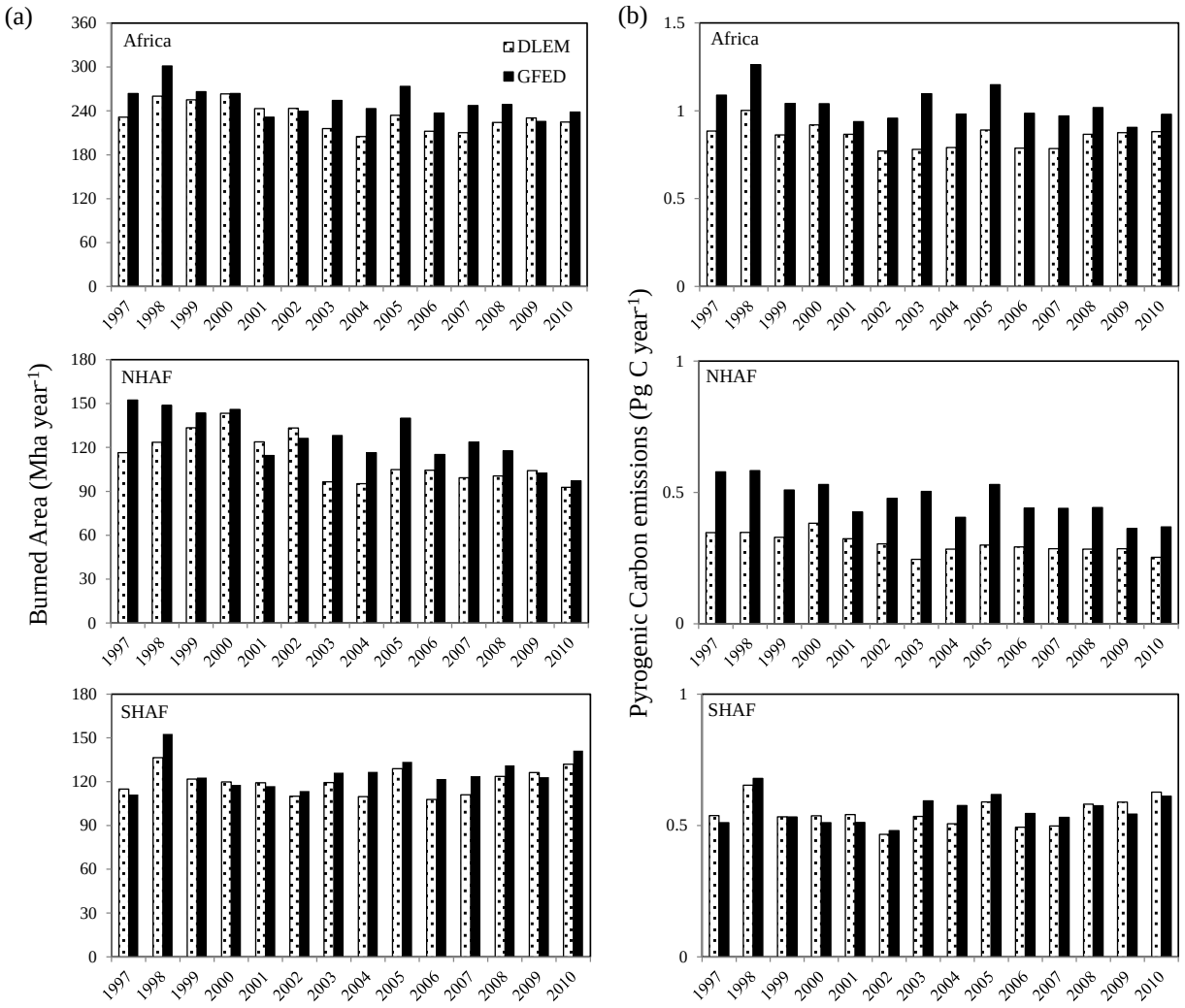

Figure 2-12. Comparisons of inter-annual variations in burned area (a) and pyrogenic carbon emissions (b) between DLEM simulations and GFED3.1 estimates in Africa, NHAF, and SHAF from 1997 to 2010.

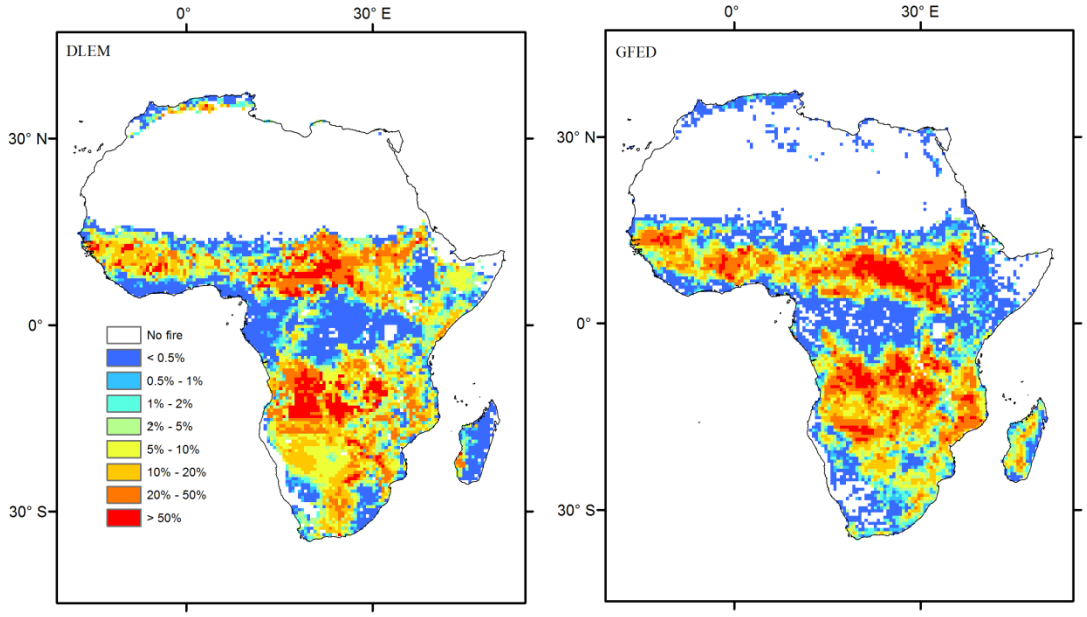

Figure 2-13. Comparison of average burned fraction during 1997-2010 between DLEM simulation and GFED3.1 estimate.

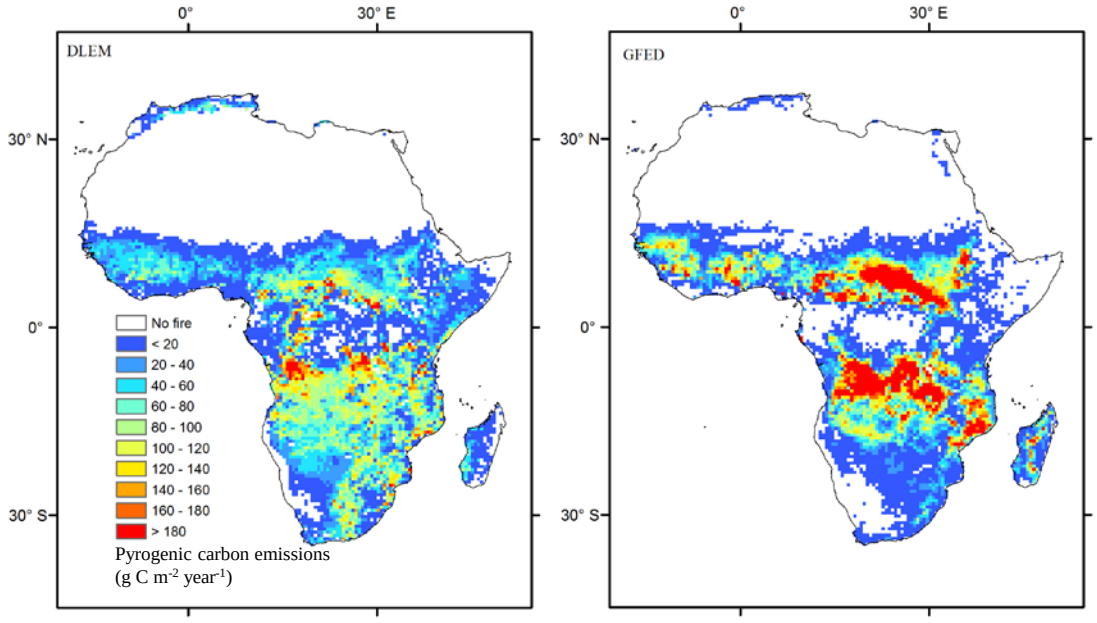

Figure 2-14. Comparison of average pyrogenic carbon emissions during 1997-2010 between DLEM simulation and GFED3.1 estimate.

3. Conclusion

A process-based fire model was developed on the platform of the DLEM. The detailed processes of fires, such as fire ignition, fire spread and duration, were explicitly estimated by considering multiple environmental factors. The fire mortality and post-fire vegetation recovery processes were also included in the DLEM. As shown by the comparison, the DLEM-fire can capture the spatial distribution and temporal variations of burned area and fire-induced carbon emissions observed by the satellite products. The DLEM-simulated carbon storage and fluxes agreed well with the benchmark datasets. Therefore, we applied the DLEM-fire model to study the changes in historical fire activities in various regions and the entire globe, and investigate fire impacts on terrestrial carbon budget.

Chapter 3. Burned area and fire emission from large fires in the Conterminous United States

Abstract

Since the mid-1980s, the frequency of wildfires in the Conterminous United States (CONUS) has increased significantly due to climate warming and frequent droughts. However, little work has been conducted to study the burned area and fire emissions of large fires at national scale. Meanwhile, the mechanisms explaining the changes in fire size needs further investigation. In this study, we synthesized fire perimeter and burn severity data sets and estimated fire-induced carbon emissions in the CONUS from 1984 to 2012 by using a process-based ecosystem model. The results show that average area burned by large fires was 14,430.51 km^2 $year^{-1}$ and large fire-induced carbon consumption was approximately 17.65 Tg C $year^{-1}$ during the study period. The inter-annual variations of burned area and carbon consumption presented significant increasing trends. The characteristic fire size in the period 2004-2012 increased by 176.1% compared to that in the period 1984-1993. Moreover, we found that the larger fires were associated with higher burn severity, and the larger fires became increasingly important in terms of their contributions to the total burned area and pyrogenic carbon emissions. Our findings imply that, once the warming and drying trends continue in the 21st century, the contributions of larger and severer fires to total burned area and fire emissions would increase with climate change.

Keywords: Burned area; fuel loading; extreme fires; burn severity; fire emissions; fire model

1. Introduction

As a natural disturbance in the earth system, fire plays a critical role in contributing to climate changes (Bowman *et al.*, 2009, Randerson *et al.*, 2006a, Ward *et al.*, 2012a) through modifying vegetation composition and distribution (Bond *et al.*, 2005a), atmospheric greenhouse gases and aerosol concentration (Bousquet *et al.*, 2006, Kasischke *et al.*, 2005, Langmann *et al.*, 2009, Van Der Werf *et al.*, 2004), terrestrial carbon budget (Bond-Lamberty *et al.*, 2007, Houghton *et al.*, 2000a, Li *et al.*, 2014b, Prentice *et al.*, 2011a), and land surface water and energy balance (Beck *et al.*, 2011, Bond-Lamberty *et al.*, 2009). In the Conterminous United States (CONUS), wildfire activities have been intensively studied at various temporal and spatial scales e.g., (Houghton *et al.*, 2000a, Liu, 2004, Schoennagel *et al.*, 2004, Westerling *et al.*, 2006a, Zhang *et al.*, 2014). It has been found that burned area declined by 98% in the CONUS during 1700-1990 due to human activities (i.e., fire suppression activities and cropland expansion) (Houghton *et al.*, 2000a), while increased substantially in the western US since the mid-1980s as influenced by climate warming, earlier spring, frequent droughts, and insect outbeark (Dennison *et al.*, 2014, Littell *et al.*, 2009, Westerling *et al.*, 2006a).

The probability of very large fires has been found to present an increasing trend in the recent decades (Barbero *et al.*, 2014, Dennison *et al.*, 2014). Though they compose a small percentage of all fires, large fires contribute the majority to the total area burned (Strauss *et al.*, 1989). “Extreme wildfire” was commonly used to defined the individual fires burning a very large area (Birch *et al.*, 2014), and “mega-fire” was to define those fires with large size as well as high burn severity (Adams, 2013, Pyne, 2007, Stephens *et al.*, 2014, Williams, 2013). Due to the large spatial extent and resistance to control, mega-fires become the most costly and dangerous wildfires (Williams, 2013).

Fires have often been grouped into several size categories to investigate the changes of fire size in different periods. For example, *Kasischke and Turetsky* (2006) studied the changes in fire size from 1959 to 1999 in boreal North America by analyzing the frequency and burned area of fires in four size categories (small, large, very large, and ultra large). They found more than a doubling of the frequency of large fire years in the 1980s and the 1990s, comparing with the 1960s and the 1970s. *Barbero et al.* (2014) built a model to investigate the occurrence of very large fires (> 5000 ha) in the western US. *Lehsten et al.* (2014) developed a concept of "characteristic fire size" to describe the relative contribution of fires to the total burned area, and applied it to investigate the spatial distribution and temporal changes of fire sizes across the boreal ecoregions. Given that the long-term fire information is available in the CONUS, these methods can be applied to study the fire size in the CONUS as well.

In the recent decade, fire-induced forest mortality presented an upward trend in the western US (Hicke *et al.*, 2013, Mantgem *et al.*, 2013). It has been recognized that fires in different levels of burn severity can induce divergent ecological consequences (Schoennagel *et al.*, 2004); low severity fires usually do not kill trees and cause less fire emissions, while high severity fires are either very hot surface fires or crown fires that may kill trees and alter vegetation composition significantly. Larger and more severe fires can lead to higher fire emissions, generate higher risk for soil erosion, and slow down post-fire plant recovery processes. At the landscape scale, burn severity has been found to be determined by weather condition, fuel characteristics, and topography (Dillon *et al.*, 2011). However, at national scale, studies regarding the general relationship between burn severity and fire size are still lacking.

The gases and particulates emitted during fire events are the major way through which fires influence atmospheric greenhouse gas concentration and air quality. At the present day, two primary approaches are used to estimate fire emissions, i.e., direct satellite-based estimation and fire model simulation. For the direct satellite-based approach, biomass burning is estimated according to fire radiative power (FRP) and biomass combustion rate (Kaiser *et al.*, 2012a, Wooster *et al.*, 2005, Zhang *et al.*, 2014), while, for the model-based simulation, biomass burning is calculated as the product of burned area, fuel loading, and combustion completeness (Seiler & Crutzen, 1980). In the fire models, burned area can be either obtained from input dataset e.g. (van der Werf *et al.*, 2010b) or from model simulations e.g. (Li *et al.*, 2012). The representation of burn severity (i.e., combustion completeness and tree mortality) in fire models is usually retrieved from the fixed vegetation parameter table without considering its temporal and spatial variations e. g. (Li *et al.*, 2012, Thonicke *et al.*, 2010). One recent metadata analysis based on in-situ measurements showed that the combustion completeness of one specific plant functional type could vary substantially across various regions and time periods (van Leeuwen *et al.*, 2014c). Thus, large uncertainties could be introduced once the fixed burn severity parameters were applied to evaluate fire emissions and fire impacts on ecosystems.

National-scale fire perimeter and burn severity datasets in the US have been developed by the Monitoring Trends in Burn Severity (MTBS) project (Eidenshink *et al.*, 2007b). They have been applied to estimate the biomass burning and forest mortality across various landscapes and regions (Dennison *et al.*, 2014, Dillon *et al.*, 2011, Ghimire *et al.*, 2012, Hicke *et al.*, 2013, Meigs *et al.*, 2011, Miller *et al.*, 2012). The MTBS fire products provided detailed information for each fire event from 1984 to present. In this study, we investigated the fire size, burned area, and burn severity by analyzing the spatially-explicit MTBS fire products spanning from 1984 to

2012. Furthermore, we incorporated the MTBS fire products into a process-based ecosystem model, the Dynamic Land Ecosystem Model (DLEM) (Tian *et al.*, 2010b), to estimate the fire-induced carbon consumption. The objectives of this study are: (1) to investigate the changing trends of fire size and burned area in the CONUS; (2) to provide a new estimation of biomass burning in the CONUS by incorporating remote-sensed burn severity; (3) to probe the relationship between fire size and burn severity; (4) to examine the influencing factors for the increased fire size and burn severity.

2. Method and Data

2.1. Data sets

2.1.1. Climate datasets and indices

In this study, climate data from 1979 to 2012 were obtained from North American Regional Reanalysis (NARR) dataset at the spatial resolution of 32-km (Mesinger *et al.*, 2006) (available at http://www.esrl.noaa.gov/psd/data/gridded/data.narr.monolevel.html). We resampled the NARR climate product to geographic coordinate system at 0.25° latitude by longitude by using ArcInfo 10.0. The z-scores of temperature and precipitation (T_z and P_z) were computed to represent the inter-annual climate variations from 1984 to 2012,

$$T_z = \frac{T - \bar{T}}{\sigma_T}$$

$$P_z = \frac{P - \bar{P}}{\sigma_P}$$

where T is the annual mean temperature (°C), $\bar{T}$ is the 29-year average annual mean temperature (°C), and σ_T is the standard deviation of 29-year annual mean temperature (°C), P is the annual

total precipitation (mm year^{-1}), $\bar{P}$ is the 29-year average precipitation (mm year^{-1}), and σ_P is the standard deviation of 29-year annual precipitation (mm year^{-1}).

2.1.2. MTBS fire database

The MTBS is "a multi-year project designed to consistently map the burn severity and perimeters of fire across all the lands of the United States from 1984 and beyond" (http://www.mtbs.gov/). The satellite-based burned severity index, i.e., Differenced Normalized Burn Ratio (dNBR), was used to retrieve fire perimeters and burn severity (Eidenshink *et al.*, 2007a). The dNBR is compared well with ground-based Composite Burn Index (CBI) in the CONUS (Cocke *et al.*, 2005, Key & Benson, 2006, Peters *et al.*, 2007, Veraverbeke *et al.*, 2011b), and deemed to be an effective approach to map burn severity (Brewer *et al.*, 2005). Based on the relationship between dNBR and CBI, satellite pixels included by fire perimeter were subjectively classified into four severity levels by analysts, namely "Unburn to Low", "Low", "Medium" and "High". MTBS burn severity was provided in the raster format at the spatial resolution of 30 meter, and fire perimeters were provided in the format of ArcGIS shapefile (see the example of the "North Fork" fire in Figure S2 in Appendix II). In this study, we used the area contained in the fire perimeter to denote burned area. It should be noted that the area contained in the fire perimeter is slightly larger than the actual area burned, because the unburnt vegetation islands were existed within the fire perimeter.

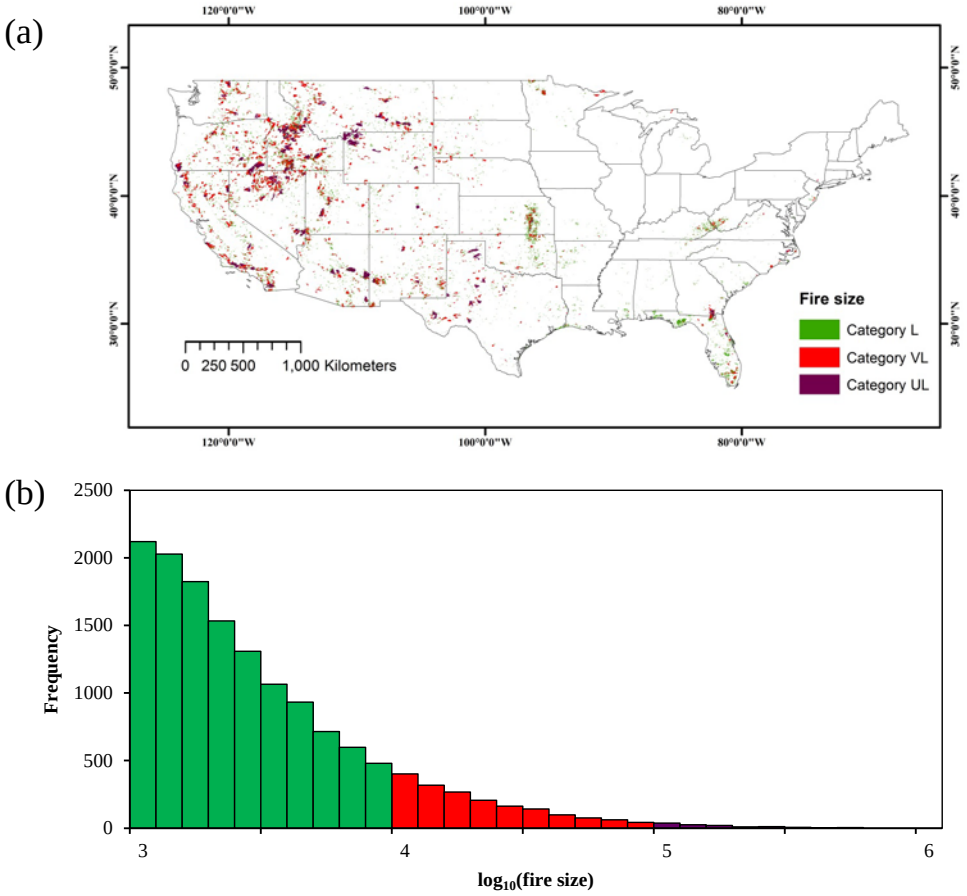

Figure 3-1. (a) Spatial distribution of fires in three size categories in the Conterminous United States, (b) the histogram of fire frequency in fire size intervals. The fire size intervals were created according to the logarithm of fire size (in acre).

MTBS project intended to map all the fires larger than 1,000 acres in the western US and fires larger than 500 acres in the eastern US (Eidenshink *et al.*, 2007a). In this study, we aimed to investigate the large fires. Therefore, fires with size less than 1,000 acres were excluded. In total, 14,495 large fires during 1984-2012 were considered in this study (Figure 3-1). We further separated these fires into three size categories, i.e., Large (L), Very Large (VL), and Ultra Large (UL). The names of fire size categories are similar to those used by *Kasischke and Turetsky*

(2006), but classification criterions are different. In this study, the fires are classified based on the fire size (acre) as below,

$$\text{Category L:} \quad 3 \leq log_{10}(fire\ size) < 4$$

$$\text{Category VL:} \quad 4 \leq log_{10}(fire\ size) < 5$$

$$\text{Category UL:} \quad log_{10}(fire\ size) \geq 5$$

For fires in each size category, we extracted monthly fire perimeters and burn severity according to fire starting dates and locations. The burn severity of one specific fire event was represented by the fractions of fire pixels in different severity levels. For example, in the "North Fork" fire, 869,025 pixels (34.2%) were burned in "Unburn to Low" severity; 167,398 pixels (6.6%) were burned in "Low" severity; 294,284 pixels (11.6%) were burned in "Moderate" severity; 1,150,086 pixels (45.3%) were burned in "High" severity; "Increased Greenness" took 52,283 pixels (2.1%); "Non-Processing Area Mask" took 7,781 pixels (0.3%).

2.1.3. Input data for driving the DLEM

In this study, the DLEM simulation period is from 1979 to 2012, and the spatial resolution of simulation is 0.25°. Georeferenced data sets were compiled to drive the DLEM, including daily climate datasets (solar radiation, precipitation, average/maximum/minimum temperature and relative humidity), monthly burned fraction and burn severity, atmospheric CO_2 concentration, nitrogen deposition, annual land cover and land use maps, soil texture and topography (elevation, slope, and aspect) for the entire CONUS. Climate data from 1979 to 2012 were retrieved from the NARR dataset (see section 2.1.1). MTBS fire perimeter was converted to grid burned fraction at the spatial resolution of 0.25°, and the burn severity in 30-meter resolution was converted to the fractions of fire pixels in the "Unburn to Low", "Low",

"Moderate", and "High" burn severity levels in each simulation grid. Other datasets (CO_2 concentration, nitrogen deposition, land use and land cover, soil texture, topography) were consistent with our previous North America studies (Liu *et al.*, 2013a, Yang *et al.*, 2014b).

2.2. Model implementation and evaluation

The implementation of the DLEM was composed of three stages: equilibrium run, spin-up, and transient run. Equilibrium run aims to determine the initial status in the year 1979. During this stage, the DLEM was fed with the average climate condition from 1979 to 1988 and other input data (atmospheric CO_2 concentration, nitrogen deposition, and land cover) in 1979, while the disturbances (such as fires, harvest, and land use change) were excluded. The equilibrium state for each grid cell was assumed to be reached when the differences in grid carbon, nitrogen, and water pools among 50 consecutive years were less than 0.1 g C m^{-2}, 0.1 g N m^{-2}, and 0.1 mm. Equilibrium run was followed by a 100-year model spin-up. In the spin-up stage, the DLEM was driven by the detrended time series of all input datasets, with fire option switched on. The detrended input datasets were constructed through random selection from the first 10 years during 1979 - 1988. In the transient mode, the DLEM was driven by the time series of all the input data from 1979 to 2012. Since MTBS fire datasets from 1979 to 1983 were not available, we simply used the fire data in 1984 to represent the fire conditions in the first 5 years of the simulation. We designed four simulations (*Sim0, Sim1, Sim2,* and *Sim3*) to investigate biomass burning from large fires in different size categories. The reference simulation (*Sim0*) included all the large fires with size over 1,000 acres detected by MTBS, while the other three simulations, namely *Sim1*, *Sim2*, and *Sim3,* included fires in each single size category, corresponding to fires in size category L, category VL, and category UL, respectively.

To evaluate the DLEM simulated carbon consumptions during biomass burning, we collected five fire products covering the entire CONUS, including Wildland Fire Emissions Information (WFEIS) v0.4 (French *et al.*, 2014), Global Fire Emissions Database (GFED) v3.1 (van der Werf *et al.*, 2010b), Fire INventory from NCAR (FINN) v1 (Wiedinmyer *et al.*, 2011b), Global Fire Assimilation System (GFAS) v1 (Kaiser *et al.*, 2012a), and Geostationary Operation Environmental Satellites (GOES) (Zhang *et al.*, 2014).

Biomass burning from WFEIS, GFED, and FINN were estimated based on burned area, fuel loading, and combustion completeness, while fire products from GFAS and GOES were computed directly from satellite-observed fire radiative power (FRP). The WFEIS is a web-based tool to compute wildfire emissions in the CONUS and Alaska at 1-km spatial resolution (http://wfeis.mtri.org/). The user can select the simulation extent, temporal period, and burned area products. In this study, we selected MTBS fire perimeter as input to drive WFEIS to estimate the carbon combustion in the CONUS from 1984 to 2010. GFED v3.1 biomass burning was downloaded from http://www.globalfiredata.org/index.html, which covers the period from 1997 to 2011 at the spatial resolution of 0.5° across the globe. For GFED, burned area is estimated according to multiple satellite images (Giglio *et al.*, 2013b), fuel loading is simulated by Carnegie-Ames-Stanford-Approach (CASA) model, and combustion completeness for leaf, stem, fine litter, and coarse woody debris are read from parameter tables. FINN estimates fuel loading according to satellite-derived land use and land cover type and a look-up table, and estimated combustion completeness through a function of tree cover (available at http://bai.acd.ucar.edu/Data/fire/). GFAS and GOES biomass burnings are computed based on the FRP retrieved from MODIS and Geostationary Operation Environmental Satellites, respectively. GFAS is downloaded from http://www.gmes-

atmosphere.eu/about/project_structure/input_data/d_fire/, and GOES biomass burning is derived from the figure 5a in *Zhang* et al., (2014).

The inter-annual variations of biomass burning estimated by these products were compared with the DLEM *sim0* simulation.

2.3. Statistical analysis

The concept of "characteristic fire size" is constructed to describe the relative contributions of fires in different size to the total burned area (Lehsten *et al.*, 2014). The fire size with the largest contribution is defined as the characteristic fire size. We estimated the characteristic fire sizes in the entire study period (1984-2012) and three sub-periods (1984-1993, 1994-2003, and 2004-2012) by using regression analysis. Firstly, fires were separated into 20 bins with equal width of logarithms of fire size (in acre). Then, un-normalized Gaussian curve was used to fit the total burned area within each bin (dependent variable) against the midpoints of that bin (independent variable),

$$y = Ne^{-\frac{(x-\mu)^2}{2\sigma^2}}$$

where parameter μ is mean of the Gaussian distribution, σ is the parameter standing for the standard deviation, and parameter N represents the maximum value of the distribution curve. The three distribution parameters were estimated according to the least-squares regression analysis. The fitted Gaussian curve is used to summarize the distribution of burned area against fire size, and estimate the characteristic fire size (i.e., 10^{μ} acre).

Mann-Kendall (MK) trend test is a non-parametric test to examine the trend significance of a time-series. In this study, we applied the MK trend test to detect the significance of the

trends in arithmetic mean fire size, burned area, and biomass burning from 1984 to 2012. The slopes of inter-annual variations in burned area and biomass burning were estimated by the least-squares linear regression analysis.

3. Results and Discussion

3.1. Burned area and fire size

From 1984 to 2012, there were totally 14,495 large fires detected by MTBS across the CONUS, and most of them occurred in the western US (Figure 3-1). Fire frequency decreases rapidly as fire size increases. The Ultra Large fires (category UL) were about 22.18% of the total burned area, while taking only 0.81% of total fire numbers (Figure 3-1 and Figure 3-2). During the study period, the annual burned area derived from all the large fires (including all three size categories) in the CONUS was approximately 14,430.51 ± 10,317.47 km^2 $year^{-1}$ (avg. ± 1 std. dev., same hereafter) with a significant upward trend at the rate of 810.29 km^2 $year^{-1}$ ($P < 0.001$; Figure 3-3). The highest annual burned area occurred in 2011 (40473.96 km^2), and the lowest burned area was in 1997 (2498.78 km^2). Similarly, significant increasing trends in burned area were detected for fires in each size category (Table 3-1). Comparing with the period 1984-1993, annual area during 2004-2012 burned by all the large fires increased by 187.3% on average, and the area burned by fires in category UL increased by 361.7%. Further analysis shows that the weight of area burned by category UL fires increased from 16.8% to 27%, while the weight of area burned by fires in category L decreased from 39.9% to 32.6% (Figure 3-3), indicating a growing importance of the UL fires in term of burned area.

Table 3-1. The averages and changing trends of burned area and biomass burning in the CONUS

	Burned area			Biomass burning		
	mean (km^2 $year^{-1}$)	**trend (km^2 $year^{-1}$)**	**P-value in MK trend test**	**mean (Tg C $year^{-1}$)**	**trend (Tg C $year^{-1}$)**	**P-value in MK trend test**
All categories	14430.51	810.29	< 0.001	17.65	0.87	< 0.01
Category L	5026.01	231.30	< 0.001	5.68	0.25	< 0.001
Category VL	6203.34	317.02	< 0.01	7.7	0.39	< 0.01
Category UL	3201.16	261.97	< 0.01	4.9	0.29	< 0.01

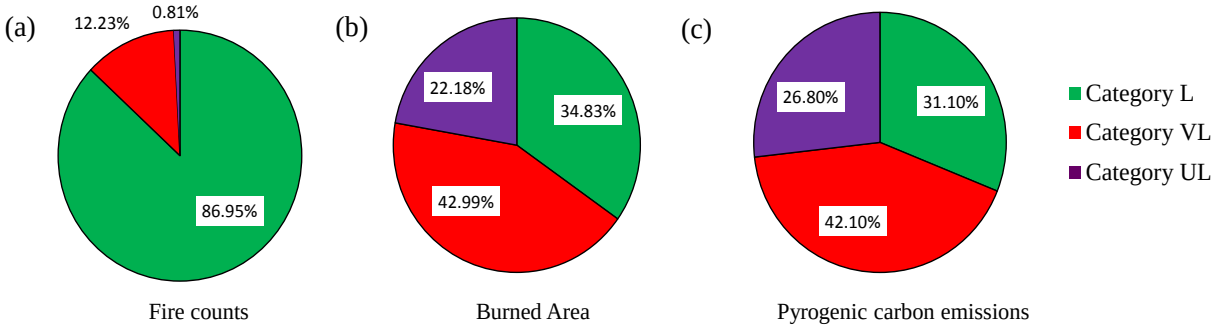

Figure 3-2. Contributions of fires in three size categories to (a) total fire counts, (b) total burned area, and (c) total biomass burning.

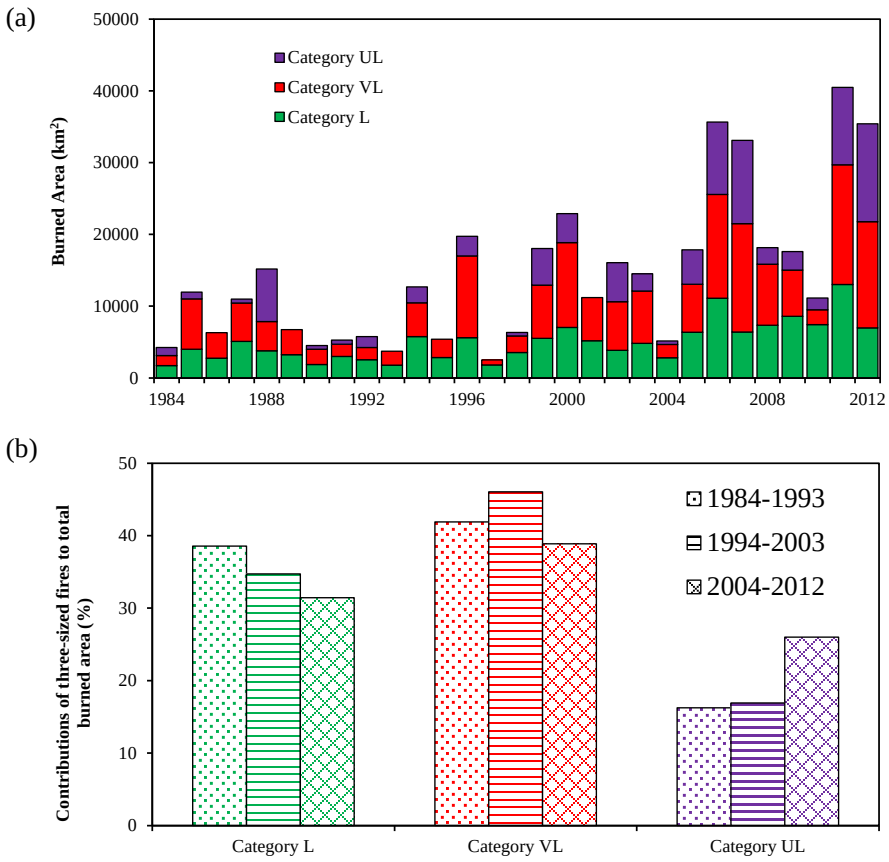

Figure 3-3. (a) Inter-annual variations of burned area during 1984 - 2012, (b) contributions of fires in three size categories in term of burned area during 1984-1993, 1994-2003, and 2004-2012.

Over the entire study period (1984-2012), the characteristic fire size was estimated to be 80 km^2 (i.e. $10^{4.296}$ acres) on average (Figure 3-4). During the three sub-periods of 1984-1993, 1994-2003, and 2004-2012, the characteristic fire sizes were estimated to be 48.32 km^2 (i.e., $10^{4.077}$ acres), 74.15 km^2 (i.e., $10^{4.263}$ acres), and 133.39 km^2 (i.e., $10^{4.518}$ acres), respectively. Compared to the first sub-period, the characteristic fire size increased by 176.1% during 2004-2012. These results indicated that the fires with maximum contribution to burned area shifted to the ones with larger size. Nevertheless, it is worth mentioning that no significant trend was found for the temporal variations of arithmetic annual mean fire size from 1984 to 2012 ($P > 0.05$,

Figure S3 in Appendix III). This is because burned area and fire frequencies increased simultaneously.

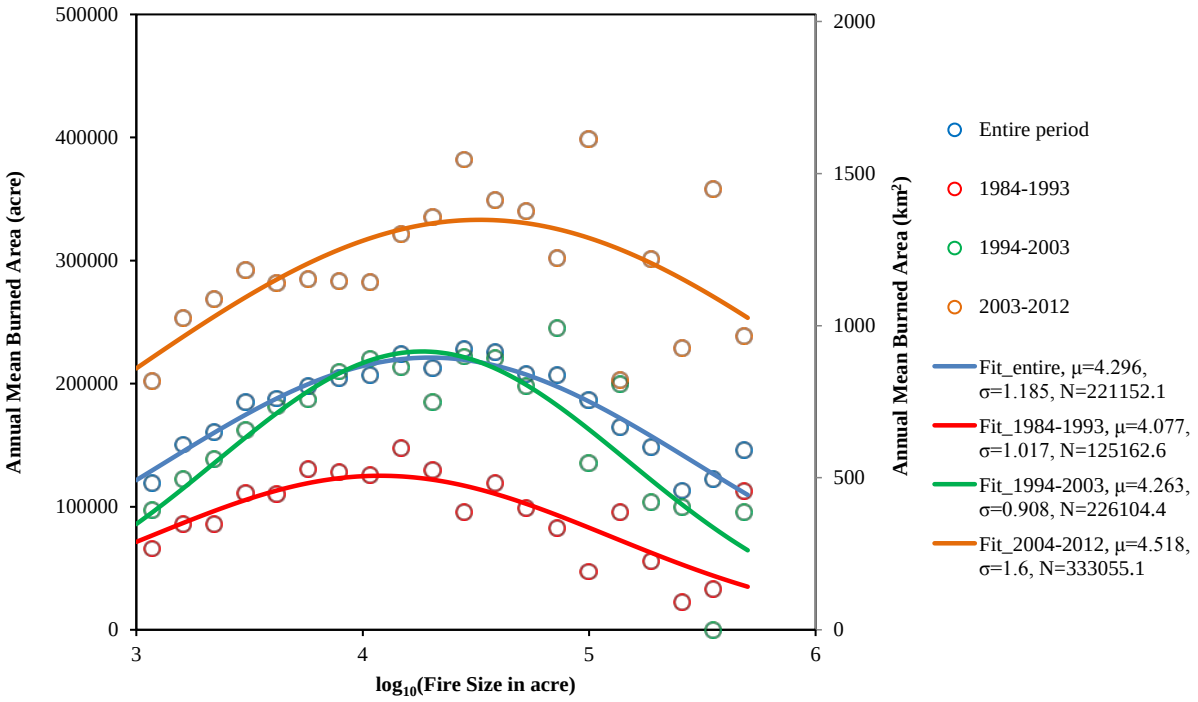

Figure 3-4. Characteristic fire size distribution in the entire study period (1984-2012), and 3 sub-periods (1984-1993, 1994-2003, and 2004-2012). The plots were fitted with non-normalized Gaussian distribution curve, and the $\boldsymbol{\mu}, \boldsymbol{\sigma}$ and $\boldsymbol{N}$ in the legends are the fitting parameters.

3.2. Biomass burning

During 1984-2012, annual biomass burning is simulated to be 17.65 ± 12.68 Tg C year^{-1} from all large fires with a significant increasing trend at the rate of 0.87 Tg C year^{-1} (Figure 3-5; Table 3-1). The largest annual biomass burning occurred in 2007 (48.11 Tg C), and the lowest biomass burning occurred in 1984 (1.6 Tg C). The carbon consumed by UL fires accounted for 26.8% of the total carbon consumption by all the large fires (Figure 3-2). It should be noted that the sum of biomass burning from *Sim1*, *Sim2*, and *Sim3* experiments was slightly higher than that estimated by *Sim0* experiment although the sum of burned area from *Sim1*, *Sim2*, and *Sim3* is equal to that of *Sim0* (Figure 3-5). This mismatch was primarily because *Sim1*, *Sim2*, and *Sim3*

only considered fires in single size category; therefore, more fuel was accumulated in *Sim1*-*Sim3* than that in *Sim0*. Compared to the period 1984-1993, annual mean biomass burning from UL fires simulated by *Sim3* increased by 1.16 Tg C year^{-1} during 1994-2003, and increased by 5.55 Tg C year^{-1} during 2004-2012; the contribution of biomass burning caused by UL fires increased from 26.6% in sub-period 1984-1993 to 29.6% in sub-period 2004-2012 (Figure 3-5). In term of biomass burning, it can be concluded that the UL fires were becoming more important in the recent years.

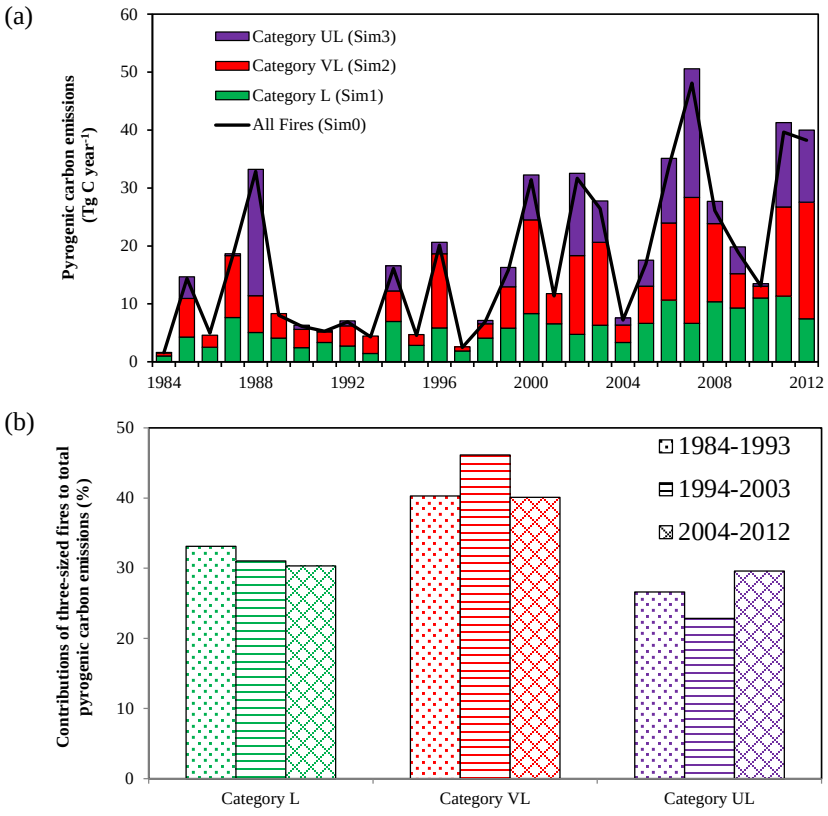

Figure 3-5. (a) Inter-annual variations of carbon consumptions in biomass burning during 1984-2012, (b) contributions of fires in three size categories in term of biomass burning during 1984-1993, 1994-2003, and 2004-2012, respectively.

The inter-annual variations of the DLEM-simulated biomass burning were compared with other five fire emission products (Figure 3-6). The results indicated that DLEM-simulated biomass burning was significantly correlated with each of them (Table 3-2), which was partially due to the fact that all the fire products have incorporated satellite information (either satellite observed burned area or FRP). During 2003-2010 (a period that all fire products covered), the DLEM-estimated annual mean biomass burning was 23.8 Tg C $year^{-1}$, which was close to the average of the other five fire products (26.1 Tg C $year^{-1}$). However, GFED v3.1 biomass burning was 69% lower than the average of the other five fire products. Some recent studies argued that fire emissions in the CONUS estimated by GFED v3.1 were likely to be underestimated (Kaiser *et al.*, 2012a, Zhang *et al.*, 2014).

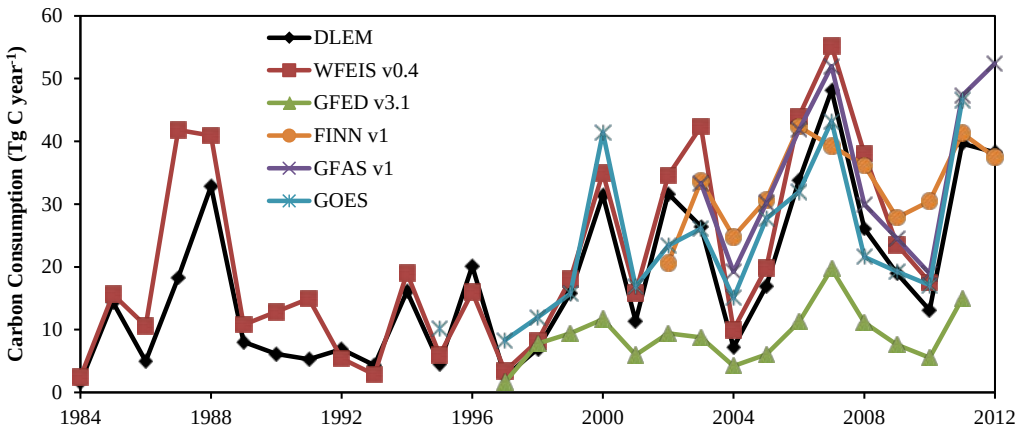

Figure 3-6. Intercomparison of annual biomass burning in the CONUS estimated by the DLEM, WFEIS v0.4, GFED v3.1, GFAS v1, GOES, and FINN v1.

Table 3-2. The biomass burning estimates from five fire emissions products and their correlations with the DLEM simulations (values in the parenthesis are estimated by the DLEM).

Fire products	Available period	Biomass burning (Tg C year^{-1})	Pearson's correlation coefficient	significance
WFEIS v0.4	1984-2010	20.9 (16.1)	0.94	$p < 0.001$
GFED v3.1	1997-2011	9 (22)	0.92	$p < 0.001$
FINN v1	2002-2012	33.2 (27.3)	0.66	$p < 0.05$
GFAS v1	2003-2012	35 (26.9)	0.95	$p < 0.001$
GOES	1995, 1997-2011	23.5 (20.9)	0.91	$p < 0.001$

One major uncertainty in the global biomass burning product comes from the parameterization of burn severity. Burn severity varies with locations, time periods, and climate conditions (see section 3.4). Thus, fire models, which parameterize burn severity by using a set of static burn severity parameters, could overestimate/underestimate biomass burning for fire events with extreme low/high burn severity. For example, as indicated by MTBS dataset, 45.3% of fire pixels within the "North Fork" fire perimeter was associated with high severity, which was much higher than the average burn severity in the CONUS (averagely, 8.64% of burned area is associated with high severity). The application of universal combustion completeness parameters based on average fire conditions could inevitably underestimate fire emissions and forest mortality caused by the "North Fork" fire. In this study, the DLEM coupled the information of satellite-derived burn severity. This strategy allowed the DLEM to better represent the large spatial and temporal variations in combustion completeness, and improve the accuracy of biomass burning estimations, particularly for the fires with extreme high severity.

3.3. Impact of climate and fuel loading on large fires

We examined the fire occurrence under four climate conditions, and the results show that 44.8%, 49.3% and 59.3% of fires in size category L, VL, and UL occurred during the relative drier and warmer years ($P_z < 0$ & $T_z > 0$) (Figure 3-7), which indicates that lower precipitation

and higher temperature stimulated the fire size, particularly for the UL fires. As indicated by the NARR climate dataset, annual temperature increased at the rate of 0.012 °C year^{-1}, and annual precipitation decreased at the rate of 2.93 mm year^{-1} in the western US (defined as the west of 97° W in this study) from 1984 to 2012 (Figure 3-8). For most ecosystems with sufficient fuel loading in the western US, the warming and drying was related to the more frequent UL fires; only in some rangeland areas, the decreases in precipitation were found to reduce fuel accumulation and suppress the occurrence of very large fires (Barbero *et al.*, 2014).

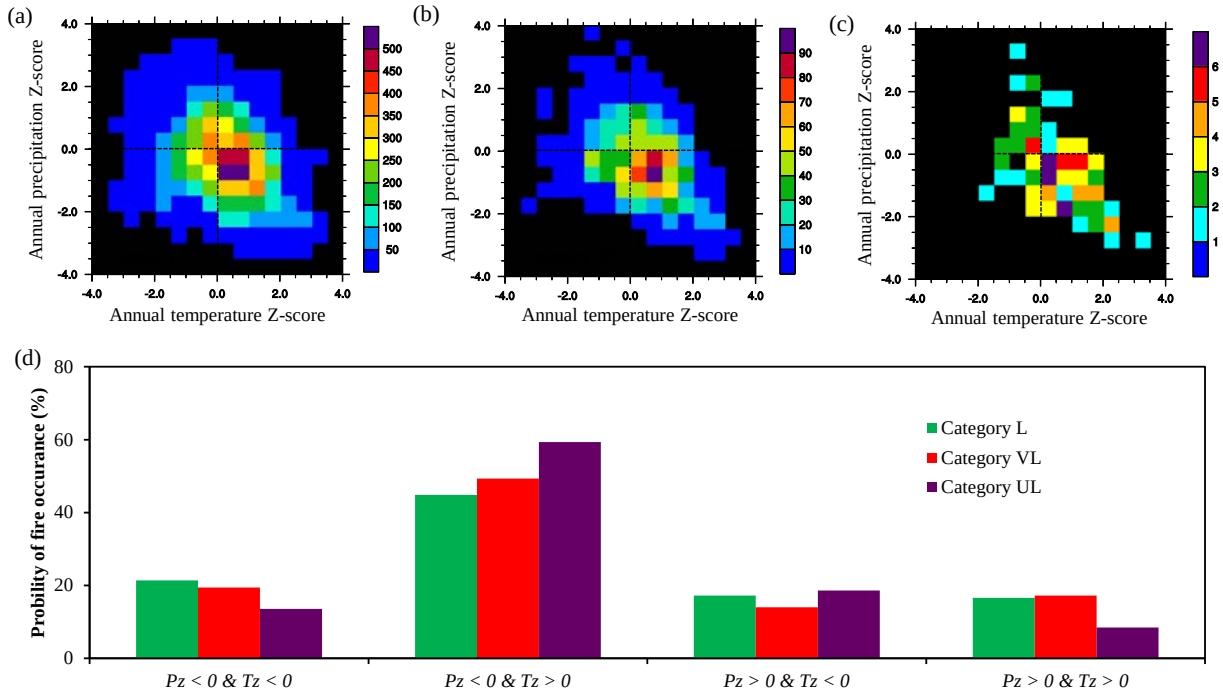

Figure 3-7. The plots of fire counts in size category L (a), category VL (b), and category UL (c) against the z-scores of annual precipitation (y-axis) and annual temperature (x-axis). (d) The probability of fire occurrence under four climate conditions: I. dry and cool ($\boldsymbol{P_z < 0}$ & $\boldsymbol{T_z < 0}$), II. dry and warm ($\boldsymbol{P_z < 0}$ & $\boldsymbol{T_z > 0}$), III. wet and cool ($\boldsymbol{P_z > 0}$ & $\boldsymbol{T_z < 0}$), and IV. wet and warm ($\boldsymbol{P_z > 0}$ & $\boldsymbol{T_z > 0}$).

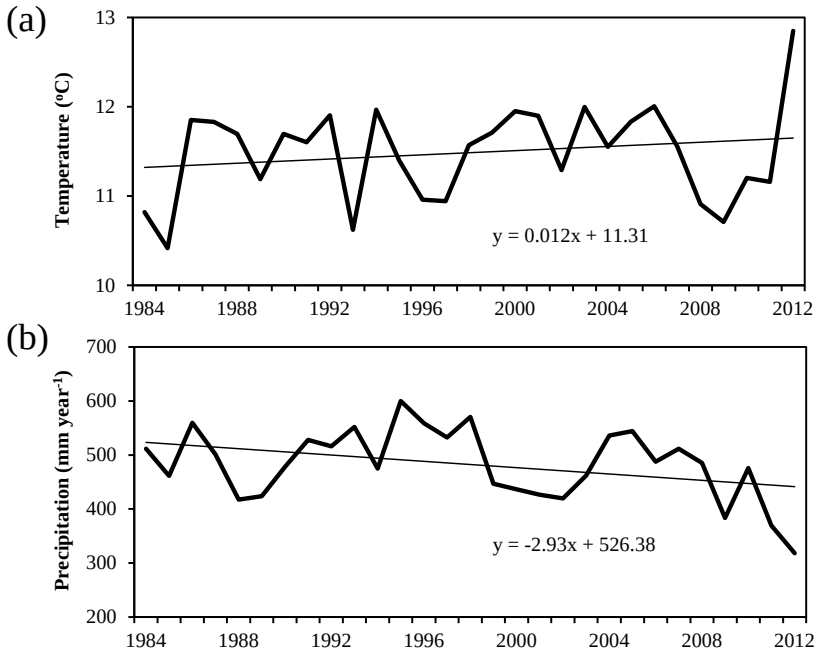

Figure 3-8. Inter-annual variations and changing trends of (a) annual mean temperature, (b) annual precipitation in the western US.

Previous fuel accumulation acted as another important factor accounting for the more frequent large wildfires (Williams, 2013). In the CONUS during the 20th century, fire activities have been suppressed substantially as a result of the fire exclusion policies (Houghton *et al.*, 2000a). The Weeks Act of 1911 established a framework between the states and federal government for cooperative firefighting, and was greatly extended with the Clark-McNary Act of 1924 and the McSweeney-McNary Act of 1928 (Houghton *et al.*, 2000a). The successful fire suppression policies promoted tree regeneration, fuel connectivity and fuel loading across all the forest types (Agee & Skinner, 2005). Therefore, the continuous fuelbed facilitated fire spread and enlarged fire sizes in the recent years.

3.4. The relationship between fire size and burn severity

Burn severity varies a lot among different fire size categories. For the area burned by fires in category L, VL, and UL, the percentages of high severity were 5.11%, 9.37%, and 12.84%, respectively (Figure 3-9). This result indicated that fires in larger size generally burned with higher severity in the CONUS. *Miller* et al. (2012) studied the percentage of high-severity wildfires in northwestern California from 1987 to 2008 and reported that the area burned with high severity was strongly related to fire size, which is consistent with our results.

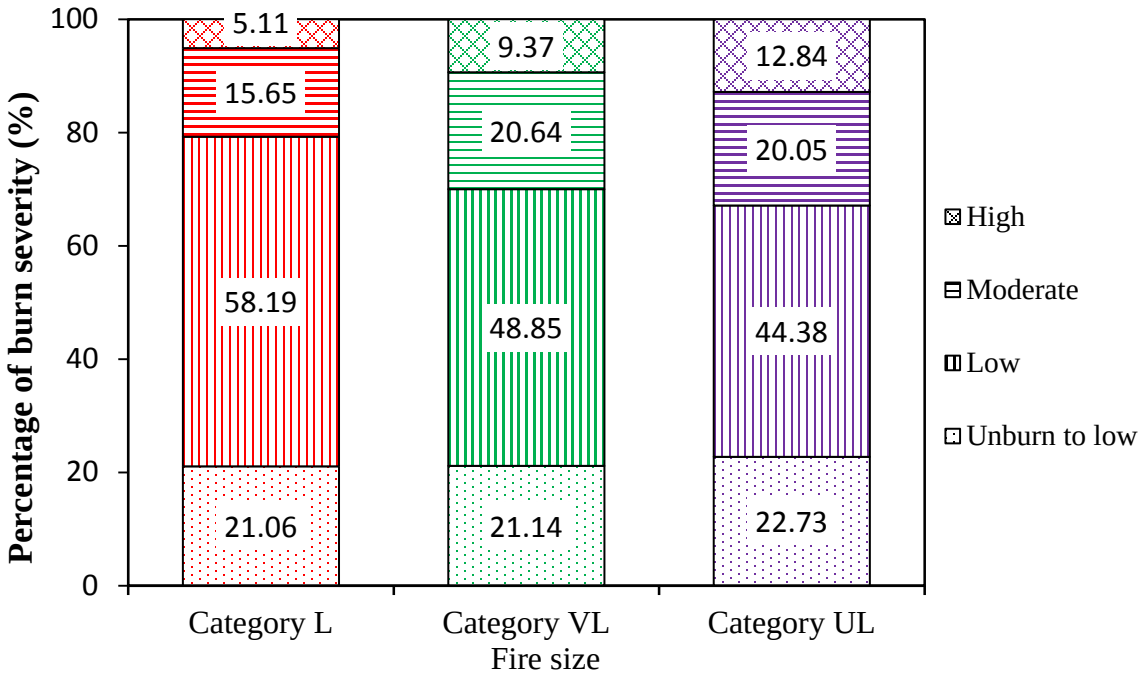

Figure 3-9. The composition of fire pixels burned in different severity levels (Unburn to Low, Low, Moderate, and High) for each size category.

Similar to fire size, burn severity can be controlled by climate and weather conditions as well. During the extreme fire weather, more energy is released, and the surface fire is more likely to converting to crown fire and leading to severer fire damage (Dillon *et al.*, 2011). Fire suppression activities in the 20th century altered fuel status by promoting the establishment of small fire-intolerant trees under the forest canopy, which formed “ladder fuel” to carry the

surface fire into the continuous canopy and enhanced the probability of catastrophic crown fires (Hurteau *et al.*, 2014, Schoennagel *et al.*, 2004). The first-time burn following long-term fire suppression activities could generate severer consequence than the burns afterwards, owing to the higher fuel accumulation (Miller *et al.*, 2012). Effective fuel treatments by removing hazard fuels, such as forest thinning and prescribed burning, are helpful to reduce the risks of high-severity fires (Pollet & Omi, 2002, Prichard *et al.*, 2010, Stephens *et al.*, 2009). Both fire size and burn severity are simultaneously affected by climatic conditions and fuel status, which explains the phenomenon that the larger fires are often associated with higher burn severity.

Moreover, topography has been recognized as another important factor in determining burn severity (Dillon *et al.*, 2011). For example, *Turesky* et al. (2011) found that soil organic layers burn deeper in south-facing slopes than north-facing slopes in interior Alaska; *Miller* et al. (2012) reported differing burn severity patterns between Sierra Nevada and northwest California, and attributed the differences to topography. Additionally, the differences in vegetation species can affect the burn severity as well (Rogers *et al.*, 2015).

3.5. Uncertainties

Our study provided a practical approach for the terrestrial model to estimate large-scale biomass burning by incorporating satellite-based burn severity. This method could greatly improve the accuracy of the model-based assessment of fire emissions and fire impact on ecosystems. Nonetheless, the uncertainties from both input datasets and model parameterizations should be beard in mind. Firstly, in the MTBS, the threshold to classify the burn severity in each satellite pixel is a quality control issue, and thus these subjectivities were inevitable introduced into the burn severity identification (Eidenshink *et al.*, 2007a). As the MTBS fire perimeter and burn severity were used to drive the DLEM simulations, the estimation of biomass burning by

the DLEM inherited the uncertainties in the MTBS datasets. Secondly, the simulated fuel loading by the DLEM was another source of uncertainty. The DLEM simulates the average fuel loading at grid level through a series of physiological and biogeochemical processes (e.g., photosynthesis, plant respiration, tissue turnover, and organic matter decomposition). Many processes, such as, insect, tornado, forest management, were not considered in this study, which might modify the fuel accumulation rate and fuel loading. Thirdly, scaling issue contributes another uncertainty source. To be compatible with the DLEM simulation, the 30-meter MTBS burn severity has to be scaled up to 0.25°. Therefore, the sub-grid variations in burn severity were neglected during the scaling-up process.

At the global scale, time-series of dNBR have been developed based on Moderate-Resolution Imaging Spectroradiometer (MODIS) dataset (Veraverbeke *et al.*, 2011b). The method to estimate biomass burning by integrating satellite-sensed burned severity should be used with caution when the study domain shifts to other regions. For example, in boreal regions, the relationship between dNBR and ground-based burn severity measurements has not been fully established; some investigators showed good relationship between dNBR and CBI (Epting *et al.*, 2005, Rogers *et al.*, 2014), while others found their correlation is weak (Hoy *et al.*, 2008, Kasischke *et al.*, 2008, Murphy *et al.*, 2008). Prior to applying satellite-based burn severity to estimating fire emissions and fire impacts, it is necessary to validate satellite-based burn severity indices against in-situ burn severity measurement.

4. Conclusions and implications

In this study, we investigated the magnitude and changing trends of burned area and pyrogenic carbon emissions from large fires in the CONUS during 1984-2012, and analyzed the relationship between burn severity and fire size. We found that both burned area and biomass

burning presented significantly upward trends; the contributions of larger fires to total burned area and pyrogenic carbon emissions were becoming higher in the recent years, owing to the warming and drying trend, previous fire suppression policies, and higher tree mortality induced by insect outbreaks; the larger fires were generally associated with higher burn severity. To the best of our knowledge, this study is the first time for the ecosystem model to estimate biomass burning in the CONUS by coupling high-resolution satellite-derived burn severity. The estimation of historical and contemporary fire emissions and fire impacts on ecosystem can be substantially improved by considering the temporal and spatial variations in burn severity.

Climate change projections indicate that the warming and drying trends would continue throughout the 21st century in the CONUS, particularly under the high greenhouse gas emissions scenario (Dai, 2011, Wuebbles *et al.*, 2014). Therefore, it is rational to expect that the contributions of larger fires in terms of burned area and fire emissions would increase continuously with the advance of climate changes. In associated with higher burn severity, the more frequent larger fires would lead to much higher fire emissions and cause severer ecological consequences in the future. The current fire regimes (such as, fire frequency, size, and severity) would be fundamentally altered. To project fire impacts on ecosystem and climate in the future, an accurate estimation of burn severity is equally important as that of burned area. Fire models with prognostic burn severity are in need to be developed.

Chapter 4. Fire-induced changes in the terrestrial carbon budget and storage in the boreal North America

Abstract

Terrestrial ecosystems in the boreal North America (BONA) are of global importance in term of climate change, due to their tremendous carbon storage and sensitivity to subtle changes in environmental conditions. As the primary agent to renew forest stand, fire play a significant role in shaping ecosystem structure and function and determining the magnitudes of terrestrial carbon fluxes and carbon storage. Although fire is ecological desirable in some boreal forests in maintaining sustainability, fire endangers human life and properties, induces higher risks in lumber production, and has strong feedbacks to regional and global climate. In the BONA, fire activities were becoming more frequent in the past several decades, and will increase more rapidly in the future. Our knowledge regarding the impacts of historical increased fires would provide useful information for forest management agencies to cope with future fires. In this study, we investigated increased fire impacts on terrestrial carbon fluxes and storage in the BONA during 1960-2010 by using a process-based ecosystem model. Our results indicate that, during the study period, pyrogenic carbon emissions were 51 ± 39.2 Tg C $year^{-1}$, with a significant increasing trend at the rate of 0.91 Tg C $year^{-2}$. As a result of the increases in fire frequency and burned area, terrestrial carbon sink was reduced by 25.4 Tg C $year^{-1}$ comparing with the constant fire scenario at the level in 1960. In the study period, the increased fires reduced vegetation, litter, and soil carbon storage by 996 Tg C, 448.3 Tg C, and 270.4 Tg C, respectively; while the more frequent fires enhanced carbon storage in woody debris pool by 417.8 Tg C. Based on these results, it is reasonable to expect that, with the advance of climate warming, increases in future fires would further the reductions in the size of terrestrial carbon

sink, alter forest composition, and cause major economic losses in lumber production as well as other human properties. Therefore, current fire management strategies need substantial adjustments to adapt to the novel fire regimes in the future.

Key words: Boreal ecosystems; terrestrial carbon budget; vegetation carbon storage; wild fire; climate change; fire emissions

1. Introduction

The dynamics of boreal ecosystems are crucial for earth system due to their tremendous organic carbon storage, and their structural and functioning sensitivity to subtle environmental changes (Chapin *et al.*, 2000, McGuire *et al.*, 2009). In the recent decades, boreal forests are significantly influenced by climate conditions and multiple anthropogenic and natural disturbances (Chen *et al.*, 2000, Kasischke *et al.*, 1995). Meanwhile, regional and global climate is affected by boreal forests according to the biophysical and biogeochemical feedbacks, such as altering land surface albedo, energy partitioning ratio, and greenhouse gases (GHG) budget (Bonan, 2008). Fire is the primary natural disturbance to renew boreal forest stands in the boreal North America (BONA) and often burn in high severity (de Groot *et al.*, 2013b, Rogers *et al.*, 2015). Although natural fires have been realized to be ecological desirable for forest sustainability (such as, create forest age structure, reduce the build-up of hazardous fuel, etc.) and allowed to burn over many landscapes by fire management agencies in the BONA (Flannigan *et al.*, 2009a), fire threatens human lives and properties in the wildland-urban interface, causes air pollution, damages domestic watersheds, and emits a sizeable amount of particles and GHG into atmosphere. Therefore, fires in the boreal ecosystems should be dealt

with caution by considering their beneficial and detrimental impacts to ecosystems, human society, and climate.

In the past several decades, fire activities in the BONA were found to present an increasing trend as a result of climate warming (Flannigan *et al.*, 2009a). Fire activities in the 1980s and the 1990s almost doubled comparing with the 1960s and the 1970s (Kasischke & Turetsky, 2006). Fire emissions substantially altered the patterns of ecosystem carbon budget across most boreal ecosystem types (Bond-Lamberty *et al.*, 2007, Mack *et al.*, 2011, Turetsky *et al.*, 2002). For example, in Alaskan forests and peatlands, it has been found that large fire emissions in the recent decades played a major role in converting these black spruce stands from carbon sink to carbon source (Turetsky *et al.*, 2011). In the long-term, ~10 - 30% of annual net primary productivity (NPP) in the upland forests lost as fire-induced carbon emissions (Harden *et al.*, 2000).

In addition to the direct pyrogenic carbon emissions, fire affects terrestrial carbon budget in the post-fire regrowth processes by reducing ecosystem productivity and modifying ecosystem respiration rate (Amiro *et al.*, 2010, Goetz *et al.*, 2012, Goulden *et al.*, 2011, Hicke *et al.*, 2003). In boreal forests, total soil respiration was found to be reduced in the early years after fire disturbances by field measurements (Amiro *et al.*, 2003). However, recent synthesis studies, such as Goulden et al., (2011) and Amiro et al., (2010), reported that stand-replacing fires caused higher heterotrophic respiration and a net ecosystem carbon loss in the early succession stage for most boreal forests. The divergences could be attributed to the differences in burn severity level and forest mortality rate in different studies. Generally, forests were carbon sources soon after stand-replacing fires, and converted to continuous carbon sink in the next few decades

(Flannigan *et al.*, 2009a). To evaluate fire impacts on terrestrial carbon budget, it is essential to consider both the direct pyrogenic carbon emissions and the changes in post-fire vegetation productivity and ecosystem respiration.

Fire in the BONA has its unique characteristics, which should be kept in mind when assessing fire impacts on ecosystems and designing forest management strategies. Firstly, fire return interval (FRI) in the boreal region is relatively long. The typical FRI in boreal forests spans from 50 to 500 years (Flannigan *et al.*, 2009a), while FRI in tundra and peatland ecosystems could be even longer (Mouillot & Field, 2005). Therefore, vegetation and fuels have sufficient time period to recover to their previous status. Secondly, fire in the BONA has higher fuel combustion rate (i.e., fire-induced carbon emissions per unit area burned) than temperate, tropical, and other boreal regions (van der Werf *et al.*, 2010b), owing to the higher fuel loading and higher burn severity. In the BONA forests, it has been identified by both satellite and field observations that high-intensity crown fires are pervasive (de Groot *et al.*, 2013a, Rogers *et al.*, 2015, Wooster & Zhang, 2004). Many tree species in the BONA (such as, black spruce and jack pine) can be classified as "Fire embracer" (Rogers *et al.*, 2015), which require severe fires to open the (semi-)serotinous cones and release seeds for regeneration. Crown fires associated with peat fires release tons of GHGs to atmosphere, and contribute to the high fuel combustion rate in the BONA.

With the advance of climate warming, future fires would be more frequent and severe in the BONA e.g., (de Groot *et al.*, 2013b, Flannigan *et al.*, 2001, Flannigan *et al.*, 2013), which would substantially modify forest composition and ecosystem carbon budget and storage. Pyrogenic carbon emissions in the BONA is projected to increase by 2.5-4.4 times by the end of

the 21st century (Balshi *et al.*, 2009b). It would be impossible for the current fire management strategies to be implemented in the future (de Groot *et al.*, 2013b). It is urgent to know how the increased fire activities will influence boreal ecosystems carbon budget and vegetation biomass. This knowledge would provide scientific background information for fire management agencies to design practical mitigation strategies to cope with future fires.

Process-based ecosystem model with fire explicitly included is an instrumental tool to examine fire emissions and fire impacts on terrestrial ecosystems (Li *et al.*, 2014a, Poulter *et al.*, 2015b, Yue *et al.*, 2015), which has been applied to study fires in the BONA (Balshi *et al.*, 2007, Chen *et al.*, 2000, Hayes *et al.*, 2011). However, previous studies put emphasis on fire-induced changes in the total ecosystem carbon budget, but neglected the changes in different components of carbon fluxes (such as, pyrogenic carbon emissions, post-fire vegetation carbon uptake, and ecosystem respiration) and various carbon pools (such as, vegetation carbon, soil carbon, and litter carbon), even though this detailed information could be particularly important to shed light on the underlying mechanisms of the responses of boreal ecosystems to fire. In this study, we attempt to bridge this knowledge gap and provide a comprehensive evaluation regarding the impacts of more frequent fires on terrestrial ecosystems in the BONA from 1960 to 2010. We select this period because it contains a sharp increases in fire activities and relatively accurate fire record. Inventory-based burned area datasets and other environmental factors were compiled together to drive a process-based ecosystem model, i.e., the Dynamic Land Ecosystem Model (DLEM). The specific objectives of this study are (1) to estimate the magnitude and changing trend of fire emissions from 1960 to 2010, (2) to quantify fire impacts on terrestrial carbon fluxes and carbon budget, and (3) to evaluate fire impacts on ecosystem carbon storage of multiple pools.

2. Methodology and data

2.1 Input data for the DLEM

This study is conducted at regional level in the BONA (Canada and Alaska) (Figure 4-1), and the simulation period is from 1948 to 2010. Input datasets are compiled at the spatial resolution of 0.25° × 0.25° to drive the DLEM, including climate conditions (average/maximum/minimum temperature, precipitation, solar radiation, and relative humidity), atmospheric CO_2 concentration, nitrogen deposition, land use and land cover change, burned area, and other static input datasets (such as, soil texture, topography, etc.).

Climate dataset was downloaded from the Terrestrial Hydrology Research Group in Princeton University (http://hydrology.princeton.edu/data.pgf.php), which blends reanalysis data (NCEP/NCAR) with observation-based dataset (Sheffield *et al.*, 2006). The land use and land cover were constructed based on multiple data sources, including Global Land Cover 2000 (GLC2000) (Bartholomé & Belward, 2005), Global Lakes and Wetlands Database (GLWD) (Lehner & Döll, 2004), and History Database of the Global Environment (HYDE) land use dataset (Klein Goldewijk *et al.*, 2011). The detailed processes to construct land use data can be referred to Liu et al., (2013). The present-day peatland distribution is identified by overlapping the wetland map from GLWD (Lehner & Döll, 2004) and the maximum peatland distribution map since the last glacial period (Yu *et al.*, 2010). Atmospheric CO_2 concentration data was downloaded from Carbon Dioxide Information Analysis Center (CDIAC, http://cdiac.ornl.gov/). Nitrogen deposition dataset was retrieved from the outputs of atmospheric chemistry transport model (http://daac.ornl.gov/CLIMATE/guides/global_N_deposition_maps.html) (Dentener *et al.*, 2006). The burned area was derived from two sources: the Canadian National Fire Database (CNFDB, http://cwfis.cfs.nrcan.gc.ca/home) (Stocks *et al.*, 2002) and the database of Fire history

in Alaska (http://afsmaps.blm.gov/). The two burned area datasets were collected from multiple fire management agencies based on aerial photography, perimeter survey, or satellite imagery (Amiro *et al.*, 2001), and digitized in Geographical Information System (GIS). The earliest fire recorded could be dated back to the early 20th century. However, it should be noted that many early fires were not preserved. Thus, our analysis focused on the period after the year of 1960.

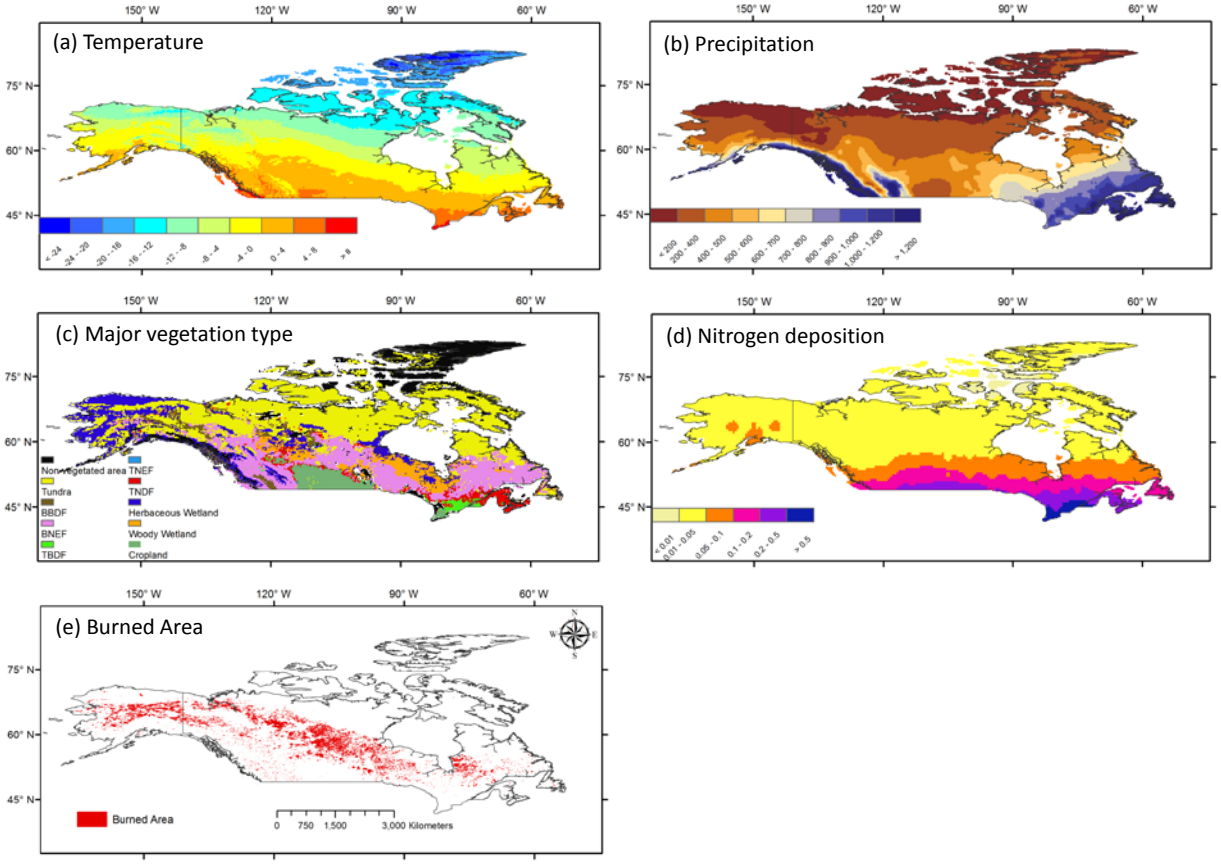

Figure 4-1. Spatial distribution of driving forces in the boreal North America. (a) Temperature (°C), (b) precipitation (mm year^{-1}), (c) major vegetation type, (d) nitrogen deposition (g N m^{-2} year^{-1}), and (e) burned area. In panel (c), BBDF refers to Boreal Broadleaf Deciduous Forest, BNEF refers to Boreal Needleleaf Evergreen Forest, TBDF refers to Temperate Broadleaf Deciduous Forest, TNEF refers to Temperate Needleleaf Evergreen Forest, and TNDF refers to Temperate Needleleaf Deciduous Forest. The temperature, precipitation, and nitrogen deposition rate are illustrated by the 51-year average during 1960-2010; major vegetation type is in the year of 2010; and burned area is represented by the fire perimeters of all the fires occurred in the 51 years.

Figure 4-2 illustrates the inter-annual variations in the input data. In the BONA from 1960 to 2010, zonal average temperature is -4.03 ± 0.71 °C (inter-annual mean ± 1 standard deviation, same hereafter), with a significant increasing trend at the rate of 0.027 °C $year^{-1}$ (Mann-Kendall trend test and Sen's slope, P-value < 0.05, same hereafter). After the year of 1997, temperature presented a declining trend, which is consistence with the recent global-warming hiatus (Kosaka & Xie, 2013). Zonal average precipitation is 532 ± 14.9 mm $year^{-1}$, with a significant increasing trend at the rate of 0.42 mm $year^{-1}$. However, precipitation decreased sharply in the last five years from 2006 to 2010. Atmospheric CO_2 concentration increased from 316.91 ppmv to 389.85 ppmv. Average atmospheric nitrogen concentration increase from 0.068 g N m^{-2} $year^{-1}$ to 0.087 g N m^{-2} $year^{-1}$. Average cropland area is 493,467 km^2. Annual burned area is 22,402.3 ± 17,950.3 km^2 $year^{-1}$, with a significant increasing trend at the rate of 377 km^2 $year^{-1}$.

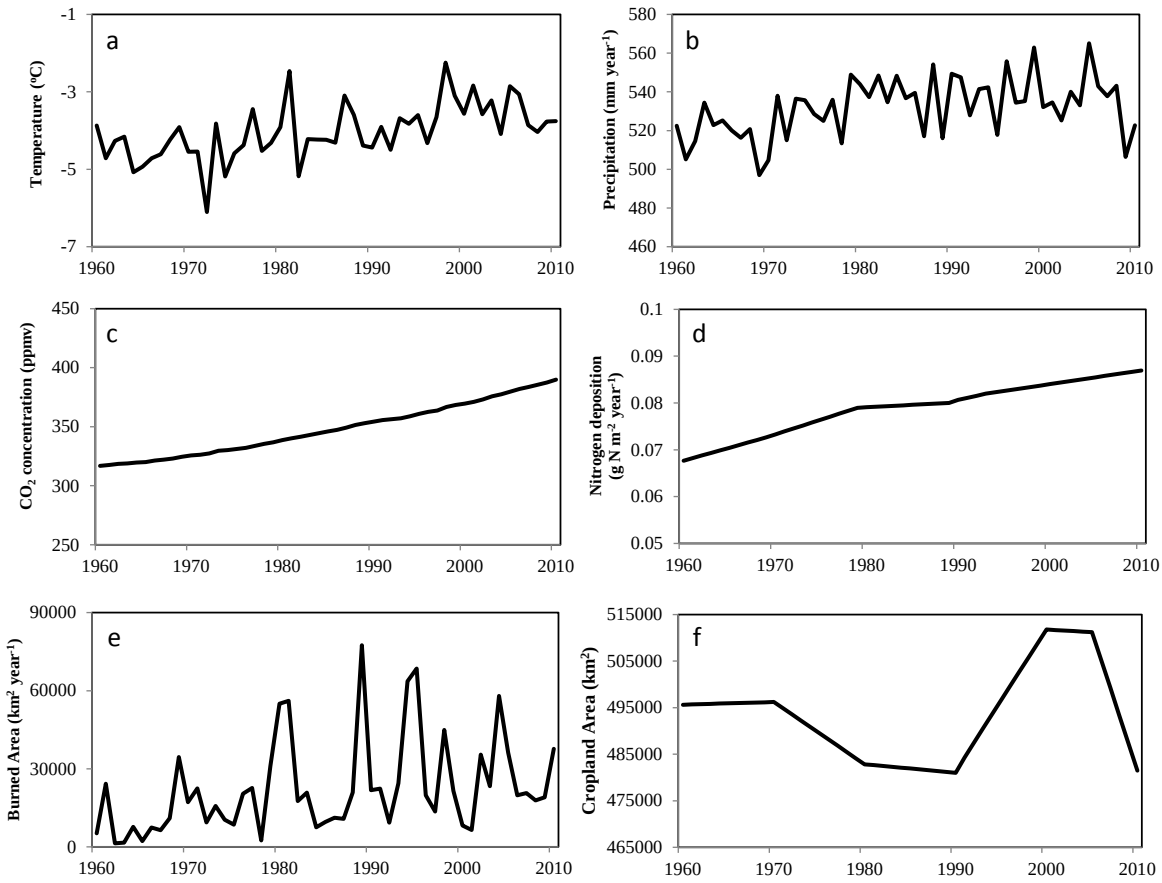

Figure 4-2. Inter-annual variations of input data to drive the DLEM in the boreal North America during 1960-2010. (a) Temperature (°C), (b) precipitation (mm $year^{-1}$), (c) atmospheric CO_2 concentration (ppmv), (d) nitrogen deposition (g N m^{-2} $year^{-1}$), (e) burned area (km^2 $year^{-1}$), and (f) cropland area (km^2).

2.2 Model implementation and experimental design

The DLEM implementation was composed of three stages, i.e., equilibrium run, spin-up, and transient run (Table 4-1). Equilibrium run aims to obtain the initial condition in the year of 1948. In this stage, the DLEM was fed with the 10-year average climate conditions during 1948-1957, and other forcing data at the level in the year of 1948. The disturbances (fire and land use change) were disregarded in this stage. For each simulation grid, equilibrium state was assumed to be reached when the carbon, nitrogen, and water storage at grid level were less than 0.1 g C m^{-2} $year^{-1}$, 0.1 g N m^{-2} $year^{-1}$, and 0.1 mm in two consecutive 50 years. Next, in the 100-year spin-

up, the DLEM was fed with detrended driving forces randomly selected during 1948-1957. In this stage, disturbances were included in the simulation. Finally, the DLEM ran in transient mode from 1948 to 2010. The simulation during 1948-1959 aims to reduce the lag effect of previous disturbances, while our analysis focused on the period of 1960-2010. For the transient run, we designed two experiments (Table 4-1) to investigate the changes in terrestrial carbon budget and contributions of fires to carbon fluxes and carbon storage in the BONA. In the "All combined" simulation, time-series of all the driving forces from 1948 to 2010 were used to drive the model. The configurations of the "All-Fire" simulation are similar to those of the "All combined" simulation except the constant burned area held at the level of 1960. The pyrogenic carbon emissions are estimated in the "All combined" simulation, and fire impacts on terrestrial carbon fluxes and carbon storage are examined by computing the differences between the "All combined" simulation and the "All-Fire" simulation.

Table 4-1. Experimental designs in this study

	Experiments	**Fire**	**Climate**	**CO_2**	**Nitrogen deposition**	**Land use/cover**	**Land management**
	Equilibrium	Excluded	10-year average	1948	1948	1948	1948
S1	All combined	1948-2010	1948-2010	1948-2010	1948-2010	1948-2010	1948-2010
S2	All-Fire	1948-1960	1948-2010	1948-2010	1948-2010	1948-2010	1948-2010

Note: "10-year average" indicates that the average climate conditions during 1948-1957 were used to drive the model; "1948" means that the data in the year 1948 was used in the simulation; "1948-2010" indicates that data in period of 1948-2010 was used in the simulation; "1948-1960" indicates that data in period of 1948-1960 was used in the simulation and the simulation after 1960 was driven by the data of 1960.

The examined terrestrial carbon fluxes as influenced by fires include gross primary productivity (GPP), terrestrial ecosystem respiration (TER), net ecosystem productivity (NEP), and net biome production (NBP). NEP is defined as the difference between GPP and TER,

$$NEP = GPP - TER$$

The size of terrestrial carbon sink is represented by NBP,

$$NBP = NEP - C_{bt} - Proddec - LUC$$

where $Proddec$ is the carbon emissions from product decay; LUC is the carbon emissions during land use change. The examined carbon storage as influenced by fires includes vegetation carbon, litter carbon, woody debris carbon, and soil carbon.

3. Results

3.1 Pyrogenic carbon emissions

During 1960-2010, pyrogenic carbon emissions in the BONA are estimated to be 50.95 ± 39.22 Tg C year^{-1}, with a significant increasing trend at the rate of 0.91 Tg C year^{-1} (Figure 4-3). Canada contributed 87.1% of the pyrogenic carbon emissions in the BONA, and Alaska contributed the left 12.9%. Pyrogenic carbon emissions presented large inter-annual variations (coefficient of variation, cv = 0.775). In the BONA, the highest burned area (77440.3 km^2 year^{-1}) and largest pyrogenic carbon emissions (157.96 Tg C year^{-1}) happened in the year of 1989, while the lowest burned area (1435.8 km^2 year^{-1}) and pyrogenic carbon emissions (3.3 Tg C year^{-1}) occurred in the year of 1962.

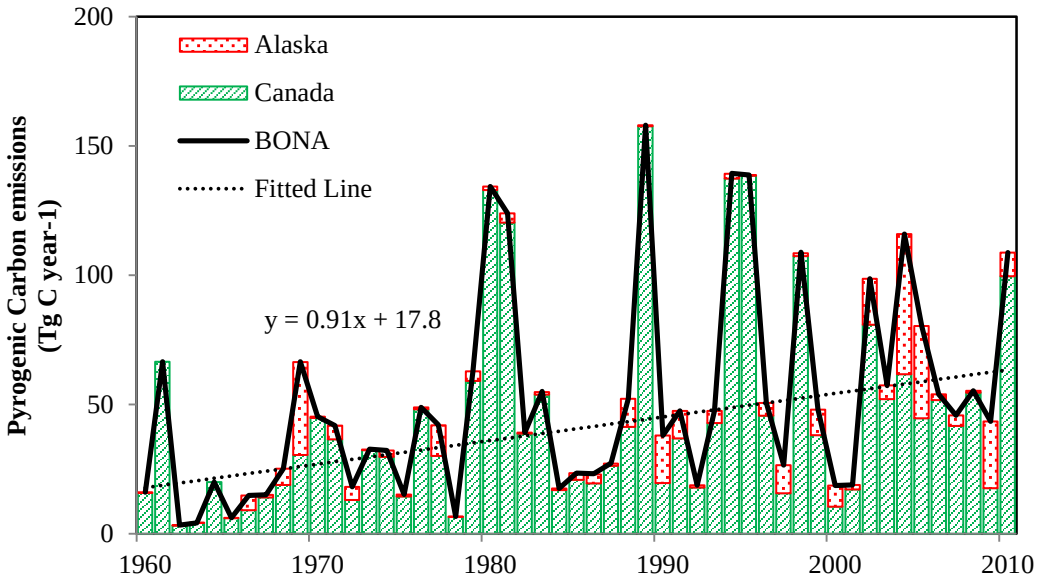

Figure 4-3. Inter-annual variations of DLEM-simulated pyrogenic carbon emissions in the BONA from 1960 to 2010.

As illustrated by Figure 4-4, in the 1960s and 1970s, pyrogenic carbon emissions in the BONA are estimated to be 23.78 Tg C year^{-1} and 34.56 Tg C year^{-1}, repectively. However, pyrogenic carbon emissions almost doubled in the following three decades (65.39 Tg C year^{-1}, 66.39 Tg C year^{-1}, and 63.37 Tg C year^{-1}). Alaska witnessed the highest pyrogenic carbon emissions in the 2000s (15 Tg C year^{-1}), which is 355.5% of the average pyrogenic carbon emissions in the first four decades and contributed 23.7% to the total pyrogenic carbon emissions in the BONA. However, in the 2000s, pyrogenic carbon emissions in Canada decreased by 19.4% comparing with those in the 1990s.

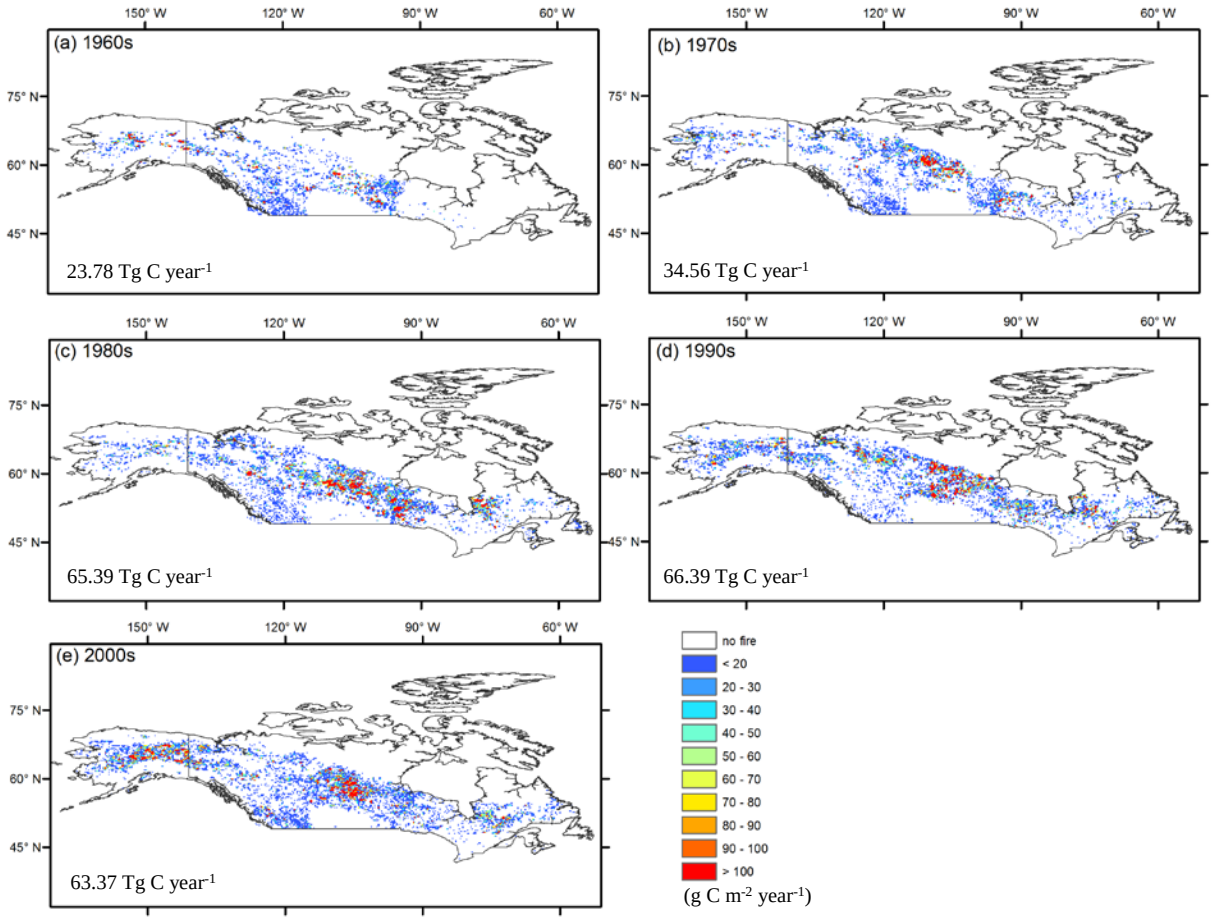

Figure 4-4. The spatial distribution of DLEM-simulated pyrogenic carbon emissions in the five decades from 1960s to 2000s.

3.2 Fire impacts on terrestrial carbon fluxes

During the 51 years in the BONA, DLEM-simulated GPP is 4897.7 ± 322.7 Tg C year^{-1}, with a significant increasing trend at the rate of 14.8 Tg C year^{-1} (Figure S4 in Appendix VI); DLEM-simulated TER is 4803.8 ± 280.16 Tg C year^{-1}, with a significant increasing trend at the rate of 13.6 Tg C year^{-1} (Figure S5 in Appendix VI); NEP is estimated to be 93.9 ± 77.1 Tg C year^{-1}. As indicated by Figure 4-5, the changes in fire activities modified the terrestrial carbon fluxes. Comparing with that in 1960, the changes in fire activities reduced GPP by 0.98 Tg C

year^{-1} in the 1960s, 3.81 Tg C year^{-1} in the 1970s, 27.95 Tg C year^{-1} in the 1980s, 39.55 Tg C year^{-1} in the 1990s, and 38.81 Tg C year^{-1} in the 2000s. The reduction in GPP is mainly caused by the fire-induced reductions in forest coverage and leaf area, which is consistence with previous satellite-based observations and field measurements (Goulden *et al.*, 2011, Hicke *et al.*, 2003). Comparing with that in 1960, the changes in fire activities reduced TER by 3.64 Tg C year^{-1} in the 1960s, 14.55 Tg C year^{-1} in the 1970s, 45.31 Tg C year^{-1} in the 1980s, 67.67 Tg C year^{-1} in the 1990s, and 71.47 Tg C year^{-1} in the 2000s (Figure 4-5). TER reduction is caused by the smaller vegetation carbon, litter carbon, and soil carbon storage induced by fires (see section 3.3 in this chapter). The reduction in ecosystem respiration simulated by the DLEM is consistence with the measurements of Amiro et al., (2003), but different to the synthesis of Goulden et al., (2011). This is because Goulden et al., (2011) mainly investigate the impacts of stand-replacing forest fires (leaving lots of standing dead boles for decomposition in the following years), while our simulation include the combined effect of all large fires in different burn severities and in various ecosystem types.

Due to the larger reduction in TER than GPP, NEP increased by 2.66 Tg C year^{-1} in the 1960s, 10.73 Tg C year^{-1} in the 1970s, 17.36 Tg C year^{-1} in the 1980s, 28.12 Tg C year^{-1} in the 1990s, and 32.65 Tg C year^{-1} in the 2000s. The increment in NEP partially offsets carbon loss during biomass burning.

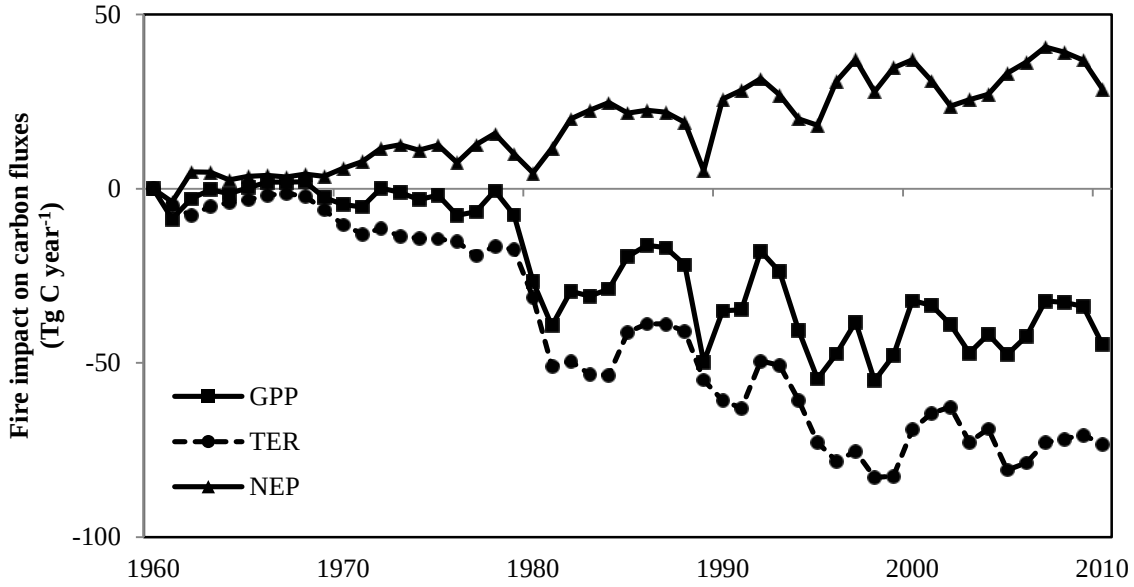

Figure 4-5. Inter-annual variations of fire-induced changes (1960-2010) in GPP, TER, and NEP in the boreal North America.

As influenced by multiple environmental factors, terrestrial ecosystems in the BONA acted as a carbon sink of 33.28 Tg C $year^{-1}$ during 1960-2010, but no significant trend was found in the inter-annual variations of NBP (Figure 4-6). In the 51 years, a total of 1697.4 Tg C was accumulated in the ecosystem. The changes in fire activities reduced the size of terrestrial carbon sink by 25.42 Tg C $year^{-1}$. Across the entire study period, the accumulated reductions in NBP caused by fires reached as high as 1296.86 Tg C. In other words, the terrestrial ecosystems would accumulate 1296.86 Tg more carbon if fire activities were kept at the level in 1960.

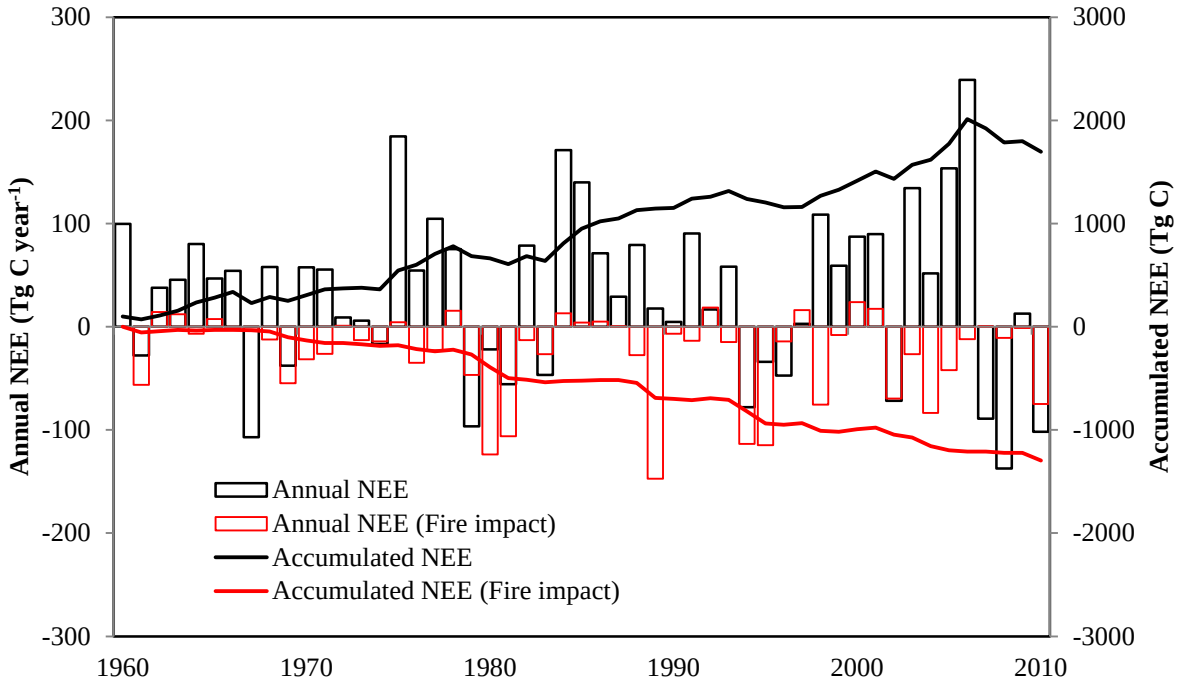

Figure 4-6. The inter-annual variations in NBP and accumulated NBP in the BONA from 1960 to 2010. The black line and histogram are the overall impacts of all the driving factors on NBP, while the red line and histogram represent the fire impacts on NBP.

3.3 Fire impacts on terrestrial carbon storage

Terrestrial organic carbon pools were modified by the changes in fire activities (Figure 4-7). Comparing with the constant fire scenario ("All-Fire" simulation), the changes in fire activities over the entire study period reduced vegetation carbon, litter carbon, and soil carbon by 996.01 Tg C, 448.28 Tg C, and 270.4 Tg C, respectively. However, carbon storage in woody debris increased by 417.83 Tg C under the impact of increased fires during the recent decades. It is worth noting that the more carbon stored in woody debris pool would be decomposed and released back to the atmosphere eventually.

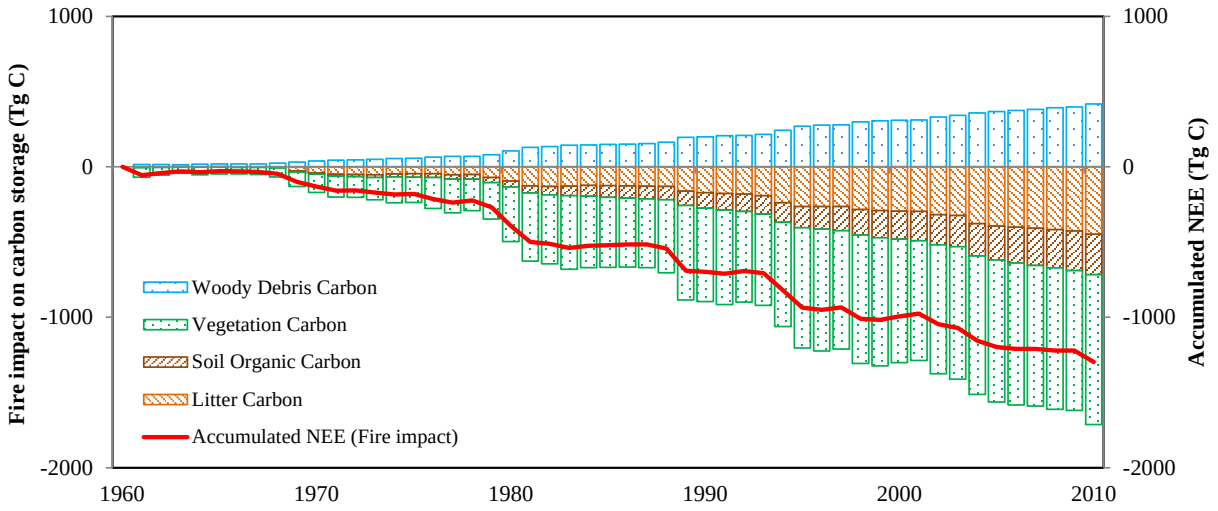

Figure 4-7. The changes in the accumulated NBP and organic carbon pools (woody debris, vegetation, soil organic carbon, and litter) under the impact of fires from 1960 to 2010.

4. Discussion

4.1 Comparison with other studies

The comparison of the DLEM-simulated pyrogenic carbon emissions with other studies indicates that our result is higher than previous estimates (Table 4-2). This is probably because of the consideration of fire emissions from peatlands and the higher combustion completeness parameters used in this study. Peatlands account for 15% to 20% of the boreal forest (Kasischke, 2000). Large amount of carbon gases can be released during peat fires (Kasischke & Bruhwiler, 2002, Turetsky *et al.*, 2011). Our study simulated peat fire emissions by coupling in-situ measurements of peatland soil carbon density and burned depth in Alaska (Turetsky *et al.*, 2011). Though the application of field measurements in Alaska to the entire BONA could introduce some uncertainties, our study is the first attempt for ecosystem model to estimate regional carbon budget by including peat fires. The larger parameters of combustion completeness used in this study also contributed to the higher pyrogenic carbon emissions. The assumption of larger

combustion completeness is based on the fact that the probability of crown fires is higher in the BONA than the other regions (de Groot *et al.*, 2013a, Rogers *et al.*, 2015).

The estimates of terrestrial carbon budget in the BONA presented large discrepancies in the previous studies (Table 4-2). The DLEM-simulated carbon sink is larger than those of Hayes et al., (2011), Gurney et al., (2004), and Baker et al., (2006), but lower than those of Balshi et al., (2007) and Peters et al., (2007). As indicated by Hayes et al., (2011), terrestrial ecosystems in the BONA trend towards net carbon release after 1986, which is similar to Kurz and Apps, 1999. However, Chen et al., (2000) and Chen et al., (2002) indicated that Canada forests still acted as net carbon sink from 1980 to 1996, even though the size of carbon sink decreased comparing to that in the previous several decades. Our simulation indicated that the BONA was a carbon sink in the first four decades of the simulation period, but converted to carbon source after 2006 (Figure 7), which is likely caused by the recent reduction in precipitation. Further investigation is in need to examine whether the recent declining in accumulated NBP will continue in the future period.

As indicated by Hayes et al., (2011) and Balshi et al., (2007), fire events reduce the size of carbon sink in the BONA. Our estimate is close to Hayes et al, (2011), but larger than Balshi et al., (2007). One improvement of our study over Hayes et al., (2011) and Balshi et al., (2007) is the investigation of fire impacts on the various components of NBP (i.e., GPP, TER, and fire emissions). Additionally, we analyzed fire-induced changes in various organic carbon pools (vegetation, litter, woody debris, and soil organic matter) at regional level, which have not been included by previous studies.

Table 4-2. Comparison of DLEM-simulated pyrogenic carbon emissions, carbon budget, and fire impacts on carbon sink with those from other studies in the boreal North America

	Data source	Study period	Literature estimates (Tg C year^{-1})	This study (Tg C year^{-1})
Pyrogenic carbon emissions	Balshi et al., (2007)	1959-2002	46.8	47.38 (average during 1960-2002)
	van der werf et al (2010)	1997-2009	54	59.37
	Hayes et al., (2011)	1997-2006	51	62.73
	French et al., (2000)	1980-1994	53	63
Carbon budget	Balshi et al., (2007)	1959-2002	81.7	33.28
	Hayes et al., (2011)	1997-2006	23.9	85.5
	Gurney et al., (2004)	1992-1996	-200	-16.82
	Baker et al., (2006)	1991-2000	-140	26.45
	Peters et al., (2007)	2000-2006	160	97.76
Fire impacts on carbon sink	Hayes et al., (2011)	1997-2006	-23.1	-25.98
	Balshi et al., (2007)	1959-2002	-15.6	-25.42 (average during 1960-2002)

Note: For the estimates in carbon budget, negative values indicate carbon source, and positive values indicate carbon sink. For fire impacts on carbon sink, negative values indicate that fires reduced the size of carbon sink.

4.2 Implications to future fires

Circumboreal fire activities were projected to increase continuously in the 21st century. Severe fire weather conditions (hot and dry) would make the large fires more difficult to be controlled, and push fire suppression capacity beyond the tipping point where even the most aggressive fire suppression activities would not be effective (de Groot *et al.*, 2013b, Flannigan *et al.*, 2009a). It is estimated that 3 - 4% of wildfires would escape regardless of large fire suppression investment. Fire suppression capacity would experience unprecedented challenges. The more frequent fires would also endanger current ecological community and forest species. In the past several decades, broadleaf deciduous trees were found to be the major post-fire tree seedling species in many Alaskan sites that were once dominated by black spruce (Adams, 2013, Barrett *et al.*, 2011, Beck *et al.*, 2011). With the increases of fires, broadleaf forest could be more prevalence, and the forest could be younger with lower fuel loading. Many unique BONA fire

characteristics (such as, long FRI and high combustion rate, as mentioned in the introduction) may not exist anymore.

Our current ability to control fire may not be effective in the coming decades (Flannigan *et al.*, 2009a). To mitigate the impacts of future fires, multiple fire-related agencies need to change their fire management policies and strategies, and more proactive forest management strategies should be implemented (de Groot *et al.*, 2013b). More fire suppression resources may need to be allocated to protect high-value areas. Fuel treatments strategies, such as prescribed fire and forest thinning, are important to manipulate future fires and mitigate fire severity (Pollet & Omi, 2002). Effective fuel treatments, which aim at removing hazardous fuel, would reduce the risk of crown fires and benefit timber production. However, this strategy should be applied with caution in forests that need severe fires for tree regeneration. For prescribed fires, appropriate plans should be designed by considering ecosystem structure, topography, and weather conditions.

4.3 Uncertainties

This study investigated the changes in terrestrial carbon budget and storage as influenced by the increased fires in the BONA by using a process-based ecosystem model. It is important to acknowledge the uncertainties in the data preparation process and model simulation stage. In this study, we used vegetation-specific parameters to calculate fire emissions, burn depth, and tree mortality across the entire region. It is difficult for this study to represent the influences of localized characteristics (such as, topography and vegetation species) on burn severity. For example, fire emissions could be underestimated in the south-facing slope and overestimated in the north-facing slope due to the local microclimate conditions and fuel moisture (Turetsky *et al.*, 2011). Recently, an empirical-based model was developed to estimate aboveground and

belowground burn severity in Alaska by considering elevation, day of burning, forest coverage, and satellite-observed fire severity index (Veraverbeke *et al.*, 2015). If all the input datasets are available in the BONA, model-simulated fire emissions estimates could be substantially improved by representing burn severity.

Secondly, uncertainties derived from model parameterization of fuel loading cannot be ignored, even though the DLEM has been evaluated in our previous studies. Fuel loading in the DLEM is simulated by a series of complex plant physiological and biogeochemical processes (such as, photosynthesis, carbon allocation, tissue turnover, and organic matter decomposition). Model parameterization of these processes contributed uncertainties in estimating fuel loading, and therefore, fuel loading and carbon budgets. Moreover, insect disturbances were not considered in this study, which has been found to affect fuel loading, fuel moisture, and burn severity in the boreal ecosystems (Chen *et al.*, 2000, Harvey *et al.*, 2014, Kurz *et al.*, 2008).

Last but not least, lag effects of disturbances contributed another important uncertainty. For example, forest regrowth in the previous disturbed land caused by fires, insects, and harvest in the late 19th century has been found to contribute to the enhancement in carbon sink during 1930-1970 (Chen *et al.*, 2000). The lag effects of previous disturbances could be as long as several decades. In this study, model simulations started at the year of 1948. Thus, lag effect of earlier disturbances was disregarded and might cause an underestimation in terrestrial carbon sink.

5. Conclusions

This study investigated increased fire activities and their impacts on terrestrial ecosystems in the BONA during 1960-2010. Significant upward trends in burned area and

pyrogenic carbon emission were found in the five decades. The increases in fires activities reduced regional GPP and TER, but enhanced the NEP. Considering both pyrogenic carbon emissions and post-fire regrowth processes, increased fires reduced terrestrial carbon sink by 25.4 Tg C $year^{-1}$ in the BONA. Meanwhile, increased fires caused decreases in vegetation, litter, and soil carbon storage, but increase in woody debris carbon storage. We acknowledge the uncertainties in this study, including the impact of lag effects of previous disturbances, insect impacts, model parameters such as burn severity, peatland burn depth etc. Nevertheless, to the best of our knowledge, it is the first time for the scientific community to evaluate the impacts of more frequent fires on the size of different components of carbon budgets and various carbon pools in the boreal North America. At last, we suggested that the current fire management strategies need substantial improvement to cope with the novel fire regimes in the future.

Chapter 5. The declining burned area and fire-induced carbon emissions in Africa

Abstract

Fire is one major disturbance in the African continent and determines vegetation composition, ecosystem carbon storage, and soil biogeochemistry characteristics. Africa has the most extensive fires in the world, including ~70% of global burned area and ~50% of global pyrogenic carbon emissions. Based on the development of satellite techniques, African fire activities have been intensively investigated during the past three decades. Spatial-temporal patterns of African fires were found to be mainly controlled by climate conditions and human activities. However, our understanding about century-scale fire regimes is still very limited due to the lack of long-term, spatially-explicit fire datasets. To bridge this knowledge gap, by using a process-based ecosystem model, we studied the spatial pattern and temporal variations of burned area and fire-induced carbon emissions from 1901 to 2010, and quantified the contributions of multiple environmental factors, including climate change, human activities, CO_2 concentration and nitrogen deposition. Our results indicated that, over the 110 years, African burned area presented a significant declining trend at the rate of -0.77 Mha $year^{-2}$ mainly caused by the intensified human activities across the African continent and climate changes in the South Hemisphere of the African continent (SHAF). Pyrogenic carbon emissions decreased at the rate of -1.6 Tg C $year^{-2}$ over the entire study period, while the decline was not significant in the last five decade. The increases in CO_2 concentration and nitrogen deposition promoted African burned area and pyrogenic carbon emissions via their influences on ecosystem carbon sequestration and fuel accumulation. In the future, human activities are expected to be more intensive and African fires will be suppressed effectively, even though the increases in CO_2

concentration and nitrogen deposition will partially offset human impacts. Future trend of fire-induced carbon emissions in Africa is subjected to uncertainties and needs further investigation.

Key words: Climate change; Wildfire; Terrestrial Ecosystem; Carbon budget; Process-based ecosystem model; Land use change; African continent

1. Introduction

Fire is one major disturbance in the earth system and almost occurred everywhere in the vegetated land across the globe (Bowman *et al.*, 2009), which has substantially altered terrestrial ecosystems, atmospheric composition, and climate conditions (Bond *et al.*, 2005b, Bowman *et al.*, 2009, Higgins *et al.*, 2007, Randerson *et al.*, 2006b, Van Der Werf *et al.*, 2004). Africa has the most extensive fires in the world. Although the African continent represents ~20% of global land area, fires in Africa accounted for ~70% of global burned area and ~50% of global pyrogenic carbon emissions (Andela & van der Werf, 2014, Giglio *et al.*, 2013b, van der Werf *et al.*, 2010b). African ecosystems have been recognized to be critical for the global carbon cycles, and are of particular vulnerable to climate change and variability (Ciais *et al.*, 2009, Pan *et al.*, 2015). Vegetation distribution, structure and functioning are determined and modified by spatial-temporal patterns of fire activities (Bond *et al.*, 2005b, Li *et al.*, 2014a). Therefore, the investigation of African burned area and fire-induced carbon emissions is of particular importance to improve our knowledge regarding global biogeochemical cycles and climate changes.

Satellite observations provided the only practical and effective approach to study the African fires and biomass burning at large scale e.g. (Barbosa *et al.*, 1999, Giglio *et al.*, 2013b,

Kaiser *et al.*, 2012b, Roy *et al.*, 2005), and have been used to disentangle the underlying mechanisms in affecting inter-annual variations of fire activities (Andela & van der Werf, 2014, Archibald *et al.*, 2009). According to satellite observations, burned area in Africa was estimated to be approximately 250 Mha $year^{-1}$ (Giglio *et al.*, 2013b, Roy *et al.*, 2008a), and fire-induced carbon emissions were estimated to be approximately 1 Pg C $year^{-1}$ in the recent decade (van der Werf *et al.*, 2010b). Over the period of 2001-2012, fire activities presented strong but opposing trends in the two African hemispheres under the impacts of climate variability and cropland expansion (Andela & van der Werf, 2014). Fires in both the North Hemisphere Africa (NHAF) and South Hemisphere Africa (SHAF) presented evident seasonality. Fire season lasts from November to February in the NHAF, and spans from June to September in SHAF (Giglio *et al.*, 2013b), which is consistent with the seasonal shift of rain belt between the two hemispheres.

Prior to the satellite era, fire records in some national parks, forest, or conservative area provided valuable information about the changes in African fire regimes (Archibald *et al.*, 2010). However, these records cannot represent the entire African continent because these lands were often intensively managed by human (Roy *et al.*, 2005). Sediment-charcoal records have been used to reconstruct fire history at regional and global levels (Bowman *et al.*, 2009). The compilation of charcoal records indicated a strong correlation between fires and climate changes (Power *et al.*, 2008), and suggested the reductions in global biomass burning after the 1870s under the impact of human activities (Marlon *et al.*, 2008b). However, it is difficult to extract the accurate time of fire occurrence and retrieve the spatial map of fires. Our knowledge about the changes in fire regimes prior to satellite era is still very limited in this most fire-abundant continent. Process-based fire models have been developed and applied to estimate burned area and fire emissions by explicitly considering environmental factors at regional and global scales

e.g. (Arora & Boer, 2005, Li *et al.*, 2012, Pechony & Shindell, 2009, Thonicke *et al.*, 2010, Yang *et al.*, 2014a). Provided that driving forces (such as, climate, cropland area, etc.) are available, fire models could be applied to study the spatially-explicit burned area and fire emissions with high temporal resolution prior to satellite era in Africa.

The African fires were controlled by multiple environmental factors, such as climate/weather condition, fuel loading, vegetation type, human activities, and cropland expansion (Archibald *et al.*, 2009). In the tropics and subtropics, the highest burned area was found in the regions with intermediate levels of fuel loading and precipitation (van der Werf *et al.*, 2008b). Fire activities in the wetter ecosystems could be enhanced by lower precipitation and longer fire season, while fire activities in the drier ecosystems could be enhanced by higher precipitation and faster fuel accumulation in the vegetation growing season. Human activities, on the one hand, could increase ignitions sources through camping, logging, arson, etc., while one the other hand, suppress fire spread by breaking fuel connectivity through cropland expansion, grazing, and road buildup (Marlon *et al.*, 2008b). However, the influences of CO_2 concentration and nitrogen deposition on fire activities are rarely investigated by previous studies, although both of them have been reported to stimulate vegetation growth and fuel accumulation (Yang *et al.*, 2014a). In the natural world, influences of these environmental factors were usually mixed together and modified fire regimes simultaneously.

In the past 50-100 years, the African continent has experienced dramatic changes in climate condition (Hulme *et al.*, 2001), atmospheric components (Dentener *et al.*, 2006), land use and land cover type (Lambin *et al.*, 2003), and population density (Ciais *et al.*, 2011). Yet, it is not clear how the long-term burned area and fire emissions in Africa changed in response to the

changes in environmental factors, and how much these multiple environmental factors contributed to African fires. The investigation into underlying mechanisms controlling the changes in African fires would provide useful knowledge for fire management practices (Archibald *et al.*, 2010), and provide insight into fire regimes in the future.

Based on the above considerations, we investigated African fires from 1901 to 2010 by using a highly-integrated, process-based terrestrial ecosystem model. Specific objectives of this study are (1) to estimate the changes in spatial-temporal patterns of burned area and pyrogenic carbon emissions, (2) to investigate underlying mechanisms and quantify contributions of climate change, human activities, and CO_2 concentration and nitrogen deposition, and (3) to discuss the possible trends of African fires in the future.

2. Methods and input data

2.1 Input data

In this study, the DLEM was run at daily time step from 1901 to 2010. Driving forces collected from various sources were compiled at the spatial resolution of 0.5° × 0.5° to drive the model, including daily climate condition (maxmum/minimum/average temperature, precipitation, solar radiation, relative humidity, wind speed, and lightning frequency), CO_2 concentration, atmospheric nitrogen deposition, land use and land cover change, human population density, and other time-invariant variables (such as, soil texture, topography, etc.). Climate conditions (except lightning frequency) were obtained from the CRU/NCEP climate dataset (https://www.earthsystemgrid.org/dataset/ucar.cgd.ccsm4.CRUNCEP.v4.TPHWL6Hrly.html). Lightning frequency is the multi-year climatology (1995-2011) of the NASA Lightning Imaging Sensor/Optical Transient Detector (Christian *et al.*, 2003), which was downloaded from

ftp://ghrc.nsstc.nasa.gov/pub/lis/climatology/HRAC/. Lightning climatology was applied to each year due to the lack of long-term observations. CO_2 concentration was downloaded from the Carbon Dioxide Information Analysis Center (http://cdiac.ornl.gov/trends/co2/). Nitrogen deposition rates were acquired from the output of atmospheric chemical transport models (Dentener *et al.*, 2006) and interpolated to annual scale. Land use change and human population density were obtained from the History Database of the Global Environment (HYDE3.1, ftp://ftp.pbl.nl/hyde/) (Klein Goldewijk *et al.*, 2011).

Spatial distribution and temporal variations of major driving forces are illustrated in Figure 5-1. As indicated by the input datasets, temperature in Africa was 24.1 ± 0.35 °C in the 110 years. In the last four decades over the study period, African temperature presented a significant increasing trend at the rate of 0.31 °C dec^{-1} (p-value < 0.05, same hereafter), and warming trend in the NHAF (0.31 °C dec^{-1}) was stronger than that in the SHAF (0.24 °C dec^{-1}). During 1901-2010, precipitation rate in Africa was 639.3 ± 31.6 mm $year^{-1}$ with no significant trend detected. Nitrogen deposition rates were 0.22 ± 0.09 g N m^{-2} $year^{-1}$, with a continuous increasing trend from 0.12 g N m^{-2} $year^{-1}$ in 1901 to 0.44 g N m^{-2} $year^{-1}$ in 2010. CO_2 concentration increased from 295 ppmv in 1901 to 387.2 ppmv in 2010. From the early 20th century to the 2000s, cropland area increased from 1.11×10^6 km^2 to 2.31×10^6 km^2 in the Africa continent, increased from 0.83×10^6 km^2 to 1.61×10^6 km^2 in the NHAF, and increased from 0.28×10^6 km^2 to 0.7×10^6 km^2 in the SHAF. During the 110 years, African population grew from 0.14 billion to 1 billion, with an accelerated growing rate in the recent decades; population in the NHAF increased from 0.1 billion to 0.7 billion; and population in the SHAF increased from 0.03 to 0.3 billion.

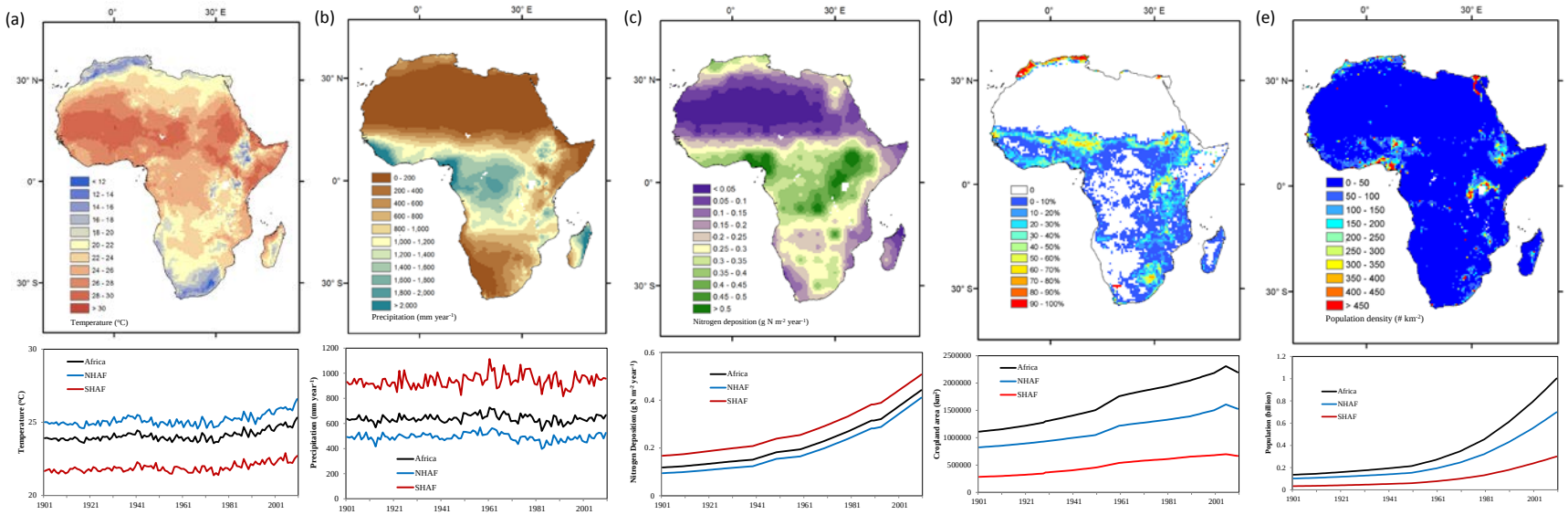

Figure 5-1. Spatial-temporal patterns of major driving forces in Africa. (a) Temperature, (b) precipitation, (c) atmospheric nitrogen deposition, (d) cropland area, and (e) population density. The maps of temperature, precipitation, nitrogen deposition are illustrated by 110-year average, while the maps of cropland area and population density are at the levels in 2010.

2.2 Model implementation and experimental design

DLEM implementation was composed of three stages, namely equilibrium run, spin-up, and transient run (Table 5-1). Equilibrium run aimed at obtaining the initial carbon/nitrogen/water conditions at the beginning of model simulation. During this stage, the DLEM was driven by the average climate condition over 1901-1930, and other driving forces at the level in 1901. For each model grid, equilibrium state was assumed to be reached when the differences in carbon, nitrogen, and water storage were less than 0.1 g C m^{-2}, 0.1 g N m^{-2}, and 0.1 mm between two consecutive 50-year periods. Equilibrium run was followed by the 100-year model spin-up. In model spin-up, driving forces were randomly selected from the period of 1901-1910.

Table 5-1. Experimental design in this study

		Climate	CO_2	Nitrogen deposition	Land use and population
Equilibrium run		1901-1930 average	1901	1901	1901
Spin-up		1901-1910 random	1901-1910 random	1901-1910 random	1901-1910 random
Transient run	**S0 Reference**	1901	1901	1901	1901
	S1 All_Com	1901-2010	1901-2010	1901-2010	1901-2010
	S2 No_Clm	1901	1901-2010	1901-2010	1901-2010
	S3 No_CO_2	1901-2010	1901	1901-2010	1901-2010
	S4 No_Ndep	1901-2010	1901-2010	1901	1901-2010
	S5 No_Hum	1901-2010	1901-2010	1901-2010	1901

Note: "1901-1930 average" refers to the 30-year average condition; "1901-1910 random" refers to the driving force randomly selected during 1901-1910; "1901" refers to the data at the level of year 1901; "1901-2010" refers to the time-series of datasets from 1901 to 2010.

At last, the DLEM was run in transient mode (including six simulations) to investigate African burned area and pyrogenic carbon emissions from 1901 to 2010, and the contributions of various factors. "S0 Reference" simulation intended to examine model internal fluctuations by keeping all the driving forces constant at the level of 1901.

The “S1 All_Com” simulation considered the combined effect of all driving forces, and represented our best estimates of the spatial pattern and temporal changes in burned area and pyrogenic carbon emissions. For the other four simulations (“S2 No_Clm”, “S3 No_CO_2”, “S4 No_Ndep”, and “S5 No_Hum”), all the driving forces varied with time throughout simulation period, expect the designated one environmental factor kept constant at the level of 1901 (Table 5-1). Specifically, climate condition was kept constant in the “S2 No_Clm” simulation; CO_2 concentration was kept constant in the “S3 No_CO_2” simulation; nitrogen deposition rates were kept constant in the “S4 No_Ndep” simulation; and human activities (i.e. land use change and population density) were kept constant in the “S5 No_Hum” simulation. Contributions of climate change, CO_2, nitrogen deposition, and human activities to burned area and pyrogenic carbon emissions were examined according to the differences between the “S1 All_com” simulation and each of the four simulations, respectively. Combined impacts of all the driving forces were examined by computing the differences between “S1 All_com” simulation and “S0 Reference” simulation.

In this study, changing trends in burned area, pyrogenic carbon emissions, and the impacts of contributing factors were estimated according to Linear Least-square Regression analysis. The trends were assumed to pass the significance test if p-value < 0.05.

3. Results

3.1 Burned area in Africa

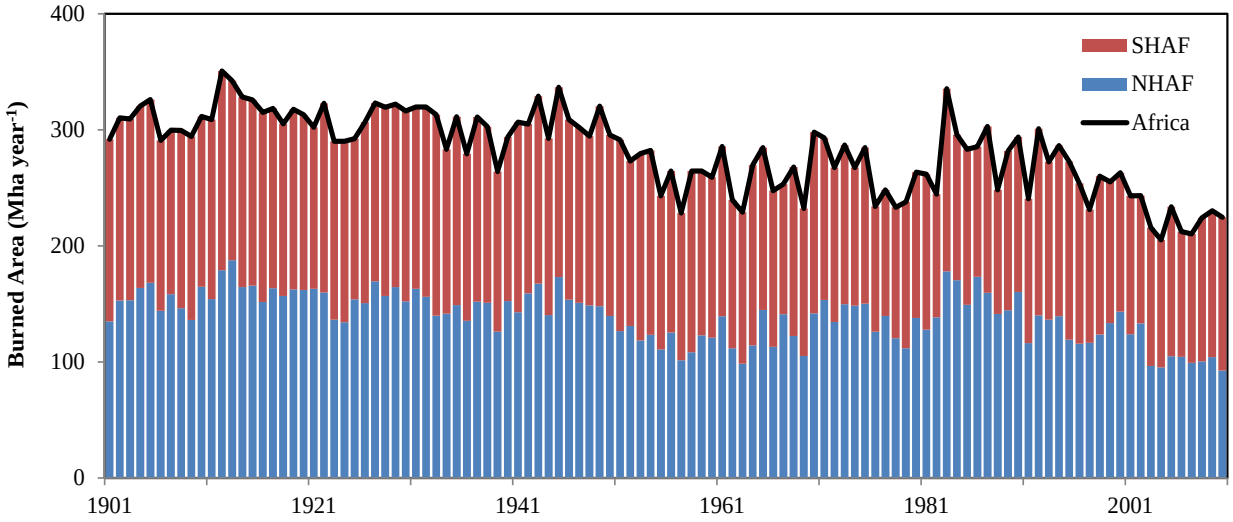

Figure 5-2. Inter-annual variations of burned area in the Africa over the period of 1901-2010.

In the 110 years, DLEM-simulated African burned area was 282.2 ± 33.4 Mha year^{-1}, with a significant declining trend of -0.77 Mha year^{-2} (Figure 5-2). Average burned areas in the NHAF and SHAF were 139.8 Mha year^{-1} and 142.4 Mha year^{-1}, respectively. Temporal variations of burned areas in both hemispheres presented significant declining trends (-0.39 Mha year^{-2} in the NHAF and -0.39 Mha year^{-2} in the SHAF). Comparing with those in the 1900s, burned areas in the 2000s decreased by 25.6%, 30.7%, and 22.4% in the African continent, NHAF, and SHAF, respectively (Table 5-2). Two peaks of burned area existed along latitudinal gradient (Figure 5-3a). One was located at between 5 °N to 15 °N, while the other one was located at between 5 °S to 20 °S. For the grids fire occurred, 43.2% presented significant declining trend,

17.9 % presented significant increase trend, and 38.9% did not present significant trend

(Figure 5-3b).

Table 5-2. Statistics of burned area and pyrogenic carbon emissions in the 1900s, 1950s and 2000s. The percentages in the parenthesis are the changes comparing with those in the 1900s.

	Burned Area (Mha year^{-1})			Pyrogenic carbon emissions (Pg C year^{-1})		
	Africa	NHAF	SHAF	Africa	NHAF	SHAF
1900s	305.5	152.3	153.2	1.05	0.36	0.68
1950s	265.1 (-13.2%)	118.9 (-21.9%)	146.1 (-4.6%)	0.84 (-20%)	0.28 (-22.2%)	0.56 (-17.6%)
2000s	224.3 (-26.6%)	105.5 (-30.7%)	118.9 (-22.4%)	0.84 (-20%)	0.29 (-19.4%)	0.54 (-20.6%)

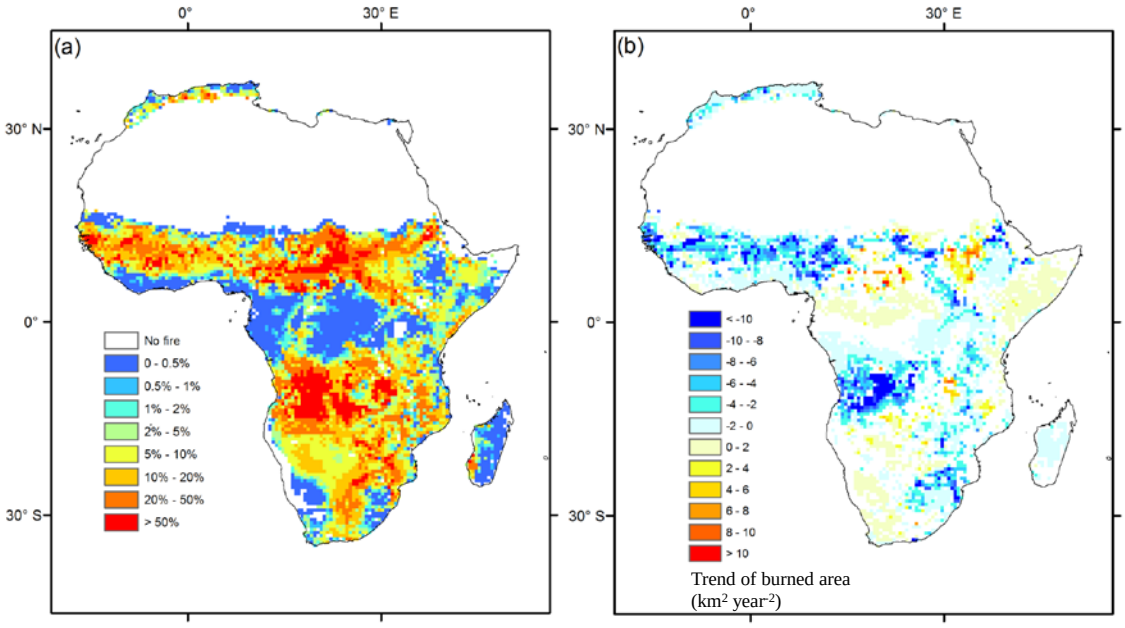

Figure 5-3. (a) DLEM-simulated spatial distribution of average burned fraction and (b) the changing trend of burned area over the period of 1901-2010. In (b), grids without significant trend are masked white.

3.2 Contributions of environmental factors to burned area

Inter-annual variations of burned area were influenced by multiple environmental factors (Figure 5-4). With the increases in population density and cropland expansion, human activities took continuous negative effects on burned area. The increases in CO_2 concentration and nitrogen deposition rates mainly played positive roles in burned area. African burned area decreased at the rate of -0.58 Mha $year^{-2}$ under the single impact of human activities, while increased at the rates of 0.09 Mha $year^{-2}$ and 0.09 Mha $year^{-2}$ under the impacts of CO_2 concentration and nitrogen deposition, respectively. Comparing with that in year 1901, burned area in the 2000s was reduced by 55.3 Mha $year^{-1}$ under the impacts of human activities, and increased by 7.9 Mha $year^{-1}$ and 7.4 Mha $year^{-1}$ due to the increases in CO_2 concentration and nitrogen deposition. Contributions of human activities were much stronger in the NHAF than those in the SHAF, due to the higher population density and faster cropland expansion in the NHAF. Contributions of climate conditions varied substantially among different decades, with a general declining trend at the rate of -0.38 Mha $year^{-2}$. Over the study period, the declining trend of burned area in the NHAF was mainly induced by human activities, while the declining trend in the SHAF was mainly caused by the changes in climate conditions.

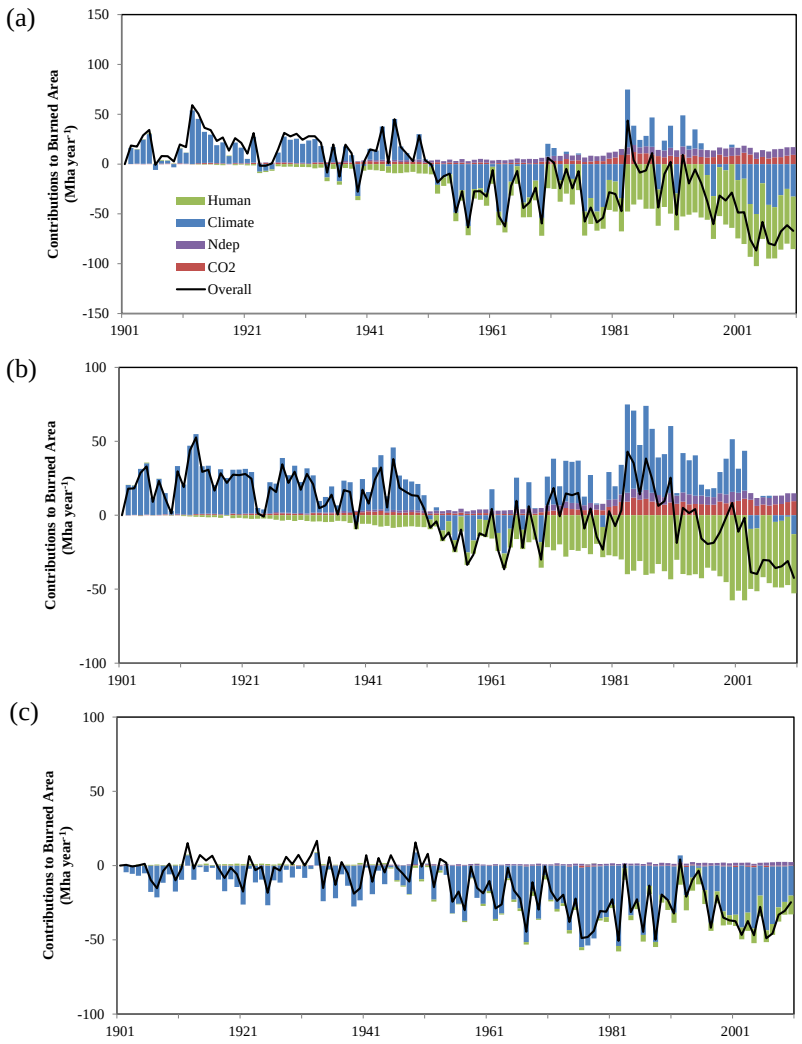

Figure 5-4. Contributions of human activities, climate changes, nitrogen deposition, CO_2 concentration, and the combined impact of multiple environmental factors to changes in burned area in the Africa (a), NHAF (b), and SHAF (c).

Figure S6 in Appendix V illustrates spatial patterns of the trends in burned area induced by the impact of single environmental factor. It can be found that human activities played a negative role across most of the African continent, due to cropland expansion and intensified human activities. However, human activities enhanced burned area in some regions, which was likely caused by the increases in anthropogenic ignition

sources. Climate changes reduced burned area in most of the Africa, but slightly enhanced burned area in the rainforest region in the central Africa. The impacts of CO_2 diverged between regions with higher fuel loading and regions with lower fuel loading, suggesting the duel effects of CO_2 increment on African burned area. In regions with lower fuel loading, the increment in CO_2 concentration enhanced carbon sequestration, fuel loading, and then burned area, while in regions with higher fuel loading, the increment in CO_2 concentration reduced stomatal conductance, suppressed plant transpiration, enhanced soil and fuel moisture content, and then reduced burned area. Increases in nitrogen deposition mainly played positive roles in enhancing burned area across the Africa continent through stimulating fuel accumulation.

3.3 Pyrogenic carbon emissions in Africa

From 1901 to 2010, pyrogenic carbon emissions in Africa were estimated to be 0.93 ± 0.11 Pg C year^{-1} with a significant declining trend of -1.6 Tg C year^{-2} (Figure 5-5). However, the declining trends were not significant in both NHAF and SHAF. African pyrogenic carbon emissions deceased significantly at the rate of -3.9 Tg C year^{-2} in the first 60 years from 1901 to 1960, but no significant trend was detected during 1961-2010. Comparing with those in the 1900s, fire-induced carbon emissions in the 2000s decreased by 20% in the African continent (Table 5-2). Yet, fire-induced carbon emissions in the 2000s were similar to those in the 1950s. For all the grids fire occurred, 32.9% presented significant declining trend, 26.2% presented significant increase trend, while 40.9% did not show significant trend (Figure 5-6b).

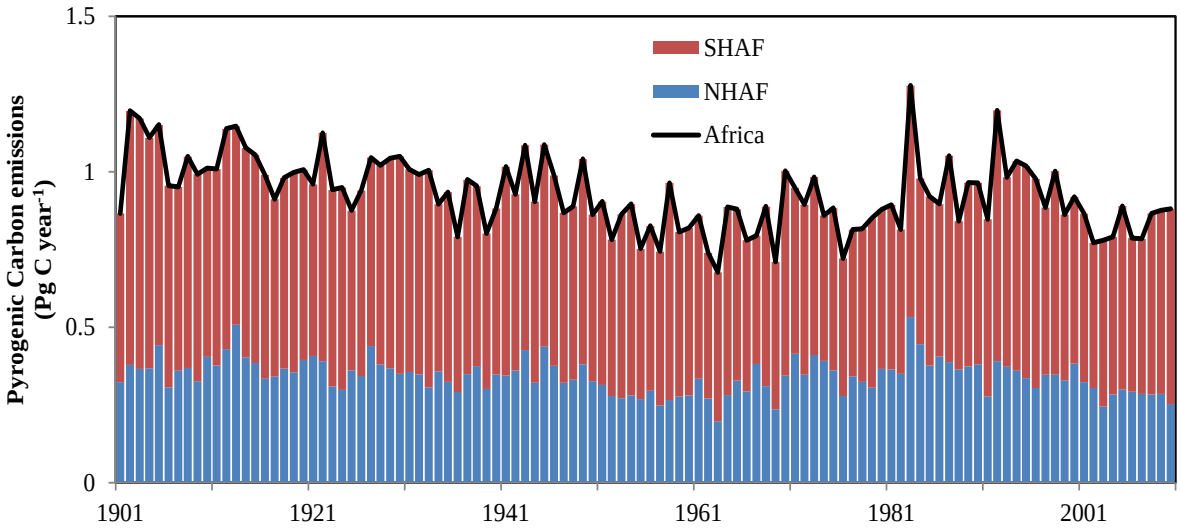

Figure 5-5. Inter-annual variations of DLEM-simulated pyrogenic carbon emissions in the Africa during 1901 to 2010.

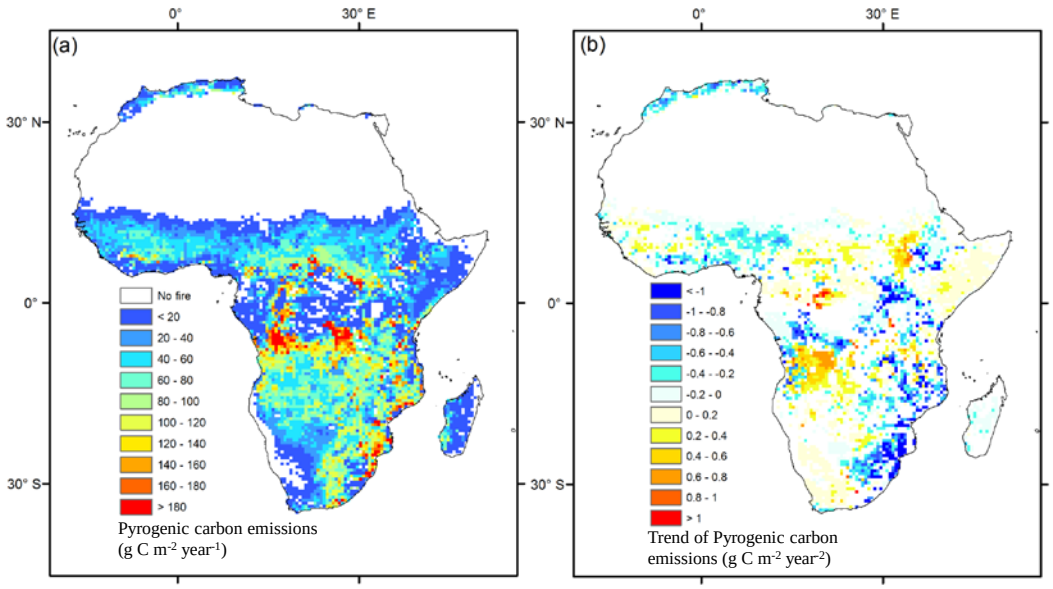

Figure 5-6. DLEM-simulated spatial distribution of pyrogenic carbon emissions (a) and the changing trend of pyrogenic carbon emissions (b) over the period of 1901-2010. In (b), grids without significant trend are masked white.

3.4 Contributions of environmental factors to pyrogenic carbon emissions

Figure 5-7 illustrates the contributions of environmental factors on pyrogenic carbon emissions. Comparing with 1901, African pyrogenic carbon emissions in the 2000s were reduced by 0.18 Pg C $year^{-1}$ under the influences of human activities, but enhanced by 0.08 Pg C $year^{-1}$ and 0.09 Pg C $year^{-1}$ under the impacts of increases in CO_2 concentration and nitrogen deposition, respectively. Contributions of climate changes varied substantially among decades. The trend of climate impacts on pyrogenic carbon emissions in Africa was not significant over the entire study period, although climate changes significantly reduced burned area (see section 3.2 in this chapter). In the last five decades, pyrogenic carbon emissions did not show significant trend. This is because the declining trend induced by human activities was largely offset by the influences of CO_2 concentration and nitrogen deposition.

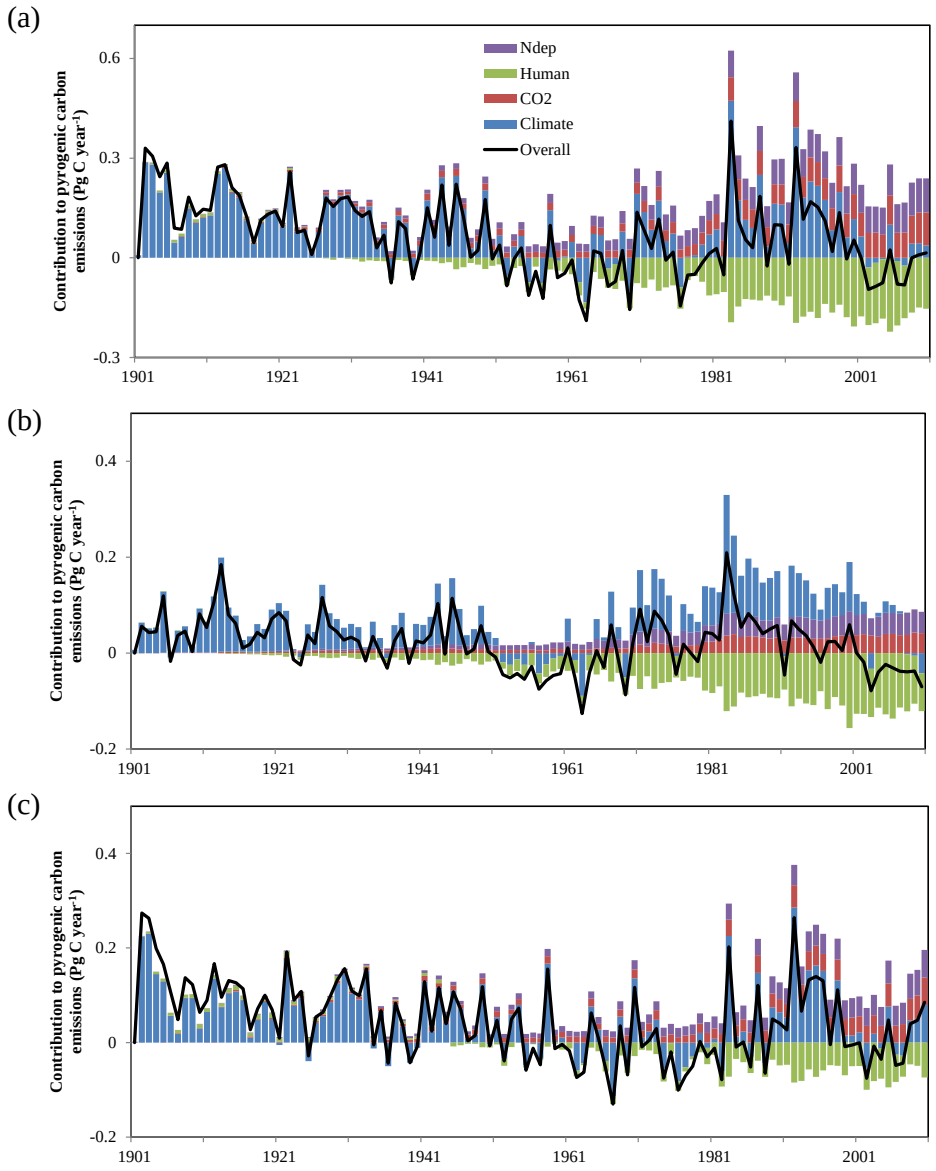

Figure 5-7. Contributions of human activities, climate changes, nitrogen deposition, CO_2 concentration, and the combined impact of multiple environmental factors to the changes in pyrogenic carbon emissions in the Africa (a), NHAF (b), and SHAF (C).

Spatial patterns of the changing trends caused by single factor are illustrated in Figure S7 in Appendix V. Human activities reduced pyrogenic carbon emissions in most of the African continent. The impacts of climate changes on pyrogenic carbon emissions

were very heterogeneous across the African continent, indicating the complex relationship between climate change and pyrogenic carbon emissions in Africa. Nitrogen deposition enhanced pyrogenic carbon emissions by stimulate fuel accumulation, and contributions of nitrogen deposition were relatively homogeneous across the Africa. The increases in CO_2 concentration stimulated pyrogenic carbon emissions in most of the continent, except tropical rainforest in the central Africa.

4. Discussions

4.1 Future implications

The DLEM simulation indicated that African burned area and fire-induced carbon emissions were reduced by human activities in the past century. According to previous findings that forest coverage and vegetation biomass were negatively correlated to burned area (Poulter *et al.*, 2015a), it can be expected that forest coverage have been enhanced by the reductions in burned area induced by human activities. As projected by the World Population Prospects (United Nations, 2013), Africa population would grow by 1.3 billion during 2013-2050, and grow by 1.8 billion from 2050 to 2010. The trends of expansions in cropland and pasture land will continue in order the meet the growing food demand in Africa (Alexandratos & Bruinsma, 2012). Therefore, more reductions in fire activities would be induced by the more intensive human activities in the 21st century. Current savannas ecosystems would be fundamentally altered, including vegetation composition, terrestrial carbon storage, and carbon exchange between land and atmosphere. Social-economic factors would dominant the trends in African fires in the future (Andela & van der Werf, 2014).

In this study, CO_2 concentration and nitrogen deposition have been found to stimulate fuel accumulation, burned area and pyrogenic carbon emissions, which have largely offset the reductions caused by human activities. It is necessary for ecosystem models to consider the impacts of changes in atmospheric composition when assessing the long-term trends of fire activities. According to the projections of atmospheric chemistry transport models, nitrogen deposition rates and CO_2 concentration are likely to increase in the future (Dentener *et al.*, 2006, Lamarque *et al.*, 2013a). More works are still in need to investigate the contributions of future changes in atmospheric composition to fire activities under different Representative Concentration Pathways (Van Vuuren *et al.*, 2011).

Fires determines African vegetation composition (Bond *et al.*, 2003). Savanna ecosystems are structurally responsive to fire disturbances (Higgins *et al.*, 2007). Numerical experiments of ecosystem model indicated that many savannas would convert to forest, and the area of closed forest could double in a world without fires (Bond *et al.*, 2005b). Meanwhile, terrestrial carbon balance could be altered substantially by fires (Li *et al.*, 2014a). Yang et al., (2015a) indicated that net primary productivity in African terrestrial ecosystems could increase by 2.59 Pg C $year^{-1}$ and the size of net carbon sink could increase by 0.17 Pg C $year^{-1}$ once African fires were put off. Therefore, changing trends in fire regimes under the impacts of multiple environmental factors should be carefully accounted when assessing the terrestrial carbon budget in future period.

4.2 Uncertainties and improvement needs

In this study, we estimated the long-term changes in African fires by using a process-based ecosystem model. Although model performance was validated against

satellite-based fire products, uncertainties from input datasets and model parameterizations should be kept in mind. Due to the relatively short observations of lightning frequency, we applied the climatology of lightning frequency to each year across the study period. This might introduce uncertainties in estimating natural ignition sources. Nitrogen deposition rates were obtained from the output of atmospheric chemical transport models due to the lack of in-situ measurements in Africa. Parameterizations of anthropogenic ignition sources and human suppression strength were developed based on the relationship between fire and population density according to satellite observations in the recent decades (Archibald *et al.*, 2009, Pechony & Shindell, 2009). Application of this human-fire relationship to historical period might bring uncertainties in estimating human impacts. Comparison of DLEM simulations against GFED3.1 fire products indicated an underestimation of DLEM-simulated pyrogenic carbon emissions in the NHAF. This underestimation was likely caused by the slow post-fire plant regrowth and lower fuel loading simulated by the DLEM. Thus, parameters regarding post-fire regrowth need to be refined. Another uncertainty was from the parameterizations of burn severity, which was estimated by using vegetation-specific parameters in this study. Thus, spatial and temporal variations in combustion completeness were largely neglected. Recently, satellite-based burn severity has been coupled into ecosystem model to estimate fire emissions and forest mortality in the United States (Yang *et al.*, 2015). At global scale, spatially-explicit burned severity dataset has been developed according to satellite observations as well (Veraverbeke *et al.*, 2011a). If compared well with ground-based measurements in Africa, burn severity

information derived from satellite observations could be coupled into ecosystem model to improve model accuracy in estimating fire emissions.

5. Conclusion

In this study, we investigated the spatial-temporal patterns of burned area and pyrogenic carbon emissions in the African continent from 1901 to 2010. Both burned area and pyrogenic carbon emissions presented significant declining trends over the study period. The intensified human activities were recognized as the major factor in determining the declines in fire activities and fire emissions, especially in the NHAF. The changes in CO_2 concentration and nitrogen deposition enhanced African burned area and pyrogenic carbon emissions. Climate changes reduced burned area in the SHAF significantly, meanwhile controlled the inter-annual and inter-decadal variations in fire activities. We acknowledge the existing uncertainties regarding input dataset and model parameterizations. Nevertheless, this study is the first attempt for ecosystem model to quantify the contributions of multiple environmental factors to the changes in African burned area and fire emissions at century scale. The declining trend in African burned area is likely to continue in the 21st century under the impacts of more intensive human activities. However, future trend in fire-induced carbon emissions and fire impacts on the terrestrial carbon budget need further investigation by considering the combined impacts of human activities, atmospheric composition and climate changes.

Chapter 6. Spatial and temporal patterns of global burned area in response to anthropogenic and environmental factors

Abstract

Fire is a critical component of the earth system, which substantially influences land surface, climate change, and ecosystem dynamics. To accurately predict the fire regimes in the 21st century, it is essential to understand the historical fire patterns and recognize the interaction among fire, human and environment factors. Until now, few efforts are put on the studies regarding to the long-term fire reconstruction and the attribution analysis of anthropogenic and environmental factors to fire regimes at global scale. To fill this knowledge gap, we developed a 0.5° × 0.5° data set of global burned area from 1901 to 2007 by coupling Global Fire Emission Database version 3 (GFED3) with a process-based fire model, and conducted factorial simulation experiments to evaluate the impacts of human, climate, and atmospheric components. The average global burned area is ~442×10^4 km^2 $year^{-1}$ during 1901-2007 and our results suggest a notable declining rate of burned area globally (1.28×10^4 km^2 $year^{-1}$). Burned area in tropics and extratropics exhibited a significant declining trend, with no significant trend detected at high latitudes. Factorial experiments indicated that human activities were the dominant factor in determining the declining trend of burned area in tropics and extratropics, and climate variation was the primary factor controlling the decadal variation of burned area at high latitudes. Elevated CO_2 and nitrogen deposition enhanced burned area in tropics and southern extratropics, but suppressed fire occurrence at high latitudes. Rising temperature and frequent droughts are becoming increasingly important and expected to increase wildfire activity in many regions of the world, particularly in extratropics.

Key words: Burned area; Dynamic Land Ecosystem Model (DLEM); Fire model; Climate change; Fire emissions

1. Introduction

Fire plays a critical role in shaping biosphere and atmospheric patterns. Fire regimes are largely regulated by climate (Morton *et al.*, 2013) and human activities (Marlon *et al.*, 2008b); meanwhile burning of biomass can speed up climate change through altering atmospheric radiative characteristics and land surface albedo (Andreae & Merlet, 2001, Langmann *et al.*, 2009, Levine *et al.*, 1995, Liu *et al.*, 2013b, Randerson *et al.*, 2006b). In the future, the global fire regimes may be quite different from the present pattern due to rapid climate change (Bowman *et al.*, 2009), and anthropogenic effects on fire might become less important than climatic influences (Pechony & Shindell, 2010). A better understanding of the interaction among fire, climate and human activities is helpful to enhance our capability of predicting future fire pattern and provide scientific information for fire management policy in the 21st century.

To date, a variety of methods have been used to retrieve fire history at local and regional scales, including charcoal records of biomass burning (Marlon *et al.*, 2008b), tree fire scars (Wallenius *et al.*, 2004), official fire records (Stocks *et al.*, 2002) and satellite observations (Eidenshink *et al.*, 2007a). At the global scale, gridded burned area has also been estimated through methods grouped into three categories: satellite observation, fire modeling, and hybrid approach. Since the early 1980s, satellite imagery has been widely used to retrieve global fire pattern (Bowman *et al.*, 2009). Numerous

satellite-based global fire products have become available in recent decade, including Global Burnt Area 2000 (GBA2000) (Grégoire *et al.*, 2003), L3JRC (Tansey *et al.*, 2008b), Global Fire Emission Database version 3 (GFED3) (Giglio *et al.*, 2010a) and so on. GFED has the longest global fire observation, spanning 15 years from 1997 to 2012, and was verified by ground fire record in various regions (Giglio *et al.*, 2010a, Giglio *et al.*, 2013b). However, studies of global fire patterns prior to the 1980s are lacking.

Mouillot and Field (2005) developed a global burned area dataset for the 20th century through a hybrid approach by incorporating satellite information, official fire records, and some fire trend assumptions. Their estimated global burned area was larger than satellite observations. For example, their estimated global burned area was 722×10^4 km^2 in 1999, while the GFED3 observed 339×10^4 km^2. Current studies regarding long-term spatial-explicit global fire history have shortcomings which hinder their application to studying fire-climate-human interactions. First, there is considerable disagreement in estimated global burned area with satellite observations in terms of temporal variation and spatial distribution; second, the effects of anthropogenic and environmental factors on fire patterns are difficult to interpret; third, temporal resolutions are relatively low, which is insufficient to study the seasonality of fire activity and emissions. Therefore, an urgent need is to develop a long-term, high resolution, gridded global burned area database consistent with satellite observations, with a consideration of both long-term climate change and human impacts.

Global fire regimes have experienced extensive anthropogenic and environmental stresses in the 20th century due to the rapid climate and land use changes (Prentice, 2010).

Anthropogenic impacts have been recognized as the primary factor in controlling the global burned area (Flannigan *et al.*, 2009b, Marlon *et al.*, 2008b, Pechony & Shindell, 2010). The impacts of climate variation have also been studied at local, regional and global level (Liu *et al.*, 2010, Westerling *et al.*, 2006b). A key message is "Climate variability and fire weather influence wildfire behavior and account for the variability in fire severity at various time scales" (Liu *et al.*, 2010). Most previous studies focused on either climate or anthropogenic factors, only a few quantitatively evaluated the impacts of both climate and human activities. Other environmental factors, such as CO_2 and nitrogen deposition also play important roles in influencing fire regimes, however, are often neglected. To understand the mechanism of fire regimes at global scale, it is essential to quantify the relative contribution of human and multiple environmental factors simultaneously.

The Dynamic Land Ecosystem Model (DLEM) (Tian *et al.*, 2010a) is a highly integrated ecosystem model that incorporates biogeochemical cycle and water cycle to estimate the interactions and feedbacks among multiple ecosystem components. In this study, we improved the DLEM by coupling a process-based fire model to estimate global burned area and the feedback of fire to the ecosystem. The objectives of this study are: (1) to develop a global historical fire dataset at 0.5 degree resolution at monthly intervals from 1901 to 2007 through integrating the GFED3 burned area information; (2) to present the global and regional fire patterns; and (3) to discuss the determinative factors controlling fire trend and quantify the relative contributions of anthropogenic and multiple environmental factors to global and regional burned areas.

2. Materials and methods

2.1. Datasets

Gridded ($0.5^{\circ}\times0.5^{\circ}$), geo-referenced data sets were compiled to drive DLEM-Fire, including satellite-observed fire climatology, climate (temperature, precipitation, relative humidity and wind speed and lightning frequency), atmospheric CO_2 concentration, population density, nitrogen deposition, land use/cover change and land management practices (cropping system, fertilization and irrigation), GDP, and topography data (elevation, slope, and aspect) for the entire globe (Table 6-1). Satellite-observed fire climatology was derived from the GFED3 burned area from 1997 to 2007, which was developed based on multiple satellite sensors (MODIS, TRMM, VIRS, and ASTR) (Giglio *et al.*, 2010a). Another satellite burned area product, MCD45A1 (Roy *et al.*, 2008a), was used for validation. Daily climate variables (1901- 2007) were generated based on CRU/NCEP dataset (http://nacp.ornl.gov/thredds/fileServer/reccapDriver/cru_ncep/analysis/readme.htm). Daily lightning frequency was collected from NASA LIS/OTD (ftp://ghrc.nsstc.nasa.gov/pub/lis/climatology/HRAC/), which is the climatology of daily lightning frequency for the period 1995-2011. Due to the lack of historical lightning data, the 17-year climatology was applied to each year across the study period. Population density (1901-2005) was extracted from the History Database of the Global Environment (HYDE3.1) (Klein Goldewijk *et al.*, 2011), and assumed no change since 2005 due to the lack of data in 2006 and 2007. The CO_2 concentration was obtained from the Carbon Dioxide Information Analysis Center (CDIAC). Land use/cover change was developed based on Synergetic Land Cover Product (SYNMAP) (Jung *et al.*, 2006) and land use

transaction data (Hurtt *et al.*, 2011). Annual deforestation rate was computed through the expansion of cropland and pasture within the grid where forest exists. Cropping system and crop phenology were identified based on a global crop geographic distribution map (Leff *et al.*, 2004) and MODIS LAI products. Gross domestic production (GDP) dataset in 2000 is from *van Vuuren et al*., (2007). Elevation, slope and aspect were derived from Global 30 Arc-Second Elevation product (https://lta.cr.usgs.gov/GTOPO30).

Table 6-1. The input datasets for DLEM-Fire[a]

Variables	**Period**	**Sources**
Climate	1901-2007	CRU/NCEP
Population density	1901-2005	HYDE3.1
Lightning frequency	climatology during 1995-2011	NASA LIS/OTD
GDP	2000	*van Vuuren et al*., [2007]
CO_2	1901 – 2007	CDIAC
Land use/cover change	1901-2007	SYNMAP and *Hurtt et al*., [2011]
Topography	Static	GTOPO30
Satellite-observed fire climatology	climatology during 1997-2007	GFED3

[a]The variables simulated by DLEM , such as soil moisture and fuel loading, are not included in this table.

2.2. Model implementation and experimental design

DLEM-Fire implementation is comprised of three stages: (1) equilibrium run, (2) spin-up, and (3) transient run. The equilibrium run aims to determine the initial condition on January 1, 1901. In the equilibrium run, the model is fed with detrended climate data from 1901 to 1930, and atmospheric composition and land cover/use pattern in 1901 to reach an equilibrium state for carbon, nitrogen, and water (i.e. the changes in annual carbon, nitrogen and water fluxes and pools are less than 0.1 g C m^{-2}, 0.1 g N m^{-2}, and 0.1 mm among consecutive years). After equilibrium state was reached, the model was run another 100 years for spin-up. In the transient mode, DLEM-Fire was driven by the time series of all input dataset and had two-type simulations: type I was run without

integrating satellite information, in which the annual satellite-adjusted scalar (v) on each grid was estimated as the quotient of the average annual burned area of GFED3 and DLEM-Fire simulated average annual burned area from 1997 to 2007; type II was run after type I simulation by coupling the satellite-adjusted scalar (v) estimated through type I simulation, and all the experiments below were based on type II simulation.

Five experiments were designed to estimate the global burned area and quantify the relative contribution of human activities, climate change, and atmospheric components (CO_2 and nitrogen deposition) respectively (Table 6-2). In the "baseline" scenario (sim0), all the forcing datasets were kept at the level in 1901 to estimate the inherent model fluctuation. The "all-Combined" scenario (sim1) considered the historical variation of all the driven factors. The "climate only" scenario (sim2) was driven by historical climate condition, but constant human activities, CO_2 concentration, and nitrogen deposition. The "human only" scenario (sim3) was forced by dynamic human activities, but static climate, CO_2 concentration, and nitrogen deposition. The "CO_2+Ndep" scenario (sim4) was forced by historical CO_2 concentration and nitrogen deposition, but static climate and human activities.

Table 6-2. Experimental design for this study[a]

Simulation	Scenario	Climate	LCLUC and Population	CO_2 and Ndep
sim0	Baseline	1901	1901	1901
sim1	All-Combined	1901-2007	1901-2005 (L), 1901-2007 (P)	1901-2007
sim2	Climate only	1901-2007	1901	1901
sim3	Human only	1901	1901-2005 (L), 1901-2007 (P)	1901
sim4	CO_2+Ndep	1901	1901	1901-2007

[a]LCLUC, land cover and land use change; Ndep, nitrogen deposition; 1901-2007 indicates the dataset in 1901-2007 was used to drive model; 1901 indicates the dataset in 1901 was used to drive model through the whole simulation period; 1901-2005 (L), 1901-2007 (P) indicates LCLUC data ends at 2005 and Population data ends at 2007.

3. Results and Discussion

3.1. Spatial patterns

During 1901-2007, our simulated global average burned area was 442.1×10^4 km^2 $year^{-1}$, of which approximately 70.2% and 10.1% occurred in Africa and Oceania, respectively (Figure 6-1). The regions with high burned fraction included Africa, Northern Australia, and South America, where fuel was sufficient and dry season was long enough; the regions with low burned fraction were distributed in cold areas (e.g. Tibet plateau), very humid areas (e.g. interior Amazon rainforest) and regions with low fuel loading (e.g. Sahara desert). In the west-east direction, maximum burned area occurred between 10° E and 40° E, which was mainly due to fire in Africa. In the north-south direction, two high burned area zones were shown clearly: one was approximately located at 10° N, and the other one was within 5° S - 20° S.

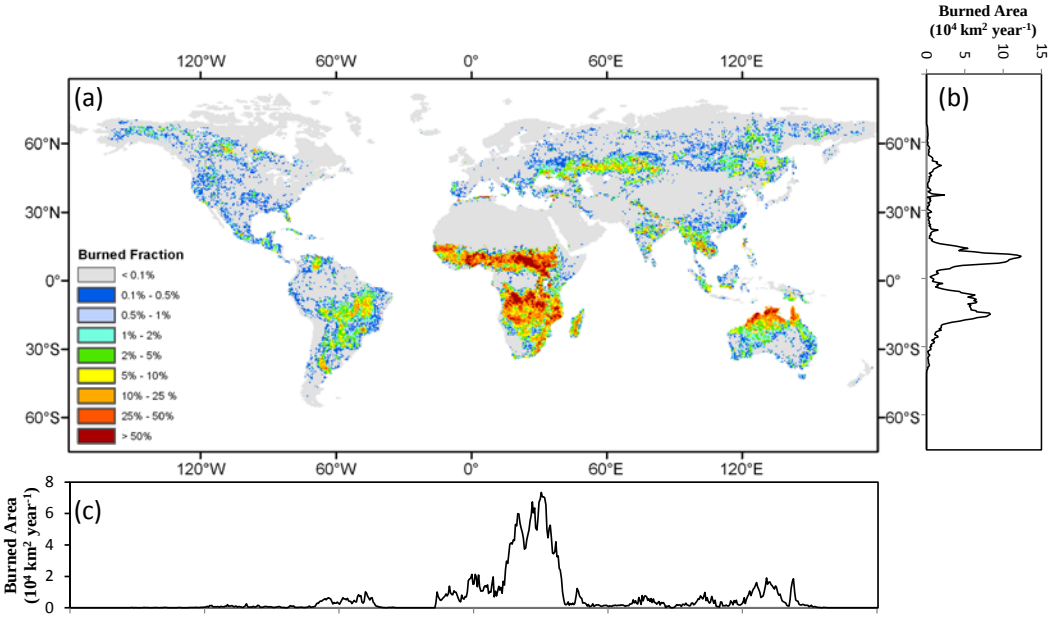

Figure 6-1. Spatial distribution of global fire. (a) Average burned fraction from 1901 to 2007, (b) zonal sum of burned area per 0.5° latitude, (c) meridional sum of burned area per 0.5° longitude.

Table 6-3 lists global burned area estimated by Satellite observations, process-based fire models, and hybrid methods. Satellite observations (GFED, MCD45A1, L3JRC, GBA2000, and GlobScar) clustered the burned area around 350×10^4 km^2 year^{-1} in the 2000s. Yet, *Randerson et al*. (2012) argued satellite imagery with coarse spatial resolution failed to detect small fires, and global burned area could be more than 400×10^4 km^2 year^{-1}. Fire models estimated a similar global burned area as satellite observations, since satellite observed fires were often used as benchmarks to calibrated fire models (Kelley *et al.*, 2013). Annual burned area from 1997 to 2004 estimated by *Kloster et al*. (2010) and *Li et al*. (2012) were 300×10^4 km^2 and 330×10^4 km^2, respectively. Our

estimated global burned area was 362.6×10^4 km^2 year^{-1} in the 2000s, which fell within the range of satellite observations.

Table 6-3. Annual global burned area estimated by different studies

Source	study period	annual burned area (10^4 km^2 year^{-1})	study approach
GFED4 [*Giglio et al.*, 2013]	1997-2011	348	multiple satellite observations
GFED3 [*Giglio et al.*, 2010]	1997-2010	363	multiple satellite observations
GFED2 [*van der Werf et al.*, 2006]	1997-2004	329	multiple satellite observations
MCD45A1 [*Roy et al.*, 2008]	2002-2010	338	satellite observation
L3JRC [*Tansey et al.*, 2008]	2000-2007	392	satellite observation
GBA2000 [*Tansey et al.*, 2004]	2000	350	satellite observation
GlobScar [*Simon et al.*, 2004]	2000	211	satellite observation
[*Randerson et al.*, 2012]	2001-2010	464	satellite observation
[*Kloster et al.*, 2010]	1997-2004	300	process-base fire model
[*Li et al.*, 2012]	1997-2004	330	process-base fire model
[*Schultz et al.*, 2008]	1960-2000	383	hybrid of official statistics and process-based fire model
[*Mouillot and Field*, 2005]	1900-2000	503	hybrid official statistics and satellite observation
This study	**1901-2007**	**442**	**hybrid of process-based fire model and satellite observation**

3.2. Temporal variations

For the period from 1901 to 2007, Mann-Kendall trend test indicated a significant decreasing trend in global burned area at the rate of 1.28×10^4 km^2 year^{-1}, with a relatively small annual variation (CV = 0.1) (Table 6-4). The largest burned area was in 1912 (552.1×10^4 km^2), and the lowest burned area appeared in 2006 (348.9×10^4 km^2). Decadal

burned area from the 1900s through the 2000s (2000s in this study refers to 2001-2007) varied between 362.9×10^4 km^2 year^{-1} and 492.3×10^4 km^2 year^{-1} (Figure 6-2). The burned area in the tropics and extratropics presented a significant declining trend, while no significant trend was detected at high latitudes.

Table 6-4. The mean, CV and trend of global and regional burned areas during 1901-2007[a]

	Mean (10^4 km^2 year^{-1})	CV	Slope (10^4 km^2 year^{-1})	Trend significance
Global	442.1	0.1	-1.28 (-0.29%)	S
N. High	4.7	0.43	-0.01 (-0.21%)	NS
N. Extra	30.4	0.43	-0.37 (-1.21%)	S
Tropics	374.7	0.09	-0.84 (-0.22%)	S
S. Extra	32.3	0.14	-0.05 (-0.15%)	S

[a]Trends were analyzed with significance of Mann-Kendall test (S for significant, P<0.05; NS for not significant, P≥0.05) and Sen's slope; CV, coefficient of variation; in the column of "Slope", the values within the parentheses are relative slope (slope normalized by the average burned area).

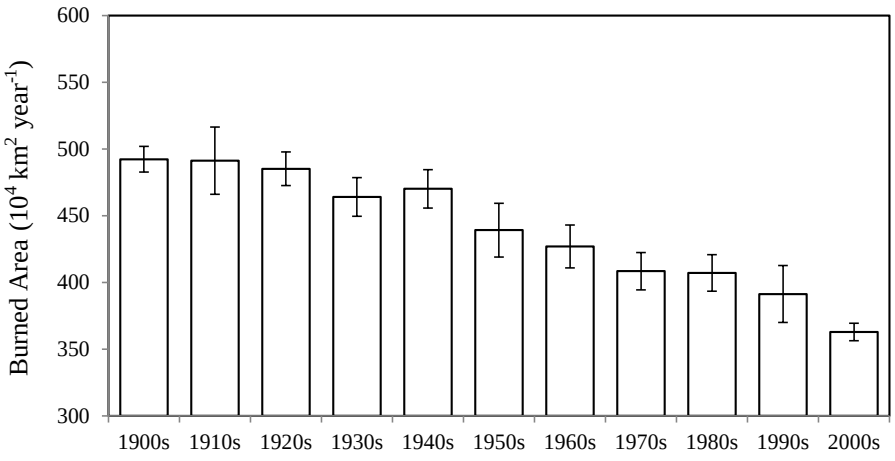

Figure 6-2. Decadal variation of global burned area. Error bar refers to the standard deviation of annual burned area within that decade.

The estimation of our study suggesting global fires declined in the 20th century was supported by Antarctic ice core record of atmospheric carbon monoxide (Wang *et al.*,

2010), charcoal records (Marlon *et al.*, 2008b), and fire model simulation of *Li et al*. (2013). *Prentice* (2010) argued present biomass burning is at a historical low because of human induced fuel loads reduction and fuel beds fragmentation. However, there are some studies presenting a different trend. As revealed by the dataset of *Mouillot and Field* (2005), 503×10^4 km^2 of land area experienced fire annually in the 20th century, with an upward trend after the 1950s. However, their dataset should be used with caution, since they made some assumptions and interpolations to quantify the burned area based on the scattered and qualitative fire records, which may bring in large uncertainties. Besides that, their dataset may not be able to reflect the variation of burned area along the variation of driving forces, as they disregarded the underlying mechanism of fire activities. *van der Werf* et al. (2013) analyzed biomass burning sources and historical methane record, and argued the historical high levels of biomass burning implied by ice core record of carbon monoxide is likely overestimated. Yet, methane concentration may not be a good indicator of biomass burning, because methane emission from fires only contributes 5.6% of global emission (Kirschke *et al.*, 2013), and explains only 15% of global emission anomalies, as compared with 70% explained by wetland emissions (Bousquet *et al.*, 2006). *Kloster et al*. (2010) simulated global burned area and found a downward trend from the 1900s to the 1960s, followed by an upward trend from the 1970s to the 1990s. The simulation of *Pechony and Shindell* (2010) showed global fire activity increases from the 1900s to the 1940s, and then decreases afterwards. These simulations contradict our estimated trend, which may be attributed to the different parameterization of anthropogenic impact on fire.

3.3. Relative contribution of human activities, climate, and atmospheric components

Previous studies have reported the impacts of climate or human activities on fire regime, while few of them quantified the relative contribution of multiple factors. The impact of atmospheric components, such as CO_2 and nitrogen deposition, was basically neglected. In this study, we conducted factorial experiments to quantify the relative contribution of human activities and multiple environmental factors from 1901 to 2007. The contribution of climate on burned area was estimated by the difference between sim2 and sim0; the contribution of human activity was estimated by the difference between sim3 and sim0; and the contribution of CO_2 and nitrogen deposition was estimated by the difference between sim4 and sim0.

3.3.1. Human activities

Anthropogenic impacts are critical factors in determining global fire patterns, since they may increase or decrease wildfire activity through grazing, clearing forests, altering ignition patterns and suppressing fires. *Marlon et al*. (2008) found an abrupt fire reduction after the 1870s in the tropics and extratropics as a response to cropland and pasture expansion. The model simulation of *Pechony and Shindell* (2010) suggested global fire as an anthropogenic-driven phenomenon in the 20th century. In our study, human impact was identified as the primary factor accounting for the declining trend in global fire activity, which reduced global burned area by 141.2×10^4 km^2 $year^{-1}$ in the 2000s (sim3 – sim0) (Figure 6-3). In the tropics, cropland area increased by 76.6%, and population increased by 310% from the 1900s to 2000s. Although it has been reported that deforestation rate and burned area in Amazonia increased substantially since the 1970s (Houghton *et al.*, 2000b), human activities remarkably reduced burned area in the

tropics as a whole region (Figure 6-3), which is mainly contributed by the fire reduction in the tropical Africa and tropical Asia. In northern extratropics, human impact continuously increased from 1900s to 1980s (Figure 6-3). Until the 1980s, burned area was reduced by 31.7×10^4 km^2 $year^{-1}$ compared to the beginning of the 20th century, in which human activities contributed 23.6×10^4 km^2 $year^{-1}$. Studies have attributed the reduction of large fires in United States during this period to extensive livestock grazing and fire suppression efforts (Belsky & Blumenthal, 1997, Savage & Swetnam, 1990). Fire models also suggested fire suppression efforts have substantially reduced the extent of wildfire in United States (Lenihan *et al.*, 2008). In China, burned area showed a downward trend from the 1950s to the 1990s. From 1981, fire suppression was strengthened across the forested region and abruptly reduced burned area (Lü *et al.*, 2006). At high latitudes, our results indicate human impact was relatively small compared with climate effects (Figure 6-3), although fire suppression was an important component in forest management (Flannigan *et al.*, 2005). Generally, in the 20th century, human activities acted as the dominant factor in determining the downward trend in the tropics and extratropics, but its impact was relatively minor at high latitudes.

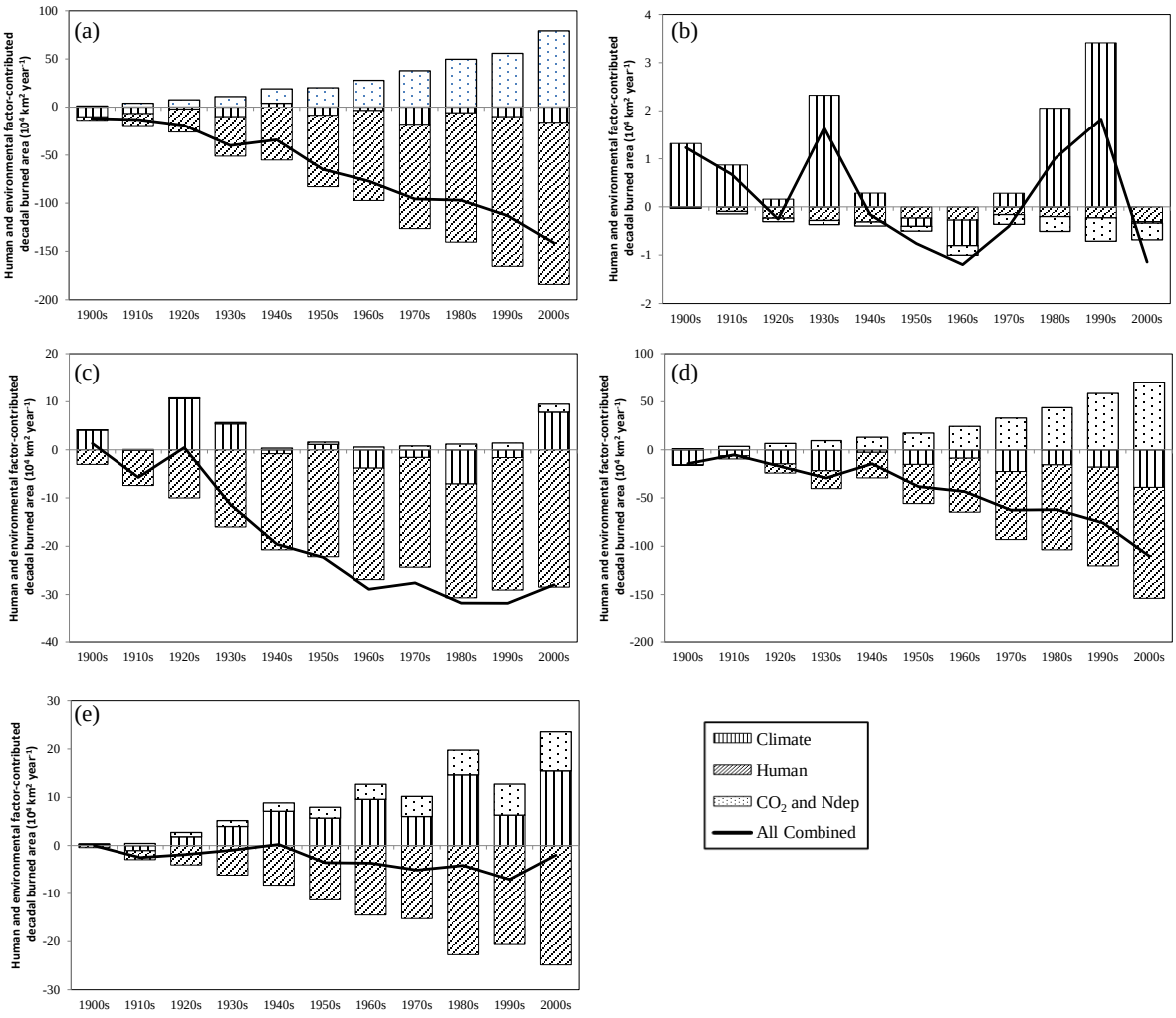

Figure 6-3. Factorial contributions to the inter-decadal variation of burned area. (a) Globe, (b) Northern high latitudes (>55° N), (c) Northern extratropics (55° N to 30° N), (d) Tropics (30° N to 20° S), and (e) Southern extratropics (>20° S).

3.3.2. Climate variation

At high latitudes, we found fire temporal pattern was closely related to climate variation (Figure 6-3). The contribution of climate variation on burned area (sim2 – sim0) dropped down from 2.3×10^4 km^2 year^{-1} to -0.5×10^4 km^2 year^{-1} during the 1930s-1960s, and increased from -0.5×10^4 km^2 year^{-1} to 3.41×10^4 km^2 year^{-1} during the 1960s-1990s.

Correspondingly, the burned area decreased by 2.8×10^4 km^2 $year^{-1}$ from the 1930s to 1960s, and increased by 3×10^4 km^2 $year^{-1}$ from the 1960s to 1990s, which indicated decadal variation of burned area at high latitudes was controlled by climate variation. Our estimated temporal pattern of burned area was comparable with other studies. The Large Fire Database (LFDB), which includes large fire information in Canada starting from 1959 (Stocks *et al.*, 2002), indicated an upward trend in the amount of area burned in Canada from 1959 to the end of the 20th century. *Wanger* (1988) described burned area in Canada as a downward trend from the 1940s to the 1960s, followed by an upward trend from the 1960s to the 1990s. Krezek-Hanes *et al.*, (2011) reported Canda burned area increased from the 1960s to the 1990s, and then decreased in the 2000s. *Flannigan et al.* (2005) suggested fire regimes in Canada were controlled by climate factors with temperature as the most important predictor to estimate burned area.

In the extratropics, climate influence was also important for fire activities. In the western United States, wildfire frequency has increased since the mid-1980s in response to the climate warming and extended fire season (Westerling *et al.*, 2006b). As demonstrated by Figure 6-3, our simulation captured the upward trend of burned area in northern extratropics from the 1980s to the 2000s. Within this period, climate dominated the fire trend, and its contribution increased from -7.1×10^4 km^2 $year^{-1}$ to 7.8×10^4 km^2 $year^{-1}$. In southern Africa, either human activities or climate change could act as the primary factor in shaping fire regimes (Archibald *et al.*, 2009). As shown in Figure 6-3, both climate and human activities were critical in southern extratropics. Although human impact was identified as the dominant factor in the extratropics, its influence was largely

counteracted by climate change. If the warming trend continues in the 21st century, climate impact may outweigh anthropogenic influence and become the primary factor in the extratropics. In general, climate variation was the primacy of fire variation at high latitudes, and is becoming increasingly important in extratropics in the context of global warming. However, the impact of climate variation was much less than anthropogenic influences in tropical regions and at the global level in the 20th century.

3.3.3. Atmospheric components

The impacts of atmospheric components on fire activity are rarely studied, because they are often covered up by the impacts of climate and human activities and its effect is difficult to detect based on short-term fire observations. The impacts of atmospheric components on ecological and hydrological processes have been verified by observations and model simulations. Theoretically, CO_2 and nitrogen deposition can stimulate fire activities by boosting ecosystem productivity, vegetation biomass, and then fuel loading (Norby *et al.*, 2010, Thomas *et al.*, 2010); at the same time, CO_2 can suppress fire occurrence by retaining more water in the soil (Nelson *et al.*, 2004) through reducing transpiration (Ainsworth & Rogers, 2007). Fire models are able to provide insight into the impact of atmospheric components on burned area (sim4 – sim0). As indicated by our simulation, the impact of atmospheric components reduced burned area at high latitudes (Figure 6-3). In the tropics and southern extratropics, elevated CO_2 and nitrogen deposition significantly stimulated fire activity (Figure 6-3). In northern extratropics, the impact of elevated CO_2 and nitrogen deposition was small, which is probably because the positive effect and negative effect counteracted each other. At the

global level, the impact of CO_2 and nitrogen deposition enhanced the burned area significantly (Figure 6-3). It is reasonable to expect atmospheric components will have more of a significant effect on global fire regimes with the continuous increasing trend in CO_2 and nitrogen deposition projected in the 21st century (Lamarque *et al.*, 2013b).

3.4. Uncertainties and future needs

The global burned area dataset of this study agrees well with satellite fire products in terms of spatial and temporal patterns, but there should be some uncertainties when interpreting the results due to the input data and fire model parameterization. The constant lightning frequency applied to each year in the study period was one source of uncertainty. Currently, the dynamic lightning dataset prior to 1995 is still unavailable. To improve the spatial pattern of burned area simulation, GFED3 observed was integrated into DLEM-Fire. Thus, the reconstructed database has inherited uncertainties from GFED3 (Giglio *et al.*, 2010a). Fire activities are a complicated phenomenon depending on numerous parameters (Pechony & Shindell, 2009). Although DLEM-Fire has addressed most critical factors influencing fire activity, some processes, such as the impact of fuel quality, have not been well represented in the current fire module. The parameterization of fire duration in the present study only considered average fire duration and natural fire breaks, which may lead DLEM-Fire to underestimate the burned area caused by megafire events that last much longer than the average fire duration. A new algorithm estimating fire duration base on fuel characteristics, fire suppression effort, and weather conditions is expected to greatly improve model performance in estimating burned area under extreme climate conditions. On the deforested land in Amazonia, trees were reburned several times within one year to clear the land, and the burned area is at

least twice the deforested area (Nepstad *et al.*, 1999). Combustion completeness and climate conditions are the two major factors determining the burning times. DLEM-Fire probably underestimated the burned area of deforestation fire. Moreover, the performance of DLEM-Fire needs further evaluation as one component within the framework of DLEM. The information collected from field observations related to fuel loading, fuel consumption, fire emissions, and fire damage to vegetation can be valuable for model development, validation and application.

4. Conclusions

In this study, we reconstructed a 0.5° × 0.5° data set of the global burned area for the 20th and early 21st centuries based on a process-based fire model and made comparisons to satellite observations. The resulting comparison indicated our reconstructed global fire history was capable of capturing the spatial and temporal patterns of global fire activities. As indicated by this dataset, the global burned area during 1901-2007 was 442.1×10^4 km^2 $year^{-1}$ and showed a significant declining trend at the rate of 1.28×10^4 km^2 $year^{-1}$. At the regional level, burned area in tropics and extratropics exhibited a significant declining trend, with no significant trend at high latitudes.

This study highlighted the evaluation of the relative contributions of human activities, climate, and atmospheric components to global and regional burned areas, and was the first time to address the importance of elevated CO_2 and nitrogen deposition to fire regimes. The factorial experiments identified human activities as the dominant factor in determining the declining trend of burned area in the tropics and extratropics, and climate variation as the primary factor in shaping the decadal variation of burned area at

high latitudes. The impact of climate change in extratropics is becoming increasingly important and may induce more fires in the context of global warming. Elevated CO_2 and nitrogen deposition enhanced burned area in tropics and southern extratropics, but suppressed fire occurrence at high latitudes. The spatial and temporal information on global burned area derived from this study can be used for ecosystem, hydrological, and climate modeling as well as by policy makers for understanding and assessing complex interactions among fire, climate and human in a changing global environment.

Chapter 7. Century-scale estimation of global pyrogenic carbon emissions and fire impacts on terrestrial carbon fluxes

Abstract

Fires have consumed sizable amount of terrestrial organic carbon, and significantly influenced ecosystems and climate system over the past century. Less work has done in century-scale assessment of the changes in global fire regimes, although the global biomass burning has been widely investigated via satellite observations in the recent decades. The knowledge of long-term fire history in the context of multiple environmental changes would enhance our understanding of future changes in fire regimes. In this study, we investigated the global pyrogenic carbon emissions and fire impacts on carbon fluxes from 1901 to 2010 by using a process-based ecosystem model. The results show a significant declining trend in global pyrogenic carbon emissions between the early 20th century and the mid-1980s and then a significant increase trend thereafter. The increase trend in the recent decades is mainly caused by the more fire activities in the ecosystems with huge carbon storage, such as peatland and tropical rainforest. The average pyrogenic carbon emission was estimated to be 2.43 ± 0.27 Pg C year^{-1} over the 110 years. Due to fire impacts, global net primary productivity, heterotrophic respiration, and net carbon sink in terrestrial ecosystems were reduced by 4.14 Pg C year^{-1}, 6 Pg C year^{-1}, and 0.57 Pg C year^{-1}, respectively. Our study suggests that, in the future, special attention should be paid on the fire activities in the current peatland and tropical rainforest ecosystems. Practical strategies, such as minimizing the forest logging and cropland expansion in these humid regions, need be applied to reduce the risks of fires and pyrogenic emissions.

Key words: The Dynamic Land Ecosystem Model (DLEM); Terrestrial carbon sink; Fire emissions; Climate change

1. Introduction

At global scale, the recent estimates of terrestrial carbon sink clustered at around 2.6 Pg C $year^{-1}$ e.g., (Poulter *et al.*, 2014, Quéré *et al.*, 2013), while the estimates of global pyrogenic carbon emissions in the recent decade clustered at around 2.0 Pg C $year^{-1}$, e.g., (Kaiser *et al.*, 2012b, Li *et al.*, 2014c, van der Werf *et al.*, 2010b) . The global fire emissions presented strong inter-annual variations. For example, as shown by the third-generation global fire emissions database (GFED3) (van der Werf *et al.*, 2010b), global pyrogenic carbon emissions were more than 2.5 Pg C $year^{-1}$ in the two El Nino years 1997 and 1998, while lower than 1.6 Pg C $year^{-1}$ in the year 2001 and 2009. The inter-annual variations in pyrogenic carbon emissions could substantially influence the size of terrestrial carbon sink. For many ecosystems, such as Canadian boreal forest and Amazon tropical forest, fire has been recognized as one of the most critical factors controlling the overall direction of carbon fluxes between land and atmosphere (Bond-Lamberty *et al.*, 2007, Gatti *et al.*, 2014).

In the recent decades, fires were extensively studied in many regions across the globe in the context of climate changes and intensified human activities, e.g., (Andela & van der Werf, 2014, Kasischke & Turetsky, 2006, Mack *et al.*, 2011, Westerling *et al.*, 2006b). The earliest estimation of global fire carbon emissions could be dated back to the 1980s (Seiler & Crutzen, 1980). However, global fires and their impacts on terrestrial

carbon balance prior to the satellite era are largely unknown. Up to date, various approaches have been use to investigate burned area and fire emissions. Generally, the methods to investigate global burned area could be classified into three categories, namely ground-based inventory data interpolation (Mouillot & Field, 2005, Schultz *et al.*, 2008), satellite observation (Giglio *et al.*, 2013b, Roy *et al.*, 2008c, Tansey *et al.*, 2008b), and model simulation (Arora & Boer, 2005, Le Page *et al.*, 2015, Li *et al.*, 2012, Pechony & Shindell, 2009, Thonicke *et al.*, 2010, Yang *et al.*, 2014a, Yue *et al.*, 2014a). Meanwhile, global fire emissions could be either estimated by the product of burned area, fuel loading and combustion completeness (Ito & Penner, 2004a, Li *et al.*, 2014c, Mouillot *et al.*, 2006, Prentice *et al.*, 2011b, Seiler & Crutzen, 1980, Thonicke *et al.*, 2010, van der Werf *et al.*, 2010b, van der Werf *et al.*, 2006a, Yue *et al.*, 2014b), or derived through the satellite-observed Fire Radiative Power (FRP) (Kaiser *et al.*, 2012b, Zhang *et al.*, 2014).

To examine the impacts of fire on ecosystem, field experiments and model simulations have been conducted at site, regional, and global level. The field fire-exclusion experiments to compare sites with different fire management strategies have been conducted in many regions across the globe e.g. (Bowman & Panton, 1995, Moreira, 2000, Tilman *et al.*, 2000). All of these experiments indicated that the long-term fire exclusion can lead to the increase of forest coverage, and frequent fires can reduce vegetation and soil carbon storage. Numerical model results show that the tree cover and biomass decreased linearly with increasing burned area (Poulter *et al.*, 2015a), and closed forest would increase from 27% to 56% of vegetated land area once the global fire activities were excluded (Bond *et al.*, 2005a). Thus, terrestrial ecosystem carbon storage

and carbon sequestration could be fundamentally modified by fires. However, the impact of fires on global carbon sink is largely unknown until two recent model-based studies by using CLM-fire model (Li *et al.*, 2014c) and ORCHIDEE model (Yue *et al.*, 2014b). Both of them designed the "Fire-on" and "Fire-off" numerical experiments, and computed the differences in carbon balance between the two experiments. It is worth noting that the estimated reductions in the terrestrial carbon sink presented large divergence between the two studies (1.0 Pg C $year^{-1}$ estimated by *Li et al.*, (2014) and 0.32 Pg C $year^{-1}$ estimated by *Yue et al.*, (2014a)). Therefore, further investigation is in need to narrow down the uncertainties.

Century-scale global burned area datasets have been reconstructed by *Mouillet and Field*, (2005) and *Yang et al.*, (2014a), independently. The dataset of *Mouillet and Field*, (2005) was developed based on fire inventory data, while the dataset of *Yang et al.*, (2014a) was reconstructed based on model simulations and constrained by satellite observation. In the present study, we conducted our investigation by using a process-based ecosystem model, the Dynamic Land Ecosystem Model (DLEM), in combination with a newly developed burned area dataset and other gridded environmental datasets. The objectives are (1) to provide a century-scale estimation of global pyrogenic carbon emissions from 1901 to 2010, (2) to evaluate the impact of fires on terrestrial carbon budget, and (3) to discuss the influences of climate, human activities, and atmospheric components on the trend of historical biomass burning and their future implications.

2. Method and Data

2.1. Model input datasets

Gridded, georeferenced data sets are compiled to drive the DLEM at the spatial resolution of 0.5°×0.5°, including climate (daily mean/maximum/minimum temperature, precipitation, downward solar radiation, and relative humidity), atmospheric CO_2 concentration, nitrogen deposition, land use/cover change, burned area, topography, soil texture, and other ancillary datasets (the data availability is described in the supporting materials). The temporal variations in the global temperature, precipitation, CO_2 concentration, and nitrogen deposition rate are illustrated in Figure 7-1.

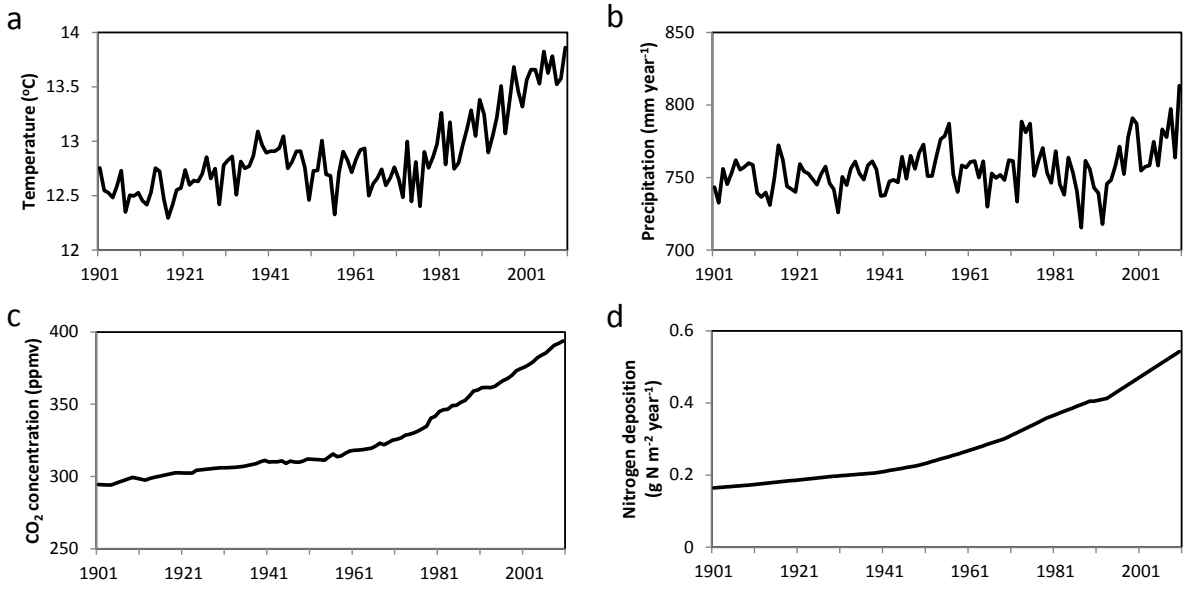

Figure 7-1. The inter-annual variations of the DLEM input dataset on land area from 1901 to 2010. (a) Global average temperature (°C), (b) precipitation (mm $year^{-1}$), (c) CO_2 concentration (ppmv), and (d) nitrogen deposition rate (g N m^{-2} $year^{-1}$)

The monthly burned area dataset used in study is consisted of two products. Burned area from 1901 to 1996 is obtained from *Yang et al.*, [2014a], while burned area from 1997 to 2010 comes from GFED3 (Giglio *et al.*, 2010a). As the dataset of *Yang et al.*, [2014a] was reconstructed based on GFED3 burned area climatology, no abrupt change exists in the transition period from 1996 to 1997. As indicated by this dataset, global burned area decreased from 547.24×10^4 km^2 year^{-1} in 1901 to 324.39×10^4 km^2 year^{-1} in 2010, with a significant declining trend of -1.84×10^4 km^2 year^{-1} (Mann-Kendall trend significance test, p-value < 0.05, same hereafter) (Figure 7-2).

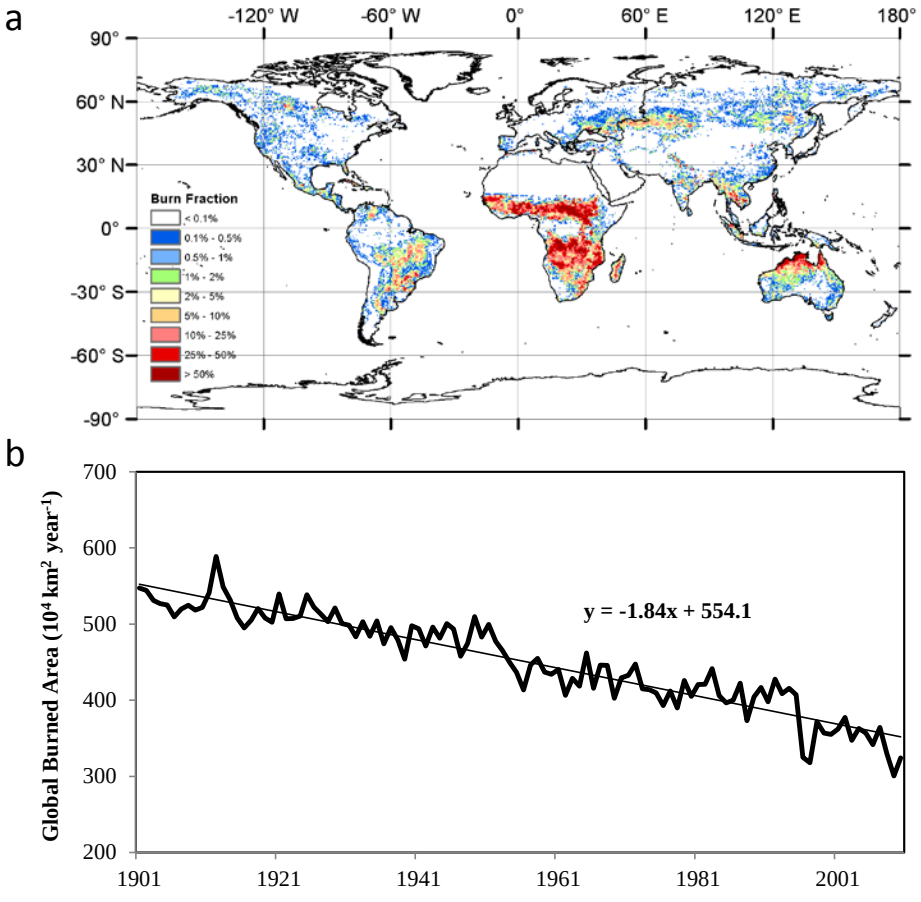

Figure 7-2. (a) Spatial distribution and (b) inter-annual variations of global burned area during 1901-2010.

2.2. Model implementation and experimental designs

To investigate the fire-induced carbon emissions and the impact of fires on global carbon fluxes, we designed two model experiments, i.e., "Fire-on" and "Fire-off", by using the DLEM. Generally, the implementation of the DLEM was composed of three stages: equilibrium run, spin-up, and transient run. The equilibrium run aimed to determine the initial condition. During the equilibrium run, the DLEM was fed with the average climate condition from 1901 to 1930 and other input data (atmospheric CO_2 concentration, nitrogen deposition, land cover) at the level of 1901, while the disturbances (such as, fires and harvest) were excluded. For each simulation grid, the equilibrium state was assumed to be reached when the changes in annual ecosystem carbon, nitrogen, and water pools were less than 0.1 g C m^{-2}, 0.1 g N m^{-2}, and 0.1 mm among 50 consecutive years. Both "Fire-on" and "Fire-off" simulations shared the same initial condition. After equilibrium state was reached, the model was run for another 100 years for spin-up purpose. During this stage, the time-series of driving forces were randomly selected within the 30 years from 1901 to 1930, and fire option was switched on in the "Fire-on" experiment, but kept closed in the "Fire-off" experiment. The different spin-up strategies for "Fire-on" and "Fire-off" experiments caused different sizes of vegetation and soil organic carbon/nitrogen storage. At last, the DLEM was run in a transient mode by feeding with the time series of all input datasets from 1901-2010.

The pyrogenic carbon emissions were estimated in the "Fire-on" experiment. The differences of net primary productivity (NPP) and ecosystem heterotrophic respiration (Rh) in "Fire-on" and "Fire-off" simulations were analyzed to denote the impacts of fires on terrestrial carbon fluxes. Net ecosystem production (NEP) was defined as the difference between NPP and

Rh. The fire impact on NEP (NEP_{fire}) was calculated according to the *NPP* and *Rh* in the "Fire-on" and "Fire-off" simulations,

$$NEP_{fire} = \left(NPP_{fire-on} - Rh_{fire-on}\right) - \left(NPP_{fire-off} - Rh_{fire-off}\right)$$

Net biome production (NBP) was analyzed to investigate the impact of fires on terrestrial carbon sink, which is defined in this study as the difference between NPP and the sum of Rh, pyrogenic carbon emissions (C_{bt}), carbon emissions during crop harvesting (C_{harv}), and biogenic methane emission (C_{CH_4}). The magnitude of fire impacts on C_{harv} and C_{CH_4} was found to be negligible comparing to its impacts on NPP and Rh. Thus, we simplified the equation of fire impacts on terrestrial carbon sink (NBP_{fire}) as,

$$NBP_{fire} = \left(NPP_{fire-on} - Rh_{fire-on} - C_{bt}\right) - \left(NPP_{fire-off} - Rh_{fire-off}\right)$$

Furthermore, we designed another two simulations, i.e., "without-CO_2" and "without-Ndep", to examine the impacts of changes in atmospheric components (CO_2 concentration and nitrogen deposition) on pyrogenic carbon emissions. In the "without-CO_2" ("without-Ndep") simulation, the model configurations were similar to the "Fire-on" experiment, except that the atmospheric CO_2 concentration (nitrogen deposition rate) was kept at the level in 1901. The differences of the simulated pyrogenic carbon emissions in "Fire-on" and "without-CO_2" simulations were assumed to be caused by the increment in CO_2 concentration during 1901-2010. Similarly, the impact of increased nitrogen deposition on pyrogenic carbon emissions can be calculated according to the differences between "Fire-on" and "without-Ndep" simulations.

3. Results

3.1. Long-term trend of pyrogenic carbon emissions

From 1901 to 2010, DLEM-simulated global pyrogenic carbon emissions were 2.43 ± 0.27 Pg C $year^{-1}$ (avg. ± 1 std. dev., same hereafter). The maximum carbon emissions occurred in the year 1912 (3.02 Pg C $year^{-1}$). Although burned areas in some other years, such as 1997 and 2009, were even lower, the minimum carbon emissions occurred in the year 2001 (1.89 Pg C $year^{-1}$), indicating a smaller combustion rate (carbon emissions per area burned, in unit g C m^{-2} burned area $year^{-1}$) in this year. Pyrogenic carbon emissions decreased significantly from the early 20^{th} century to the mid-1980s at the rate of -0.0086 Pg C $year^{-1}$, but followed by a significant increase at the rate of 0.014 Pg C $year^{-1}$ from 1984 to 2010 (Figure 7-3). The upward trend in pyrogenic carbon emissions after the year 1984 were mainly contributed by the large increases in the low-latitudes (defined as 30° N to 30° S in this study) and mid-latitudes (defined as 30° N to 55° N, and 30° S to 55° S). The pyrogenic carbon emissions in the low-latitudes and mid-latitudes increased significantly at 0.011 Pg C $year^{-1}$ and 0.006 Pg C $year^{-1}$. However, the trend in pyrogenic carbon emissions in the high-latitudes (defined as 55° N and north) was not significant after the 1980s, which is similar to *Balshi et al.*, (2007) indicating that, in the boreal North America (Canada and Alaska), the fire emissions in the 1990s were lower than those in the 1980s.

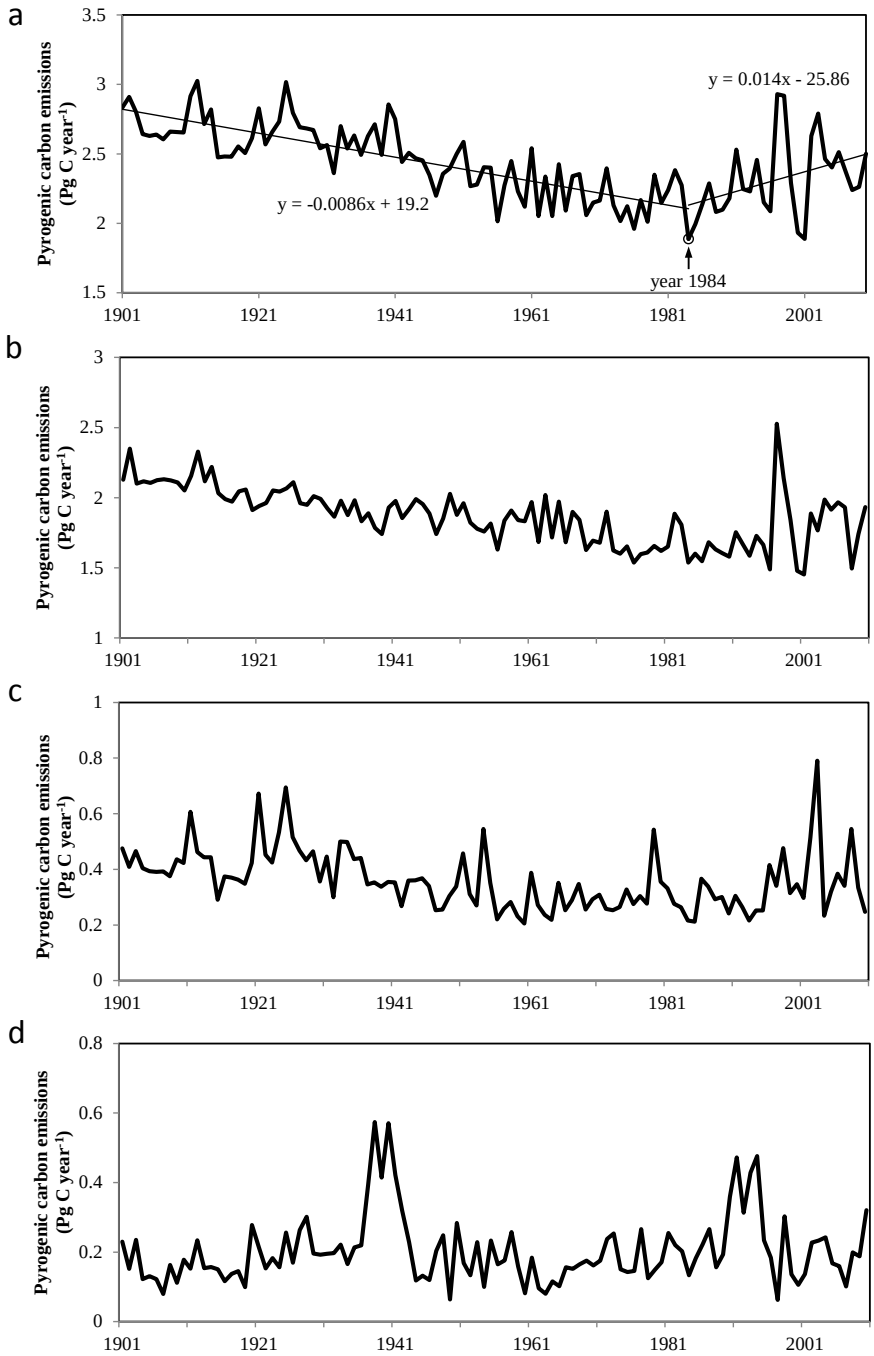

Figure 7-3. Inter-annual variations of pyrogenic carbon emissions from 1901 to 2010 at global level (a), in the low-latitudes (b), mid-latitudes (c), and high-latitudes (d).

3.2. Spatial pattern of pyrogenic carbon emissions

In the low-latitudes, 1.87 ± 0.2 Pg C organic carbon was burned annually, which contributed 77% to the global total amount. The pyrogenic carbon emissions in the mid-latitudes and high-latitudes contributed 14.8% and 8.2%, respectively. At continental level, the pyrogenic carbon emissions in Africa contributed the most (44%) to global total, followed by Asia (19.8%), South America (18.1%), North America (10.7%), Oceania (5.3%) and Europe (2.1%) (Table 7-1). Over the area affected by fires, the global average combustion rate was 537.85 g C m^{-2} burned area $year^{-1}$. The highest combustion rate occurred in North America (2549.02 g C m^{-2} burned area $year^{-1}$), while the lowest were found in Oceania (300.23 g C m^{-2} burned area $year^{-1}$) and Africa (344.27 g C m^{-2} burned area $year^{-1}$). Generally, the combustion rate in the pan-tropical regions was lower than that in the pan-boreal regions (Figure 7-4). The different combustion rate could be attributed to the fuel loading, fire return interval, and vegetation composition. In the tropical savanna regions, the frequent fires reduced fuel loading, and thus fuel combustion rate; while fires in the boreal forest have longer return interval, and left sufficient time for forest recovery and fuel accumulation. The crown fire is a common fire type in the boreal North America (Rogers *et al.*, 2015), which substantially alters vegetation composition and combusts much more fuels than the tropical savanna fire.

Table 7-1. The statistics of average burned area, pyrogenic carbon emissions, and combustion rate from 1901 to 2010 at global and continental scales. The values within the parentheses denote their contributions to the global total amount.

	Burned area ($\times 10^4$ km^2 year^{-1})	**Pyrogenic carbon emissions (Pg C year^{-1})**	**Combustion rate (g C m^{-2} burned area year^{-1})**
Globe	451.8 (100%)	2.43 (100%)	537.85
Africa	310.8 (68.8%)	1.07 (44%)	344.27
Asia	46.2 (10.2%)	0.48 (19.8%)	1038.96
Oceania	43.3 (9.6%)	0.13 (5.3%)	300.23
South America	36.2 (8%)	0.44 (18.1%)	1215.47
North America	10.2 (2.3%)	0.26 (10.7%)	2549.02
Europe	5.1 (1.1%)	0.05 (2.1%)	980.39

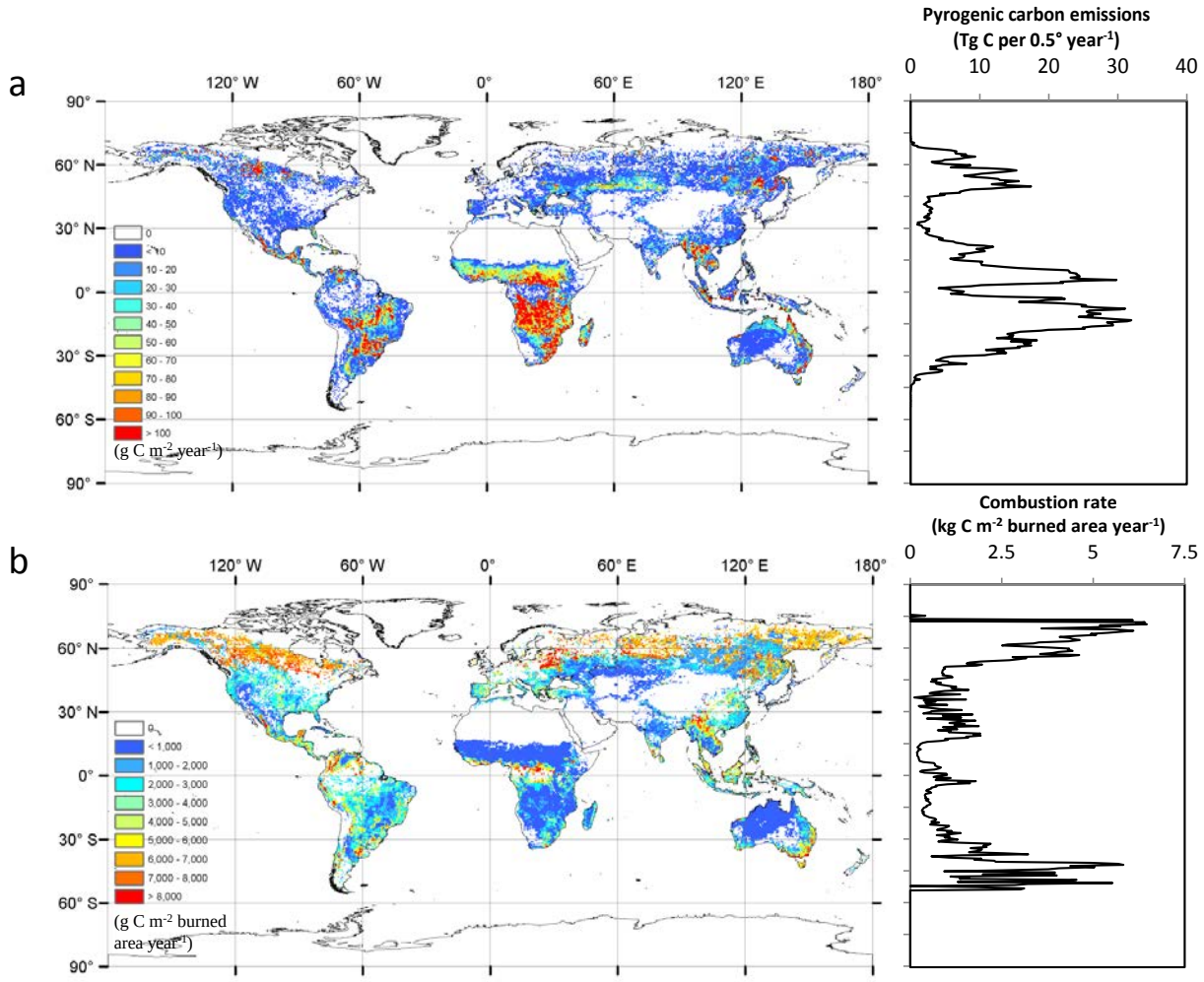

Figure 7-4. (a) The spatial distribution of the 110-year average pyrogenic carbon emissions at grid level (g C m^{-2} $year^{-1}$), and (b) combustion rate in the area affected by fires (g C m^{-2} burned area $year^{-1}$).

3.3. Fire impact on terrestrial carbon budget

During the 110 years, the global terrestrial NPP were estimated to be 50.22 Pg C $year^{-1}$ and 54.36 Pg C $year^{-1}$ in the "Fire-on" and "Fire-off" simulations, respectively (Figure 7-5). Under the impact of fires, the globally NPP was reduced by 4.14 Pg C $year^{-1}$, with the largest NPP reduction occurred in Africa (2.59 Pg C $year^{-1}$) (Table 7-2). The NPP reduction in the "Fire-on" simulation was primarily caused by the less forest coverage and lower soil fertility. The global Rh were estimated to be 46.79 Pg C $year^{-1}$ and 52.79 Pg C $year^{-1}$ in the "Fire-on" and

"Fire-off" simulations in the study period (Figure 7-5). Global Rh was reduced by 6 Pg C $year^{-1}$ by fire activities, with the largest reduction in Africa (3.49 Pg C $year^{-1}$) as well. The lower Rh in the "Fire-on" simulation could be attributed to the lower amounts of litter and soil organic materials for microbial decomposition. The Rh reduction caused by fires was higher than the reduction in NPP. Therefore, the global NEP in the "Fire-on" simulation was 1.86 Pg C $year^{-1}$ higher than that in the "Fire-off" simulation. Combining the fire-induced NEP change and the pyrogenic carbon emissions together, terrestrial carbon sink was estimated to be reduced by 0.57 Pg C $year^{-1}$ under the influences of global fires. Three continents with largest reduction in terrestrial carbon sink were Asia (0.18 Pg C $year^{-1}$), Africa (0.17 Pg C $year^{-1}$), and North America (0.14 Pg C $year^{-1}$), sequentially.

Table 7-2. The impact of fires on terrestrial carbon fluxes and carbon budget at global and continental scales during 1901 – 2010.

	NPP change (Pg C $year^{-1}$)	**Rh change (Pg C $year^{-1}$)**	**NEP change (Pg C $year^{-1}$)**	**NBP change (Pg C $year^{-1}$)**
Globe	-4.14	-6	1.86	-0.57
Africa	-2.59	-3.49	0.9	-0.17
Asia	-0.5	-0.8	0.3	-0.18
Oceania	-0.24	-0.36	0.12	-0.01
South America	-0.59	-0.97	0.38	-0.06
North America	-0.17	-0.29	0.12	-0.14
Europe	-0.05	-0.09	0.04	-0.01

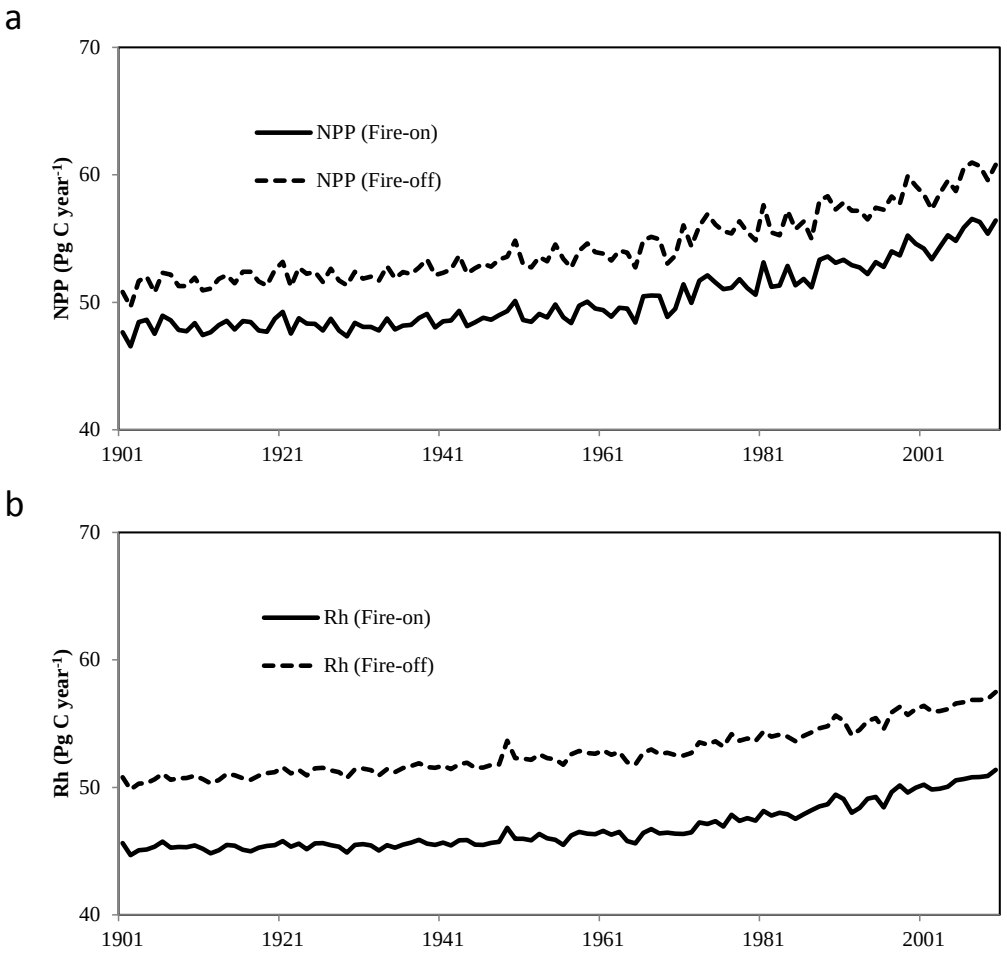

Figure 7-5. The temporal variations of global net primary productivity (a) and heterotrophic respiration (b) simulated by the DLEM.

In the meridional direction, the fire-induced reductions in NPP and Rh presented double-peak pattern, with one peak located at between 0° and 15° N and the other peak located at between 0° and 20° S (Figure 7-6). In the low-latitudes, NPP was reduced by 3.92 Pg C year^{-1}, contributing 94.7% of the global NPP reduction; Rh was reduced by 5.52 Pg C year^{-1}, contributing 92% of the global Rh reduction. The reductions in NPP and Rh in the mid- and high-latitudes were much lower than those in the low-latitudes. The fire-induced reduction in

carbon sink was mainly contributed by two latitudinal bands: one was located at between 46° N to 70° N, contributing 48.1% of global fire-induced NBP reduction, the other one was located at between 10° N to 20° S, contributing 42.1% of the global fire-induced NBP reduction (Figure 7-6).

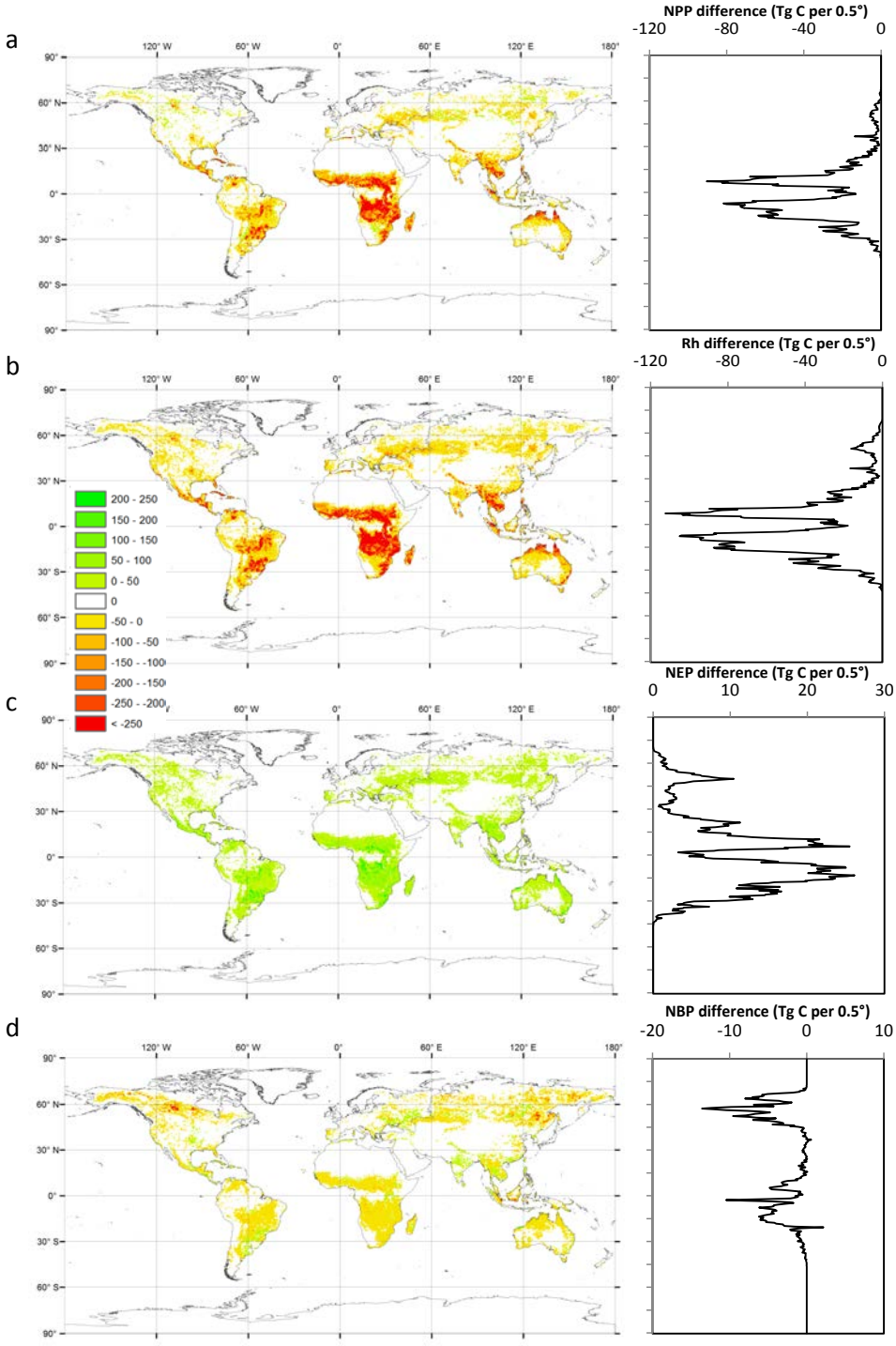

Figure 7-6. Fire-induced changes in net primary productivity (a), heterotrophic respiration (b), net ecosystem production (c), and net biome production (d), which are calculated as the differences of each variable between the “Fire-on” and “Fire-off” simulations.

4. Discussions

4.1. Changing trends of pyrogenic carbon emissions during 1901-2010

The burned areas in the tropics and extra-tropics have been found to have declining trends in the last century (Marlon *et al.*, 2008a, Yang *et al.*, 2014a). The satellite observations indicated that the trend in global burned area continues in the first decade of this century (Giglio *et al.*, 2013b). Prior to the 1980s, the downward trend in burned area is the major factor determining the declining of pyrogenic carbon emissions simulated by the DLEM. Previous studies identified human activities as the main factor in controlling the trends in burned area and pyrogenic carbon emissions: fire suppression activities inhibited fire durations, while cropland expansion broke the fuel continuity and reduced fire spread (Marlon *et al.*, 2008a). However, after the mid-1980s, the trend of pyrogenic carbon emissions reversed, which contradict the continuous decrease trend in burned area. The reversed trend in the recent decades can be explained by the significant increase in the combustion rate from 1985 to 2010 (Figure 7-7), which was caused by the increased burned area in the ecosystem with higher carbon storage (such as, tropical rainforest), and CO_2 and nitrogen deposition induced higher fuel loading.

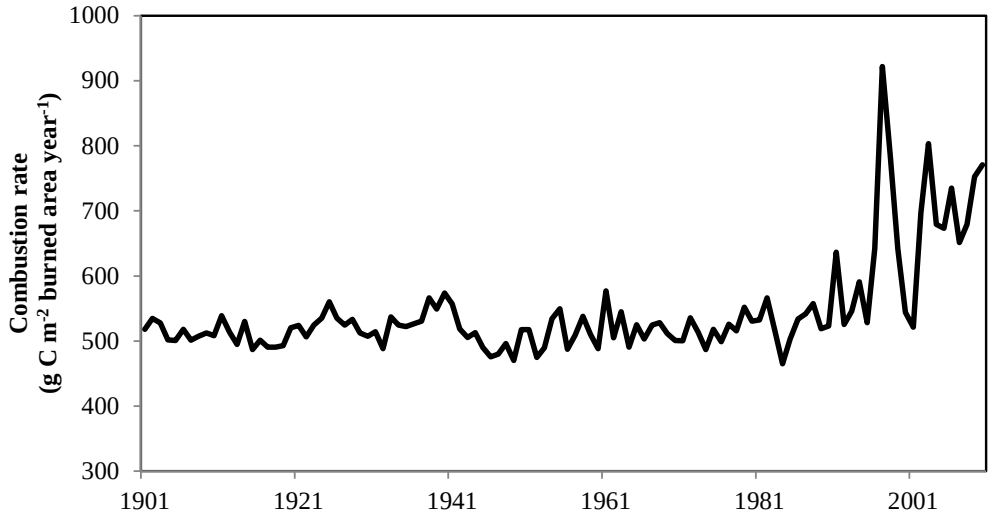

Figure 7-7. Inter-annual variations in the global average combustion rate during 1901-2010.

In the recent decades, the tropical deforestation area increased dramatically. It has been recorded that forest clear-cutting area increased from 18,165 km^2 in 2001 to 23,750 km^2 in 2004 in Brazilian Amazon basin, and increased from 17,000 km^2 in 1997 to 21,000 km^2 in 2003 in Indonesia (Santilli *et al.*, 2005). Fire is one economical and widely-used practice to clear the tropical forested land and prepare for agricultural cultivation. Different with other fire types, the trees were usually reburned several times by the deforestation fires within one year to thoroughly clear the land. Thus, the burned area could be several times of the deforested area, and the combustion completeness is very high (Nepstad *et al.*, 1999). Since the 1990s, the importance of tropical peatland fires have been widely recognized and studied. The carbon emissions from deep-burning peatland fires in Indonesia were estimated to be 0.95 Pg C in 1997 and 1998 (Page *et al.*, 2002, van der Werf *et al.*, 2010b). In the recent decades, human activities in the Southeast Asia peatland, such as logging, drainage, and plantation development, reduced the forest canopy and dried up the fuel, which made peatland soil easier to catch fire (Turetsky *et al.*, 2015). In the

boreal peatland regions, the recent global warming enhanced the fire risk. It has been reported that an unprecedented Alaska peatland fire in 2007 released 2.1 Tg C to the atmosphere (Mack *et al.*, 2011).

In many regions of the mid-latitudes, burned area since the 1980s presented substantial increases. For example, in the western United States (US), the total burned area increased at the rate of 355 km^2 $year^{-1}$ from 1984 to 2011 (Dennison *et al.*, 2014). The increment in burned area in the western US could be largely attributed to the climate warming, earlier spring, and more frequent droughts (Westerling *et al.*, 2006b). In the early and middle 20^{th} century, the fire suppression policies inhibited fire spread and duration (Houghton *et al.*, 2000a), which, therefore, enhanced fuel accumulation and induced higher fire emissions in the 21^{st} century. From 1984 to 2012, the pyrogenic carbon emissions in the conterminous US were reported to be 17.65 ± 12.68 Tg C $year^{-1}$ with a significant increasing trend at the rate of 0.87 Tg C $year^{-1}$ (Yang *et al.*, 2015). It is worth noting that burned area and fire emissions in some areas in the mid-latitudes, such as China, witnessed continuous decline from the 1950s to the 2000s under the intensified fire suppression activities (Lü *et al.*, 2006). Nevertheless, the declining trend in China did not reverse the increasing trend in the entire mid-latitudes after the 1980s.

As indicated by the model input datasets, the average CO_2 concentration increased from 294.5 ppmv to 393.7 ppmv, and the average nitrogen deposition rate over the land area increased from 0.16 g N m^{-2} $year^{-1}$ to 0.54 g N m^{-2} $year^{-1}$ during 1901-2010 (Figure 7-1). The changes in atmospheric components have been reported to stimulate the terrestrial carbon sequestration and vegetation carbon storage e.g. (Lu *et al.*, 2012, Tian *et al.*, 2011). We further examined the impacts of CO_2 and nitrogen deposition on pyrogenic carbon emissions. The results showed that

both the changes in CO_2 and nitrogen deposition rate positively contributed to the global pyrogenic carbon emissions, and their influences increased with time (Figure 7-8). Comparing with the year 1901, CO_2 increment enhanced global pyrogenic carbon emissions by 0.1 Pg C $year^{-1}$, 0.13 Pg C $year^{-1}$, and 0.16 Pg C $year^{-1}$ in the 1980s, the 1990s and the 2000s, respectively; meanwhile, nitrogen deposition enhanced global pyrogenic carbon emissions by 0.08 Pg C $year^{-1}$, 0.1 Pg C $year^{-1}$, and 0.13 Pg C $year^{-1}$ in the 1980s, the 1990s and the 2000s, respectively. The increments in CO_2 concentration and nitrogen deposition contributed to the upward trend of pyrogenic carbon emissions.

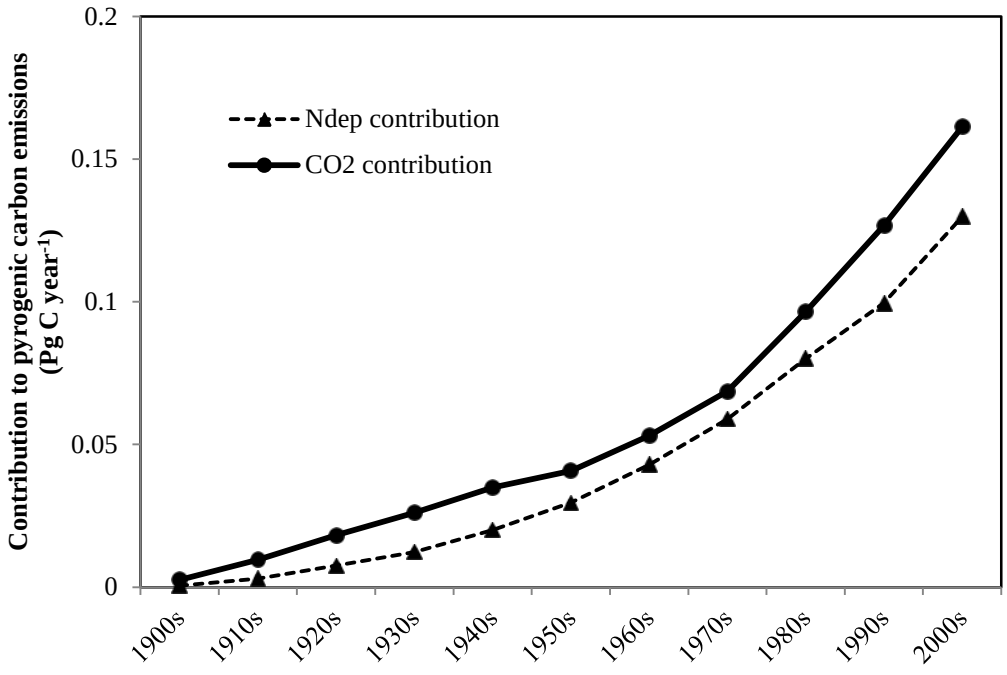

Figure 7-8. The contributions of the atmospheric CO_2 and nitrogen deposition to the pyrogenic carbon emissions from the 1900s to the 2000s.

4.2. Comparison with other studies

Mouillet et al., (2006) showed that the global pyrogenic carbon emissions at the beginning of the 20th century were 1.5-2.7 Pg C $year^{-1}$, and increased to 2.7-3.3 Pg C $year^{-1}$ by

the end of the 20th century. However, our study indicated that global pyrogenic carbon emissions were 2.7 Pg C $year^{-1}$ in the 1900s, and decreased to 2.36 Pg C $year^{-1}$ in the 1990s. The discrepancies could be mainly attributed into the large differences between the global burned area dataset used by *Mouillet et al.*, (2006) and the one used in this study. From 1997 to 2000, the burned area dataset used in *Mouillet et al.*, (2006) indicates that the global burned area is 602 $\times 10^4$ km^2 $year^{-1}$, which is 51.3% higher than GFED3.1 burned area. The declining trend of burned area used in our study is more consistent with the charcoal-based reconstruction of fire history (Marlon *et al.*, 2008a). Nevertheless, both our study and *Mouillet et al.*, (2006) show that global pyrogenic carbon emissions present significant increasing trend after the mid-1980s.

In this study, the DLEM simulations indicated that fire activities reduced the terrestrial carbon sink by 0.57 Pg C $year^{-1}$, which falls between the estimates of *Li et al.*, (2014) (1 Pg C $year^{-1}$) and *Yue et al.*, (2014) (0.32 Pg C $year^{-1}$). Our estimated global pyrogenic carbon emissions are 2.43 Pg C $year^{-1}$, which are 27.9% higher than *Li et al.*, (2014) and *Yue et al.*, (2014) (1.9 Pg C $year^{-1}$). Both *Li et al.*, (2014) and *Yue et al.*, (2014) simulated the burned area by fire models, while our study used the satellite-constrained global burned area as input dataset, which has similar spatial pattern to satellite observations. For the three studies, large differences exist in the fire-induced reductions in NPP and Rh. *Li et al.*, (2014) showed that fire activities reduced global NPP by 1.9 Pg C $year^{-1}$, and *Yue et al.*, (2014) showed that the fire-induced reduction in NPP was negligible, while our estimated NPP reduction was 4.14 Pg C $year^{-1}$. The post-fire reduction in vegetation biomass and ecosystem productivity have been widely recorded across various climate zones, e.g., (Dore *et al.*, 2012, Hicke *et al.*, 2003). The fire-induced changes in vegetation composition and forest coverage can also contribute to the changes in NPP. Therefore, the reductions in NPP estimated by this study and *Li et al.*, (2014) are more

reasonable than that in *Yue et al.*, (2014). All of the three studies agreed that the fire enlarged the global NEP, but reduced the size of terrestrial carbon sink.

4.3. Future implications

In the future, fires are projected to increase in many areas of the globe under the impact of climate change (Flannigan *et al.*, 2001, Flannigan *et al.*, 2013, Kloster *et al.*, 2012, Liu *et al.*, 2010, Pechony & Shindell, 2010). Many current humid regions would become drier and prone to fire activities. In the tropical rainforest, the droughts will be more popular and the forest will be easier to catch fires (Phillips *et al.*, 2009). For example, in the historical period, the humid interior Amazon basin is difficult to be ignited and resist to the fire-driven deforestation; however, the percentage of Amazon basin resist to deforestation fire is projected to decrease from 58% in the contemporary period to 24% in the 2050s (Le Page *et al.*, 2010). Similarly, the fires in the pan-boreal regions would also be more popular when the future climate warming dry up the fuel and soil, and induce earlier soil melt. In the North America boreal forest, carbon consumption by fires was projected to be 2.5-4.4 times its current level (Balshi *et al.*, 2009a). Once the current fire-resist ecosystems, such as boreal peatland and humid rainforest, convert to fire-prone systems under the impact of future climate warming, the regional terrestrial carbon sink would diminish, or even become net carbon source (Davidson *et al.*, 2012, Turetsky *et al.*, 2002). The fires are strongly influenced by human activities. For the tropical peatland, human activities facilitated the peatfire ignitions by reducing the forest canopy and draining the water (Turetsky *et al.*, 2015). In the future, peatland protection strategies, such as, minimizing the forest logging and cropland expansion, would be critical to reduce fire-induced reduction in carbon sink. Due to their huge carbon storage, more attention should be paid on fires in the peatland and tropical rainforest regions in the context of future climate warming.

In the 21st century, CO_2 concentration and nitrogen deposition rate are projected to increase continuously (Lamarque *et al.*, 2013c, Van Vuuren *et al.*, 2011). It can be expected that the fertilization effects of CO_2 and nitrogen deposition would further enhance ecosystem productivity and enlarge the terrestrial carbon sink until the CO_2 and nitrogen saturation points are reached (Keenan *et al.*, 2011). Meanwhile, the CO_2 and nitrogen deposition would be expected to further promote fuel accumulation and lead to higher carbon emissions from biomass burning (Martin Calvo *et al.*, 2014).

4.4. Uncertainties and improvements needed

In this study, some uncertainties exist in the model parameterization and input datasets, and need further improvement. First, in the current DLEM version, we considered the post-fire reduction in the fraction of forest area and the gradual recovery of tree coverage (Chen *et al.*, 2013), but neglected the grass occupation in the previous forest area. Therefore, ecosystem productivity in the early succession stage might be underestimated. To completely consider the post-fire vegetation succession, the ecosystem model is required to simulate the succession processes and the dynamics of both canopy and understory layers. Second, we used the burned area as input data to drive the DLEM. One merit of this strategy is the improvement in the representation of fire spatial pattern, as this input burned area dataset was constructed by incorporating satellite observation. Nevertheless, this method disregarded the feedbacks of ecosystems to fire, and may bring some uncertainties to the simulated carbon fluxes influenced by fires. Third, we used vegetation specific parameters to identify burn severity (combustion completeness and forest mortality), but did not consider the impacts of topography, vegetation species, and weather conditions on burn severity. In the field measurement, combustion completeness and forest mortality have been reported to differ substantially depending on the

locations, times of fire occurrence, and vegetation species (Rogers *et al.*, 2015, van Leeuwen *et al.*, 2014b). The Differenced Normalized Burned Ratio (dNBR) is a satellite-based burned severity index, which was found to be in good correlation with ground-based Composite Burn Index (CBI) in many regions e.g., (Cocke *et al.*, 2005, Miller & Thode, 2007). The regional and global dNBR datasets have been developed based on MODIS and LANDSAT images, and coupled into ecosystem model to investigate burn severity and biomass burning in the United States (Yang *et al.*, 2015). To represent the burn severity prior to satellite era or in future period, it is in urgent need to develop a prognostic fire model to simulate the burn severity based on fuel characteristics and environmental conditions. It should be noted that, in this study, the contributions of elevated CO_2 and nitrogen deposition to carbon emissions were estimated via their impacts on ecosystem carbon storage and fuel loading. Previous study reported that the elevated CO_2 and nitrogen deposition can modify the burned area and then fire emissions (Yang *et al.*, 2014a), which were not considered in this study and need further investigation.

5. Conclusions

Our dynamic land ecosystem model has simulated the spatial and temporal patterns of global pyrogenic carbon emissions from 1901 to 2010. We found a significant increasing trend of carbon emissions after the mid-1980s, resulting from multiple environmental changes and variations including climate change, land use/cover change, rising atmospheric CO_2 concentration and nitrogen deposition. Terrestrial carbon sink was found to be largely reduced due to fire activities. This study improves our current understanding about the magnitude and spatiotemporal patterns of century-scale pyrogenic carbon emissions and the impacts of fires on terrestrial carbon budget. We acknowledge certain caveats related to the representation of biogeochemical processes in modeling dynamic post-fire succession, the temporal and spatial

resolution of burned area datasets, and parameters such as burn severity etc. Nevertheless, our study integrated existing environmental information and mechanisms of fire impacts on terrestrial ecosystems, and provided useful information for future implications.

Chapter 8. General conclusions and improvement needs

In this study, long-term trend of fire activities and their impacts on ecosystems were investigated at both regional and global scales. A process-based fire model (DLEM-fire) was developed on the platform of one existing terrestrial ecosystem model, and its performance was validated by benchmark datasets. Spatially-explicit burned area data were collected from satellite observations and inventory-based fire records, or reconstructed by model simulations at decadal and century scales. Together with other environmental factors (such as, climate change, land use and land cover change, atmospheric composition, etc.), burned area datasets were used to drive the DLEM to study fire-induced carbon emissions and fire impacts on ecosystem carbon storage and carbon budgets. Meanwhile, underlying mechanisms of the changes in fire regimes and contributions from environmental factors were analyzed and quantified through numerical experiments by the DLEM.

The major conclusions are listed as below:

(1) In the CONUS during 1984-2012, both burned area and biomass burning presented significantly upwards trends; the contributions of larger fires were becoming higher in the recent years, owing to the warming and drying trend and previous fire suppression policies; the larger fires were generally associated with higher burn severity.

(2) In the BONA during 1960-2010, the increasing fires activities reduced regional GPP and TER, but enhanced the NEP. As a result of more frequent fires in the 51 years, terrestrial carbon sink in the BONA was reduced by 25.42 Tg C $year^{-1}$, comparing to the scenario with

constant fires in 1960. The increases in burned area caused a net decrease in vegetation, litter, and soil carbon storage, but an increase in woody debris carbon storage.

(3) In the African continent from 1901 to 2010, both burned area and pyrogenic carbon emissions presented significant declining trends. The intensified human activities were recognized as the major factor in determining the declines in fire activities and fire emissions, especially in the NHAF. The changes in CO_2 concentration and nitrogen deposition enhanced African burned area and pyrogenic carbon emissions. Climate changes reduced burned area in the SHAF significantly, meanwhile controlled the inter-annual and inter-decadal variations in fire activities.

(4) Global burned area during 1901-2007 was 442.1×10^4 km^2 $year^{-1}$ and showed a significant declining trend at the rate of 1.28×10^4 km^2 $year^{-1}$. Burned area in tropics and extratropics exhibited a significant declining trend. The factorial experiments identified human activities as the dominant factor in determining the declining trend of burned area in the tropics and extratropics, and climate variation as the primary factor in shaping the decadal variation of burned area at high latitudes.

(5) Over the period of 1901-2010, global pyrogenic carbon emissions were estimated to be 2.43 Pg C $year^{-1}$, and terrestrial carbon sink was found to be reduced by 0.57 Pg C $year^{-1}$ due to fire activities. Large increases in global pyrogenic carbon emissions and global average combustion rate were found after the mid-1980s, resulting from multiple environmental changes (climate change, rising atmospheric CO_2 concentration and nitrogen deposition) and intensified human activities.

Uncertainties were identified in this study. First, in current DLEM version, we explicitly considered post-fire reduction in the fraction of forest area and the gradual recovery of tree coverage, but neglected the growth of herbaceous vegetation in the former forest area. To completely account for post-fire trajectory of carbon storage and fluxes, ecosystem model is required to simulate vegetation succession processes and the dynamics of both canopy and understory layers. Second, we used vegetation specific parameters to identify burn severity (combustion completeness and forest mortality). In field measurements, combustion completeness and post-fire tree mortality have been reported to differ substantially depending on local topography, climate/weather condition, and vegetation species. It is in urgent need to develop a prognostic fire model to simulate burn severity based on fuel characteristics and environmental conditions. Third, the parameterization of fire duration in the present study only considered average fire duration and natural fire breaks, which may lead DLEM-Fire to underestimate the burned area caused by megafire events that last much longer than the average fire duration. A new algorithm estimating fire duration base on fuel characteristics, fire suppression effort, and weather conditions is in need to be developed to improve model performance in estimating burned area under extreme climate conditions. Fourth, due to the relatively short observations of lightning frequency, we applied the climatology of lightning frequency to each year across the study period. This might introduce uncertainties in estimating natural ignition sources.

Nevertheless, this study is the first attempt for ecosystem model to investigate long-term fire activities and quantify the contributions of multiple environmental factors at regional and global scales. These findings could provide useful knowledge to design specific fire management strategies for different regions. The fire model developed in this study can be coupled into the

earth system models, and improve the accuracy of projections in future climate and global biogeochemical cycles.

References

Adams MA (2013) Mega-fires, tipping points and ecosystem services: Managing forests and woodlands in an uncertain future. Forest Ecology and Management, **294**, 250-261.

Agee JK, Skinner CN (2005) Basic principles of forest fuel reduction treatments. Forest Ecology and Management, **211**, 83-96.

Ainsworth EA, Rogers A (2007) The response of photosynthesis and stomatal conductance to rising [CO2]: mechanisms and environmental interactions. Plant, cell & environment, **30**, 258-270.

Alexandratos N, Bruinsma J (2012) World agriculture towards 2030/2050: the 2012 revision. ESA Work. Pap, **3**.

Amiro B, Barr A, Barr J *et al.* (2010) Ecosystem carbon dioxide fluxes after disturbance in forests of North America. Journal of Geophysical Research: Biogeosciences (2005–2012), **115**.

Amiro B, Todd J, Wotton B *et al.* (2001) Direct carbon emissions from Canadian forest fires, 1959-1999. Canadian Journal of Forest Research, **31**, 512-525.

Amiro BD, Macpherson JI, Desjardins RL, Chen JM, Liu J (2003) Post-fire carbon dioxide fluxes in the western Canadian boreal forest: evidence from towers, aircraft and remote sensing. Agricultural and Forest Meteorology, **115**, 91-107.

Andela N, Van Der Werf GR (2014) Recent trends in African fires driven by cropland expansion and El Nino to La Nina transition. Nature Climate Change, **4**, 791-795.

Andreae MO, Merlet P (2001) Emission of trace gases and aerosols from biomass burning. Global Biogeochemical Cycles, **15**, 955-966.

Archibald S, Nickless A, Govender N, Scholes R, Lehsten V (2010) Climate and the inter-annual variability of fire in southern Africa: a meta-analysis using long-term field data and satellite-derived burnt area data. Global Ecology and Biogeography, **19**, 794-809.

Archibald S, Roy DP, Wilgen V, Brian W, Scholes RJ (2009) What limits fire? An examination of drivers of burnt area in Southern Africa. Global Change Biology, **15**, 613-630.

Archibald S, Staver AC, Levin SA (2012) Evolution of human-driven fire regimes in Africa. Proceedings of the National Academy of Sciences, **109**, 847-852.

Arora VK, Boer GJ (2005) Fire as an interactive component of dynamic vegetation models. Journal of Geophysical Research: Biogeosciences (2005–2012), **110**.

Balshi M, Mcguire A, Duffy P, Flannigan M, Kicklighter D, Melillo J (2009a) Vulnerability of carbon storage in North American boreal forests to wildfires during the 21st century. Global change biology, **15**, 1491-1510.

Balshi M, Mcguire AD, Zhuang Q *et al.* (2007) The role of historical fire disturbance in the carbon dynamics of the pan-boreal region: A process-based analysis. Journal of Geophysical Research: Biogeosciences (2005–2012), **112**.

Balshi MS, Mcguire AD, Duffy P, Flannigan M, Kicklighter DW, Melillo J (2009b) Vulnerability of carbon storage in North American boreal forests to wildfires during the 21st century. Global Change Biology, **15**, 1491-1510.

Balshi MS, Mcguire AD, Duffy P, Flannigan M, Walsh J, Melillo J (2009c) Assessing the response of area burned to changing climate in western boreal North America using a Multivariate Adaptive Regression Splines (MARS) approach. Global Change Biology, **15**, 578-600.
Barbero R, Abatzoglou J, Steel EA, Larkin NK (2014) Modeling very large-fire occurrences over the continental United States from weather and climate forcing. Environmental research letters, **9**, 124009.
Barbosa PM, Stroppiana D, Grégoire JM, Cardoso Pereira JM (1999) An assessment of vegetation fire in Africa (1981–1991): Burned areas, burned biomass, and atmospheric emissions. Global Biogeochemical Cycles, **13**, 933-950.
Barrett K, Mcguire A, Hoy EE, Kasischke E (2011) Potential shifts in dominant forest cover in interior Alaska driven by variations in fire severity. Ecological applications, **21**, 2380-2396.
Bartholomé E, Belward A (2005) GLC2000: a new approach to global land cover mapping from Earth observation data. International Journal of Remote Sensing, **26**, 1959-1977.
Beck PS, Goetz SJ, Mack MC, Alexander HD, Jin Y, Randerson JT, Loranty M (2011) The impacts and implications of an intensifying fire regime on Alaskan boreal forest composition and albedo. Global Change Biology, **17**, 2853-2866.
Belsky AJ, Blumenthal DM (1997) Effects of livestock grazing on stand dynamics and soils in upland forests of the Interior West. Conservation Biology, **11**, 315-327.
Birch DS, Penelope M, Crystal AK, Andrew TH, Alistair MSS (2014) Is proportion burned severely related to daily area burned? Environmental Research Letters, **9**, 064011.
Bonan GB (2008) Forests and climate change: forcings, feedbacks, and the climate benefits of forests. science, **320**, 1444-1449.
Bond-Lamberty B, Peckham SD, Ahl DE, Gower ST (2007) Fire as the dominant driver of central Canadian boreal forest carbon balance. Nature, **450**, 89-92.
Bond-Lamberty B, Peckham SD, Gower ST, Ewers BE (2009) Effects of fire on regional evapotranspiration in the central Canadian boreal forest. Global change biology, **15**, 1242-1254.
Bond W, Midgley G, Woodward F (2003) What controls South African vegetation-climate or fire? South African Journal of Botany, **69**, 79-91.
Bond W, Woodward F, Midgley G (2005a) The global distribution of ecosystems in a world without fire. New Phytologist, **165**, 525-538.
Bond WJ, Keeley JE (2005) Fire as a global 'herbivore': the ecology and evolution of flammable ecosystems. Trends in Ecology & Evolution, **20**, 387-394.
Bond WJ, Woodward FI, Midgley GF (2005b) The global distribution of ecosystems in a world without fire. New Phytologist, **165**, 525-538.
Bousquet P, Ciais P, Miller J *et al.* (2006) Contribution of anthropogenic and natural sources to atmospheric methane variability. Nature, **443**, 439-443.
Bowman D, Panton W (1995) Munmarlary revisited: response of a north Australian Eucalyptus tetrodonta savanna protected from fire for 20 years. Australian Journal of Ecology, **20**, 526-531.
Bowman DM, Balch JK, Artaxo P *et al.* (2009) Fire in the Earth system. science, **324**, 481-484.

Brewer CK, Winne JC, Redmond RL, Opitz DW, Mangrich MV (2005) Classifying and mapping wildfire severity: a comparison of methods. Photogrammetric Engineering and Remote Sensing, **71**, 1311-1320.
Campbell J, Donato D, Azuma D, Law B (2007) Pyrogenic carbon emission from a large wildfire in Oregon, United States. Journal of Geophysical Research: Biogeosciences (2005–2012), **112**.
Chang D, Song Y (2009) Comparison of L3JRC and MODIS global burned area products from 2000 to 2007. Journal of Geophysical Research: Atmospheres, **114**, D16106.
Chapin F, Mcguire A, Randerson J *et al.* (2000) Arctic and boreal ecosystems of western North America as components of the climate system. Global Change Biology, **6**, 211-223.
Chen G, Tian H, Huang C, Prior SA, Pan S (2013) Integrating a process-based ecosystem model with Landsat imagery to assess impacts of forest disturbance on terrestrial carbon dynamics: Case studies in Alabama and Mississippi. Journal of Geophysical Research: Biogeosciences, **118**, 1208-1224.
Chen G, Tian H, Zhang C *et al.* (2012) Drought in the Southern United States over the 20th century: variability and its impacts on terrestrial ecosystem productivity and carbon storage. Climatic change, **114**, 379-397.
Chen J, Chen W, Liu J, Cihlar J, Gray S (2000) Annual carbon balance of Canada's forests during 1895–1996. Global Biogeochemical Cycles, **14**, 839-849.
Christian HJ, Blakeslee RJ, Boccippio DJ *et al.* (2003) Global frequency and distribution of lightning as observed from space by the Optical Transient Detector. Journal of Geophysical Research: Atmospheres (1984–2012), **108**, ACL 4-1-ACL 4-15.
Ciais P, Bombelli A, Williams M *et al.* (2011) The carbon balance of Africa: synthesis of recent research studies. Philosophical Transactions of the Royal Society of London A: Mathematical, Physical and Engineering Sciences, **369**, 2038-2057.
Ciais P, Piao S-L, Cadule P, Friedlingstein P, Chédin A (2009) Variability and recent trends in the African terrestrial carbon balance. Biogeosciences, **6**, 1935-1948.
Cocke AE, Fulé PZ, Crouse JE (2005) Comparison of burn severity assessments using Differenced Normalized Burn Ratio and ground data. International Journal of Wildland Fire, **14**, 189-198.
Dai A (2011) Drought under global warming: a review. Wiley Interdisciplinary Reviews: Climate Change, **2**, 45-65.
Davidson EA, De Araújo AC, Artaxo P *et al.* (2012) The Amazon basin in transition. Nature, **481**, 321-328.
De Groot WJ, Cantin AS, Flannigan MD, Soja AJ, Gowman LM, Newbery A (2013a) A comparison of Canadian and Russian boreal forest fire regimes. Forest Ecology and Management, **294**, 23-34.
De Groot WJ, Flannigan MD, Cantin AS (2013b) Climate change impacts on future boreal fire regimes. Forest Ecology and Management, **294**, 35-44.
Dennison PE, Brewer SC, Arnold JD, Moritz MA (2014) Large wildfire trends in the western United States, 1984–2011. Geophysical Research Letters, **41**, 2928-2933.
Dentener F, Drevet J, Lamarque J *et al.* (2006) Nitrogen and sulfur deposition on regional and global scales: a multimodel evaluation. Global Biogeochemical Cycles, **20**.

Dillon GK, Holden ZA, Morgan P, Crimmins MA, Heyerdahl EK, Luce CH (2011) Both topography and climate affected forest and woodland burn severity in two regions of the western US, 1984 to 2006. Ecosphere, **2**, art130.

Dore S, Montes-Helu M, Hart SC *et al.* (2012) Recovery of ponderosa pine ecosystem carbon and water fluxes from thinning and stand-replacing fire. Global change biology, **18**, 3171-3185.

Eidenshink J, Schwind B, Brewer K, Zhu Z-L, Quayle B, Howard S (2007a) project for monitoring trends in burn severity. Fire Ecology.

Eidenshink J, Schwind B, Brewer K, Zhu Z-L, Quayle B, Howard S (2007b) project for monitoring trends in burn severity. Fire Ecology, **2007**.

Epting J, Verbyla D, Sorbel B (2005) Evaluation of remotely sensed indices for assessing burn severity in interior Alaska using Landsat TM and ETM+. Remote Sensing of Environment, **96**, 328-339.

Flannigan M, Campbell I, Wotton M, Carcaillet C, Richard P, Bergeron Y (2001) Future fire in Canada's boreal forest: paleoecology results and general circulation model-regional climate model simulations. Canadian Journal of Forest Research, **31**, 854-864.

Flannigan M, Cantin AS, De Groot WJ, Wotton M, Newbery A, Gowman LM (2013) Global wildland fire season severity in the 21st century. Forest Ecology and Management, **294**, 54-61.

Flannigan M, Stocks B, Turetsky M, Wotton M (2009a) Impacts of climate change on fire activity and fire management in the circumboreal forest. Global Change Biology, **15**, 549-560.

Flannigan MD, Krawchuk MA, De Groot WJ, Wotton BM, Gowman LM (2009b) Implications of changing climate for global wildland fire. International Journal of Wildland Fire, **18**, 483-507.

Flannigan MD, Logan KA, Amiro BD, Skinner WR, Stocks B (2005) Future area burned in Canada. Climatic Change, **72**, 1-16.

French NH, Mckenzie D, Erickson T *et al.* (2014) Modeling Regional-Scale Wildland Fire Emissions with the Wildland Fire Emissions Information System*. Earth Interactions, **18**, 1-26.

Gatti L, Gloor M, Miller J *et al.* (2014) Drought sensitivity of Amazonian carbon balance revealed by atmospheric measurements. Nature, **506**, 76-80.

Ghimire B, Williams CA, Collatz GJ, Vanderhoof M (2012) Fire-induced carbon emissions and regrowth uptake in western US forests: Documenting variation across forest types, fire severity, and climate regions. Journal of Geophysical Research: Biogeosciences (2005–2012), **117**.

Giglio L, Randerson J, Van Der Werf G, Kasibhatla P, Collatz G, Morton D, Defries R (2010a) Assessing variability and long-term trends in burned area by merging multiple satellite fire products. Biogeosciences, **7**.

Giglio L, Randerson J, Van Der Werf G, Kasibhatla P, Collatz G, Morton D, Defries R (2010b) Assessing variability and long-term trends in burned area by merging multiple satellite fire products. Biogeosciences, **6**, 1171-1186.

Giglio L, Randerson JT, Van Der Werf GR (2013a) Analysis of Daily, Monthly, and Annual Burned Area Using the Fourth Generation Global Fire Emissions Database (GFED4). Journal of Geophysical Research, **accepted**.

Giglio L, Randerson JT, Werf GR (2013b) Analysis of daily, monthly, and annual burned area using the fourth-generation global fire emissions database (GFED4). Journal of Geophysical Research: Biogeosciences, **118**, 317-328.
Goetz SJ, Bond-Lamberty B, Law BE *et al.* (2012) Observations and assessment of forest carbon dynamics following disturbance in North America. Journal of Geophysical Research: Biogeosciences (2005–2012), **117**.
Goulden ML, Mcmillan A, Winston GC, Rocha AV, Manies KL, Harden JW, Bond-Lamberty B (2011) Patterns of NPP, GPP, respiration, and NEP during boreal forest succession. Global Change Biology, **17**, 855-871.
Grégoire J-M, Tansey K, Silva J (2003) The GBA2000 initiative: developing a global burnt area database from SPOT-VEGETATION imagery. International Journal of Remote Sensing, **24**, 1369-1376.
Harden J, Trumbore S, Stocks B, Hirsch A, Gower S, O'neill K, Kasischke E (2000) The role of fire in the boreal carbon budget. Global Change Biology, **6**, 174-184.
Harvey BJ, Donato DC, Romme WH, Turner MG (2014) Fire severity and tree regeneration following bark beetle outbreaks: the role of outbreak stage and burning conditions. Ecological applications, **24**, 1608-1625.
Hayes DJ, Mcguire AD, Kicklighter DW, Gurney KR, Burnside T, Melillo JM (2011) Is the northern high-latitude land-based CO2 sink weakening? Global Biogeochemical Cycles, **25**.
Hicke JA, Asner GP, Kasischke ES *et al.* (2003) Postfire response of North American boreal forest net primary productivity analyzed with satellite observations. Global Change Biology, **9**, 1145-1157.
Hicke JA, Meddens AJ, Allen CD, Kolden CA (2013) Carbon stocks of trees killed by bark beetles and wildfire in the western United States. Environmental Research Letters, **8**, 035032.
Higgins SI, Bond WJ, February EC *et al.* (2007) Effects of four decades of fire manipulation on woody vegetation structure in savanna. Ecology, **88**, 1119-1125.
Hoelzemann JJ, Schultz MG, Brasseur GP, Granier C, Simon M (2004) Global Wildland Fire Emission Model (GWEM): Evaluating the use of global area burnt satellite data. Journal of Geophysical Research, **109**, D14S04.
Hooijer A, Page S, Canadell J, Silvius M, Kwadijk J, Wösten H, Jauhiainen J (2010) Current and future CO [subscript 2] emissions from drained peatlands in Southeast Asia.
Houghton R, Hackler J, Lawrence K (2000a) Changes in terrestrial carbon storage in the United States. 2: The role of fire and fire management. Global Ecology and Biogeography, **9**, 145-170.
Houghton R, Skole D, Nobre CA, Hackler J, Lawrence K, Chomentowski WH (2000b) Annual fluxes of carbon from deforestation and regrowth in the Brazilian Amazon. Nature, **403**, 301-304.
Hoy EE, French NH, Turetsky MR, Trigg SN, Kasischke ES (2008) Evaluating the potential of Landsat TM/ETM+ imagery for assessing fire severity in Alaskan black spruce forests. International Journal of Wildland Fire, **17**, 500-514.
Hulme M, Doherty R, Ngara T, New M, Lister D (2001) African climate change: 1900-2100. Climate research, **17**, 145-168.

Hurteau MD, Bradford JB, Fulé PZ, Taylor AH, Martin KL (2014) Climate change, fire management, and ecological services in the southwestern US. Forest Ecology and Management, **327**, 280-289.
Hurtt G, Chini LP, Frolking S *et al.* (2011) Harmonization of land-use scenarios for the period 1500–2100: 600 years of global gridded annual land-use transitions, wood harvest, and resulting secondary lands. Climatic Change, **109**, 117-161.
Ito A, Penner JE (2004a) Global estimates of biomass burning emissions based on satellite imagery for the year 2000. Journal of Geophysical Research: Atmospheres (1984–2012), **109**.
Ito A, Penner JE (2004b) Global estimates of biomass burning emissions based on satellite imagery for the year 2000. Journal of Geophysical Research, **109**, D14S05.
Jain AK, Tao Z, Yang X, Gillespie C (2006) Estimates of global biomass burning emissions for reactive greenhouse gases (CO, NMHCs, and NOx) and CO2. Journal of Geophysical Research, **111**, D06304.
Jin Y, Randerson JT, Goetz SJ, Beck PS, Loranty MM, Goulden ML (2012) The influence of burn severity on postfire vegetation recovery and albedo change during early succession in North American boreal forests. Journal of Geophysical Research: Biogeosciences (2005–2012), **117**.
Jung M, Henkel K, Herold M, Churkina G (2006) Exploiting synergies of global land cover products for carbon cycle modeling. Remote Sensing of Environment, **101**, 534-553.
Jung M, Reichstein M, Margolis HA *et al.* (2011) Global patterns of land-atmosphere fluxes of carbon dioxide, latent heat, and sensible heat derived from eddy covariance, satellite, and meteorological observations. Journal of Geophysical Research: Biogeosciences (2005–2012), **116**.
Kaiser J, Heil A, Andreae M *et al.* (2012a) Biomass burning emissions estimated with a global fire assimilation system based on observed fire radiative power. Biogeosciences, **9**.
Kaiser J, Heil A, Andreae M *et al.* (2012b) Biomass burning emissions estimated with a global fire assimilation system based on observed fire radiative power. Biogeosciences, **9**, 527-554.
Kasischke ES (2000) Boreal ecosystems in the global carbon cycle. In: *Fire, climate change, and carbon cycling in the boreal forest.* pp Page., Springer.
Kasischke ES, Bruhwiler LP (2002) Emissions of carbon dioxide, carbon monoxide, and methane from boreal forest fires in 1998. Journal of Geophysical Research: Atmospheres (1984–2012), **107**, FFR 2-1-FFR 2-14.
Kasischke ES, Christensen Jr N, Stocks BJ (1995) Fire, global warming, and the carbon balance of boreal forests. Ecological applications, 437-451.
Kasischke ES, Hyer EJ, Novelli PC *et al.* (2005) Influences of boreal fire emissions on Northern Hemisphere atmospheric carbon and carbon monoxide. Global Biogeochemical Cycles, **19**.
Kasischke ES, Turetsky MR (2006) Recent changes in the fire regime across the North American boreal region—spatial and temporal patterns of burning across Canada and Alaska. Geophysical Research Letters, **33**.
Kasischke ES, Turetsky MR, Ottmar RD, French NH, Hoy EE, Kane ES (2008) Evaluation of the composite burn index for assessing fire severity in Alaskan black spruce forests. International Journal of Wildland Fire, **17**, 515-526.

Keenan T, Maria Serra J, Lloret F, Ninyerola M, Sabate S (2011) Predicting the future of forests in the Mediterranean under climate change, with niche-and process-based models: CO2 matters! Global change biology, **17**, 565-579.

Kelley D, Prentice I, Harrison S, Wang H, Simard M, Fisher J, Willis K (2013) A comprehensive benchmarking system for evaluating global vegetation models. Biogeosciences, **10**, 3313-3340.

Key CH, Benson NC (2006) Landscape assessment (LA). FIREMON: Fire effects monitoring and inventory system. Gen. Tech. Rep. RMRS-GTR-164-CD, Fort Collins, CO: US Department of Agriculture, Forest Service, Rocky Mountain Research Station.

Kirschke S, Bousquet P, Ciais P *et al.* (2013) Three decades of global methane sources and sinks. Nature Geoscience, **6**, 813-823.

Klein Goldewijk K, Beusen A, Van Drecht G, De Vos M (2011) The HYDE 3.1 spatially explicit database of human-induced global land-use change over the past 12,000 years. Global Ecology and Biogeography, **20**, 73-86.

Kloster S, Mahowald N, Randerson J, Lawrence P (2012) The impacts of climate, land use, and demography on fires during the 21st century simulated by CLM-CN. Biogeosciences, **9**.

Knorr W, Lehsten V, Arneth A (2012) Determinants and predictability of global wildfire emissions. Atmos. Chem. Phys, **12**, 6845-6861.

Knutti R, Sedláček J (2013) Robustness and uncertainties in the new CMIP5 climate model projections. Nature Climate Change, **3**, 369-373.

Konovalov IB, Beekmann M, Kuznetsova IN, Yurova A, Zvyagintsev AM (2011) Atmospheric impacts of the 2010 Russian wildfires: integrating modelling and measurements of an extreme air pollution episode in the Moscow region. Atmos. Chem. Phys., **11**, 10031-10056.

Korontzi S, Roy DP, Justice CO, Ward DE (2004) Modeling and sensitivity analysis of fire emissions in southern Africa during SAFARI 2000. Remote Sensing of Environment, **92**, 255-275.

Kosaka Y, Xie S-P (2013) Recent global-warming hiatus tied to equatorial Pacific surface cooling. Nature, **501**, 403-407.

Kurz WA, Dymond C, Stinson G *et al.* (2008) Mountain pine beetle and forest carbon feedback to climate change. Nature, **452**, 987-990.

Lamarque J-F, Dentener F, Mcconnell J *et al.* (2013a) Multi-model mean nitrogen and sulfur deposition from the Atmospheric Chemistry and Climate Model Intercomparison Project (ACCMIP): evaluation historical and projected changes. Atmospheric Chemistry and Physics, **13**.

Lamarque J, Shindell DT, Josse B *et al.* (2013b) The Atmospheric Chemistry and Climate Model Intercomparison Project (ACCMIP): overview and description of models, simulations and climate diagnostics. Geoscientific Model Development, **6**, 179-206.

Lamarque JF, Dentener F, Mcconnell J *et al.* (2013c) Multi-model mean nitrogen and sulfur deposition from the Atmospheric Chemistry and Climate Model Intercomparison Project (ACCMIP): evaluation of historical and projected future changes. Atmos. Chem. Phys., **13**, 7997-8018.

Lambin EF, Geist HJ, Lepers E (2003) Dynamics of land-use and land-cover change in tropical regions. Annual review of environment and resources, **28**, 205-241.

Langmann B, Duncan B, Textor C, Trentmann J, Van Der Werf GR (2009) Vegetation fire emissions and their impact on air pollution and climate. Atmospheric Environment, **43**, 107-116.
Le Page Y, Morton D, Bond-Lamberty B, Pereira J, Hurtt G (2015) HESFIRE: a global fire model to explore the role of anthropogenic and weather drivers. Biogeosciences, **12**, 887-903.
Le Page Y, Van Der Werf G, Morton D, Pereira J (2010) Modeling fire-driven deforestation potential in Amazonia under current and projected climate conditions. Journal of Geophysical Research: Biogeosciences (2005–2012), **115**.
Leff B, Ramankutty N, Foley JA (2004) Geographic distribution of major crops across the world. Global Biogeochemical Cycles, **18**.
Lehner B, Döll P (2004) Development and validation of a global database of lakes, reservoirs and wetlands. Journal of Hydrology, **296**, 1-22.
Lehsten V, Groot WJ, Flannigan M, George C, Harmand P, Balzter H (2014) Wildfires in boreal ecoregions: Evaluating the power law assumption and intra-annual and interannual variations. Journal of Geophysical Research: Biogeosciences, **119**, 14-23.
Lenihan JM, Bachelet D, Neilson RP, Drapek R (2008) Simulated response of conterminous United States ecosystems to climate change at different levels of fire suppression, CO 2 emission rate, and growth response to CO 2. Global and Planetary Change, **64**, 16-25.
Levine JS, Cofer Iii WR, Cahoon Jr DR, Winstead EL (1995) A driver for global change. Environmental Science & Technology, **29**, 120A-125A.
Li F, Bond-Lamberty B, Levis S (2014a) Quantifying the role of fire in the Earth system–Part 2: Impact on the net carbon balance of global terrestrial ecosystems for the 20th century. Biogeosciences, **11**, 1345-1360.
Li F, Bond-Lamberty B, Levis S (2014b) Quantifying the role of fire in the Earth system – Part 2: Impact on the net carbon balance of global terrestrial ecosystems for the 20th century. Biogeosciences, **11**, 1345-1360.
Li F, Bond-Lamberty B, Levis S (2014c) Quantifying the role of fire in the Earth system – Part 2: Impact on the net carbon balance of global terrestrial ecosystems for the 20th century. Biogeosciences, **11**, 1345-1360.
Li F, Levis S, Ward D (2013) Quantifying the role of fire in the Earth system–Part 1: Improved global fire modeling in the Community Earth System Model (CESM1). Biogeosciences, **10**, 2293-2314.
Li F, Zeng X, Levis S (2012) A process-based fire parameterization of intermediate complexity in a Dynamic Global Vegetation Model. Biogeosciences, **9**, 2761-2780.
Littell JS, Mckenzie D, Peterson DL, Westerling AL (2009) Climate and wildfire area burned in western US ecoprovinces, 1916-2003. Ecological Applications, **19**, 1003-1021.
Liu M, Tian H, Yang Q, Yang J, Song X, Lohrenz SE, Cai WJ (2013a) Long-term trends in evapotranspiration and runoff over the drainage basins of the Gulf of Mexico during 1901–2008. Water Resources Research, **49**, 1988-2012.
Liu Y (2004) Variability of wildland fire emissions across the contiguous United States. Atmospheric Environment, **38**, 3489-3499.
Liu Y, Goodrick SL, Stanturf JA (2013b) Future US wildfire potential trends projected using a dynamically downscaled climate change scenario. Forest Ecology and Management, **294**, 120-135.

Liu Y, Stanturf J, Goodrick S (2010) Trends in global wildfire potential in a changing climate. Forest Ecology and Management, **259**, 685-697.
Lü A, Tian H, Liu M, Liu J, Melillo JM (2006) Spatial and temporal patterns of carbon emissions from forest fires in China from 1950 to 2000. Journal of Geophysical Research: Atmospheres (1984–2012), **111**.
Lu C, Tian H (2013) Net greenhouse gas balance in response to nitrogen enrichment: perspectives from a coupled biogeochemical model. Global change biology, **19**, 571-588.
Lu C, Tian H, Liu M, Ren W, Xu X, Chen G, Zhang C (2012) Effect of nitrogen deposition on China's terrestrial carbon uptake in the context of multifactor environmental changes. Ecological applications, **22**, 53-75.
Lyons EA, Jin Y, Randerson JT (2008) Changes in surface albedo after fire in boreal forest ecosystems of interior Alaska assessed using MODIS satellite observations. Journal of Geophysical Research: Biogeosciences (2005–2012), **113**.
Mack MC, Bret-Harte MS, Hollingsworth TN, Jandt RR, Schuur EA, Shaver GR, Verbyla DL (2011) Carbon loss from an unprecedented Arctic tundra wildfire. Nature, **475**, 489-492.
Mantgem PJ, Nesmith JC, Keifer M, Knapp EE, Flint A, Flint L (2013) Climatic stress increases forest fire severity across the western United States. Ecology letters, **16**, 1151-1156.
Marlon JR, Bartlein P, Carcaillet C *et al.* (2008a) Climate and human influences on global biomass burning over the past two millennia. Nature Geoscience, **1**, 697-702.
Marlon JR, Bartlein PJ, Carcaillet C *et al.* (2008b) Climate and human influences on global biomass burning over the past two millennia. Nature Geoscience, **1**, 697-702.
Martin Calvo M, Prentice I, Harrison S (2014) Climate vs. carbon dioxide controls on biomass burning: a model analysis of the glacial-interglacial contrast. Biogeosciences Discussions, **11**, 2569-2593.
Mcguire AD, Anderson LG, Christensen TR *et al.* (2009) Sensitivity of the carbon cycle in the Arctic to climate change. Ecological Monographs, **79**, 523-555.
Meigs GW, Donato DC, Campbell JL, Martin JG, Law BE (2009) Forest fire impacts on carbon uptake, storage, and emission: the role of burn severity in the Eastern Cascades, Oregon. Ecosystems, **12**, 1246-1267.
Meigs GW, Turner DP, Ritts WD, Yang Z, Law BE (2011) Landscape-scale simulation of heterogeneous fire effects on pyrogenic carbon emissions, tree mortality, and net ecosystem production. Ecosystems, **14**, 758-775.
Mesinger F, Dimego G, Kalnay E *et al.* (2006) North American regional reanalysis. Bulletin of the American Meteorological Society, **87**.
Miller J, Skinner C, Safford H, Knapp EE, Ramirez C (2012) Trends and causes of severity, size, and number of fires in northwestern California, USA. Ecological Applications, **22**, 184-203.
Miller JD, Thode AE (2007) Quantifying burn severity in a heterogeneous landscape with a relative version of the delta Normalized Burn Ratio (dNBR). Remote Sensing of Environment, **109**, 66-80.
Moreira AG (2000) Effects of fire protection on savanna structure in Central Brazil. Journal of biogeography, **27**, 1021-1029.
Morton D, Collatz G, Wang D, Randerson J, Giglio L, Chen Y (2013) Satellite-based assessment of climate controls on US burned area. Biogeosciences, **10**.

Mouillot F, Field CB (2005) Fire history and the global carbon budget: a 1× 1 fire history reconstruction for the 20th century. Global Change Biology, **11**, 398-420.
Mouillot F, Narasimha A, Balkanski Y, Lamarque JF, Field CB (2006) Global carbon emissions from biomass burning in the 20th century. Geophysical Research Letters, **33**.
Murphy KA, Reynolds JH, Koltun JM (2008) Evaluating the ability of the differenced Normalized Burn Ratio (dNBR) to predict ecologically significant burn severity in Alaskan boreal forests. International Journal of Wildland Fire, **17**, 490-499.
Nelson JA, Morgan JA, Lecain DR, Mosier AR, Milchunas DG, Parton BA (2004) Elevated CO2 increases soil moisture and enhances plant water relations in a long-term field study in semi-arid shortgrass steppe of Colorado. Plant and Soil, **259**, 169-179.
Nemani RR, Keeling CD, Hashimoto H *et al.* (2003) Climate-driven increases in global terrestrial net primary production from 1982 to 1999. science, **300**, 1560-1563.
Nepstad DC, Verssimo A, Alencar A *et al.* (1999) Large-scale impoverishment of Amazonian forests by logging and fire. Nature, **398**, 505-508.
Norby RJ, Warren JM, Iversen CM, Medlyn BE, Mcmurtrie RE (2010) CO2 enhancement of forest productivity constrained by limited nitrogen availability. Proceedings of the National Academy of Sciences, **107**, 19368-19373.
Page SE, Siegert F, Rieley JO, Boehm H-DV, Jaya A, Limin S (2002) The amount of carbon released from peat and forest fires in Indonesia during 1997. Nature, **420**, 61-65.
Pan S, Dangal S, Tao B, Yang J, Tian H (2015) Increased terrestrial net primary production in Africa in response to multiple environmental changes. Ecosystem Health and Sustainability.
Pan S, Tian H, Dangal SR *et al.* (2014) Complex spatiotemporal responses of global terrestrial primary production to climate change and increasing atmospheric CO2 in the 21st century. PloS one, **9**, e112810.
Pechony O, Shindell D (2009) Fire parameterization on a global scale. Journal of Geophysical Research: Atmospheres (1984–2012), **114**.
Pechony O, Shindell DT (2010) Driving forces of global wildfires over the past millennium and the forthcoming century. Proceedings of the National Academy of Sciences, **107**, 19167-19170.
Peters W, Jacobson AR, Sweeney C *et al.* (2007) An atmospheric perspective on North American carbon dioxide exchange: CarbonTracker. Proceedings of the National Academy of Sciences, **104**, 18925-18930.
Pfeiffer M, Kaplan J (2012) SPITFIRE-2: an improved fire module for Dynamic Global Vegetation Models. Geoscientific Model Development Discussions, **5**, 2347-2443.
Phillips OL, Aragão LE, Lewis SL *et al.* (2009) Drought sensitivity of the Amazon rainforest. science, **323**, 1344-1347.
Plummer S, Arino O, Simon M, Steffen W (2006) Establishing a earth observation product service for the terrestrial carbon community: The GLOBCARBON initiative. Mitigation and adaptation strategies for global change, **11**, 97-111.
Pollet J, Omi PN (2002) Effect of thinning and prescribed burning on crown fire severity in ponderosa pine forests. International Journal of Wildland Fire, **11**, 1-10.
Poulter B, Cadule P, Cheiney A *et al.* (2015a) Sensitivity of global terrestrial carbon cycle dynamics to variability in satellite-observed burned area. Global Biogeochemical Cycles.

Poulter B, Cadule P, Cheiney A *et al.* (2015b) Sensitivity of global terrestrial carbon cycle dynamics to variability in satellite-observed burned area. Global Biogeochemical Cycles, **29**, 207-222.
Poulter B, Frank D, Ciais P *et al.* (2014) Contribution of semi-arid ecosystems to interannual variability of the global carbon cycle. Nature, **509**, 600-603.
Power MJ, Marlon J, Ortiz N *et al.* (2008) Changes in fire regimes since the Last Glacial Maximum: an assessment based on a global synthesis and analysis of charcoal data. Climate Dynamics, **30**, 887-907.
Prentice I, Kelley D, Foster P, Friedlingstein P, Harrison S, Bartlein P (2011a) Modeling fire and the terrestrial carbon balance. Global Biogeochemical Cycles, **25**.
Prentice IC (2010) The burning issue. science, **330**, 1636-1637.
Prentice IC, Kelley DI, Foster PN, Friedlingstein P, Harrison SP, Bartlein PJ (2011b) Modeling fire and the terrestrial carbon balance. Global Biogeochemical Cycles, **25**, GB3005.
Prentice S, Mackerras D (1977) The ratio of cloud to cloud-ground lightning flashes in thunderstorms. Journal of Applied Meteorology, **16**, 545-550.
Prichard SJ, Peterson DL, Jacobson K (2010) Fuel treatments reduce the severity of wildfire effects in dry mixed conifer forest, Washington, USA. Canadian Journal of Forest Research, **40**, 1615-1626.
Pyne SJ (2007) Megaburning: the meaning of megafires and the means of the management. Proceedings of the Wildfire.
Quéré CL, Andres RJ, Boden T *et al.* (2013) The global carbon budget 1959–2011. Earth System Science Data, **5**, 165-185.
Randerson J, Liu H, Flanner M *et al.* (2006a) The impact of boreal forest fire on climate warming. science, **314**, 1130-1132.
Randerson JT, Chen Y, Van Der Werf GR, Rogers BM, Morton DC (2012) Global burned area and biomass burning emissions from small fires. Journal of Geophysical Research: Biogeosciences, **117**, G04012.
Randerson JT, Liu H, Flanner MG *et al.* (2006b) The impact of boreal forest fire on climate warming. science, **314**, 1130-1132.
Ren W, Tian H, Tao B *et al.* (2011) Impacts of tropospheric ozone and climate change on net primary productivity and net carbon exchange of China's forest ecosystems. Global Ecology and Biogeography, **20**, 391-406.
Rogers B, Randerson J, Bonan G (2013) High-latitude cooling associated with landscape changes from North American boreal forest fires. Biogeosciences, **10**, 699-718.
Rogers BM, Soja AJ, Goulden ML, Randerson JT (2015) Influence of tree species on continental differences in boreal fires and climate feedbacks. Nature Geoscience.
Rogers BM, Veraverbeke S, Azzari G *et al.* (2014) Quantifying fire-wide carbon emissions in interior Alaska using field measurements and Landsat imagery. Journal of Geophysical Research: Biogeosciences, 2014JG002657.
Roy D, Boschetti L, Justice C, Ju J (2008a) The collection 5 MODIS burned area product—Global evaluation by comparison with the MODIS active fire product. Remote Sensing of Environment, **112**, 3690-3707.
Roy D, Frost P, Justice C *et al.* (2005) The Southern Africa Fire Network (SAFNet) regional burned-area product-validation protocol. International Journal of Remote Sensing, **26**, 4265-4292.

Roy DP, Boschetti L (2009) Southern Africa validation of the MODIS, L3JRC, and GlobCarbon burned-area products. Geoscience and Remote Sensing, IEEE Transactions on, **47**, 1032-1044.
Roy DP, Boschetti L, Justice C, Ju J (2008b) The collection 5 MODIS burned area product—Global evaluation by comparison with the MODIS active fire product. Remote Sensing of Environment, **112**, 3690-3707.
Roy DP, Boschetti L, Justice CO, Ju J (2008c) The collection 5 MODIS burned area product—Global evaluation by comparison with the MODIS active fire product. Remote Sensing of Environment, **112**, 3690-3707.
Ruesch A, Gibbs H (2008) New IPCC Tier-1 Global Biomass Carbon Map For the Year 2000. Available online from the Carbon Dioxide Information Analysis Center [http://cdiac.ornl.gov], Oak Ridge National Laboratory, Oak Ridge, Tennessee.
Santilli M, Moutinho P, Schwartzman S, Nepstad D, Curran L, Nobre C (2005) Tropical deforestation and the Kyoto Protocol. Climatic Change, **71**, 267-276.
Savage M, Swetnam TW (1990) Early 19th-century fire decline following sheep pasturing in a Navajo ponderosa pine forest. Ecology, 2374-2378.
Schoennagel T, Veblen TT, Romme WH (2004) The interaction of fire, fuels, and climate across Rocky Mountain forests. BioScience, **54**, 661-676.
Schultz MG, Heil A, Hoelzemann JJ *et al.* (2008) Global wildland fire emissions from 1960 to 2000. Global Biogeochemical Cycles, **22**.
Seiler W, Crutzen PJ (1980) Estimates of gross and net fluxes of carbon between the biosphere and the atmosphere from biomass burning. Climatic Change, **2**, 207-247.
Sheffield J, Goteti G, Wood EF (2006) Development of a 50-year high-resolution global dataset of meteorological forcings for land surface modeling. Journal of Climate, **19**, 3088-3111.
Simon M, Plummer S, Fierens F, Hoelzemann J, Arino O (2004) Burnt area detection at global scale using ATSR-2: The GLOBSCAR products and their qualification. Journal of Geophysical Research, **109**, D14S02.
Stephens SL, Burrows N, Buyantuyev A *et al.* (2014) Temperate and boreal forest mega-fires: characteristics and challenges. Frontiers in Ecology and the Environment.
Stephens SL, Moghaddas JJ, Edminster C *et al.* (2009) Fire treatment effects on vegetation structure, fuels, and potential fire severity in western US forests. Ecological Applications, **19**, 305-320.
Stocks B, Mason J, Todd J *et al.* (2002) Large forest fires in Canada, 1959–1997. Journal of Geophysical Research: Atmospheres (1984–2012), **107**, FFR 5-1-FFR 5-12.
Strauss D, Bednar L, Mees R (1989) Do one percent of the forest fires cause ninety-nine percent of the damage? Forest Science, **35**, 319-328.
Tansey K, Grégoire J-M, Defourny P, Leigh R, Pekel J-F, Van Bogaert E, Bartholomé E (2008a) A new, global, multi-annual (2000–2007) burnt area product at 1 km resolution. Geophysical Research Letters, **35**, L01401.
Tansey K, Grégoire JM, Defourny P, Leigh R, Pekel JF, Van Bogaert E, Bartholomé E (2008b) A new, global, multi-annual (2000–2007) burnt area product at 1 km resolution. Geophysical Research Letters, **35**.
Tao B, Tian H, Ren W *et al.* (2014) Increasing Mississippi river discharge throughout the 21st century influenced by changes in climate, land use, and atmospheric CO2. Geophysical Research Letters, **41**, 4978-4986.

Thomas RQ, Canham CD, Weathers KC, Goodale CL (2010) Increased tree carbon storage in response to nitrogen deposition in the US. Nature Geoscience, **3**, 13-17.
Thonicke K, Spessa A, Prentice I, Harrison S, Dong L, Carmona-Moreno C (2010) The influence of vegetation, fire spread and fire behaviour on biomass burning and trace gas emissions: results from a process-based model. Biogeosciences, **7**, 1991-2011.
Thonicke K, Venevsky S, Sitch S, Cramer W (2001) The role of fire disturbance for global vegetation dynamics: coupling fire into a Dynamic Global Vegetation Model. Global Ecology and Biogeography, **10**, 661-677.
Tian H, Chen G, Liu M *et al.* (2010a) Model estimates of net primary productivity, evapotranspiration, and water use efficiency in the terrestrial ecosystems of the southern United States during 1895–2007. Forest Ecology and Management, **259**, 1311-1327.
Tian H, Chen G, Lu C *et al.* (2014) North American terrestrial CO2 uptake largely offset by CH4 and N2O emissions: toward a full accounting of the greenhouse gas budget. Climatic Change, 1-14.
Tian H, Melillo J, Lu C *et al.* (2011) China's terrestrial carbon balance: contributions from multiple global change factors. Global Biogeochemical Cycles, **25**.
Tian H, Xu X, Liu M, Ren W, Zhang C, Chen G, Lu C (2010b) Spatial and temporal patterns of CH4 and N2O fluxes in terrestrial ecosystems of North America during 1979–2008: application of a global biogeochemistry model. Biogeosciences, **7**, 2673-2694.
Tilman D, Reich P, Phillips H *et al.* (2000) Fire suppression and ecosystem carbon storage. Ecology, **81**, 2680-2685.
Turetsky M, Wieder K, Halsey L, Vitt D (2002) Current disturbance and the diminishing peatland carbon sink. Geophysical Research Letters, **29**, 21-21-21-24.
Turetsky MR, Benscoter B, Page S, Rein G, Van Der Werf GR, Watts A (2015) Global vulnerability of peatlands to fire and carbon loss. Nature Geoscience, **8**, 11-14.
Turetsky MR, Kane ES, Harden JW, Ottmar RD, Manies KL, Hoy E, Kasischke ES (2011) Recent acceleration of biomass burning and carbon losses in Alaskan forests and peatlands. Nature Geoscience, **4**, 27-31.
United Nations (2013) World Population Prospects: The 2012 Revision, Highlights and Advance Tables (Working Paper No. ESA/P/WP. 228). pp Page, New York: United Nations Publications.
Van Der Werf G, Dempewolf J, Trigg S *et al.* (2008a) Climate regulation of fire emissions and deforestation in equatorial Asia. Proceedings of the National Academy of Sciences, **105**, 20350-20355.
Van Der Werf GR, Randerson JT, Collatz GJ *et al.* (2004) Continental-scale partitioning of fire emissions during the 1997 to 2001 El Nino/La Nina period. science, **303**, 73-76.
Van Der Werf GR, Randerson JT, Giglio L *et al.* (2010a) Global fire emissions and the contribution of deforestation, savanna, forest, agricultural, and peat fires (1997–2009). Atmos. Chem. Phys, **10**, 11,707-711,735.
Van Der Werf GR, Randerson JT, Giglio L *et al.* (2010b) Global fire emissions and the contribution of deforestation, savanna, forest, agricultural, and peat fires (1997–2009). Atmospheric Chemistry and Physics, **10**, 11707-11735.
Van Der Werf GR, Randerson JT, Giglio L, Collatz GJ, Kasibhatla PS, Arellano Jr A (2006a) Interannual variability in global biomass burning emissions from 1997 to 2004. Atmospheric Chemistry and Physics, **6**, 3423-3441.

Van Der Werf GR, Randerson JT, Giglio L, Collatz GJ, Kasibhatla PS, Arellano Jr A (2006b) Interannual variability of global biomass burning emissions from 1997 to 2004. Atmospheric Chemistry and Physics Discussions, **6**, 3175-3226.
Van Der Werf GR, Randerson JT, Giglio L, Gobron N, Dolman A (2008b) Climate controls on the variability of fires in the tropics and subtropics. Global Biogeochemical Cycles, **22**.
Van Leeuwen T, Van Der Werf G, Hoffmann A *et al.* (2014a) Biomass burning fuel consumption rates: a field measurement database. Biogeosciences, **11**, 7305-7329.
Van Leeuwen T, Van Der Werf G, Hoffmann A *et al.* (2014b) Biomass burning fuel consumption rates: a field measurement database.
Van Leeuwen TT, Van Der Werf GR, Hoffmann AA *et al.* (2014c) Biomass burning fuel consumption rates: a field measurement database. Biogeosciences Discuss., **11**, 8115-8180.
Van Vuuren DP, Edmonds J, Kainuma M *et al.* (2011) The representative concentration pathways: an overview. Climatic Change, **109**, 5-31.
Venevsky S, Thonicke K, Sitch S, Cramer W (2002) Simulating fire regimes in human-dominated ecosystems: Iberian Peninsula case study. Global Change Biology, **8**, 984-998.
Veraverbeke S, Lhermitte S, Verstraeten WW, Goossens R (2011a) A time-integrated MODIS burn severity assessment using the multi-temporal differenced Normalized Burn Ratio (dNBR MT). International Journal of Applied Earth Observation and Geoinformation, **13**, 52-58.
Veraverbeke S, Lhermitte S, Verstraeten WW, Goossens R (2011b) A time-integrated MODIS burn severity assessment using the multi-temporal differenced normalized burn ratio ($dNBR_{MT}$). International Journal of Applied Earth Observation and Geoinformation, **13**, 52-58.
Veraverbeke S, Rogers B, Randerson J (2015) Daily burned area and carbon emissions from boreal fires in Alaska. Biogeosciences, **12**, 3579-3601.
Wallenius TH, Kuuluvainen T, Vanha-Majamaa I (2004) Fire history in relation to site type and vegetation in Vienansalo wilderness in eastern Fennoscandia, Russia. Canadian Journal of Forest Research, **34**, 1400-1409.
Wang Z, Chappellaz J, Park K, Mak J (2010) Large variations in Southern Hemisphere biomass burning during the last 650 years. science, **330**, 1663-1666.
Ward D, Kloster S, Mahowald N, Rogers B, Randerson J, Hess P (2012a) The changing radiative forcing of fires: global model estimates for past, present and future. Atmospheric Chemistry & Physics Discussions, **12**.
Ward D, Kloster S, Mahowald N, Rogers B, Randerson J, Hess P (2012b) The changing radiative forcing of fires: global model estimates for past, present and future. Atmospheric Chemistry and Physics, **12**, 10857-10886.
Westerling A, Hidalgo HG, Cayan DR, Swetnam TW (2006a) Warming and earlier spring increase western US forest wildfire activity. science, **313**, 940-943.
Westerling AL, Hidalgo HG, Cayan DR, Swetnam TW (2006b) Warming and earlier spring increase western US forest wildfire activity. science, **313**, 940-943.
Westerling AL, Turner MG, Smithwick EA, Romme WH, Ryan MG (2011) Continued warming could transform Greater Yellowstone fire regimes by mid-21st century. Proceedings of the National Academy of Sciences, **108**, 13165-13170.

Wiedinmyer C, Akagi S, Yokelson RJ, Emmons L, Al-Saadi J, Orlando J, Soja A (2011a) The Fire INventory from NCAR (FINN): A high resolution global model to estimate the emissions from open burning. Geoscientific Model Development, **4**, 625.
Wiedinmyer C, Akagi SK, Yokelson RJ, Emmons LK, Al-Saadi JA, Orlando JJ, Soja AJ (2011b) The Fire INventory from NCAR (FINN): a high resolution global model to estimate the emissions from open burning. Geosci. Model Dev., **4**, 625-641.
Williams J (2013) Exploring the onset of high-impact mega-fires through a forest land management prism. Forest Ecology and Management, **294**, 4-10.
Wooster M, Zhang Y (2004) Boreal forest fires burn less intensely in Russia than in North America. Geophysical Research Letters, **31**.
Wooster MJ, Roberts G, Perry G, Kaufman Y (2005) Retrieval of biomass combustion rates and totals from fire radiative power observations: FRP derivation and calibration relationships between biomass consumption and fire radiative energy release. Journal of Geophysical Research: Atmospheres (1984–2012), **110**.
Wuebbles D, Meehl G, Hayhoe K *et al.* (2014) CMIP5 climate model analyses: Climate extremes in the United States. Bulletin of the American Meteorological Society, **95**, 571-583.
Xiao J, Ollinger SV, Frolking S *et al.* (2014) Data-driven diagnostics of terrestrial carbon dynamics over North America. Agricultural and Forest Meteorology, **197**, 142-157.
Yang J, Tian H, Tao B, Ren W, Kush J, Liu Y, Wang Y (2014a) Spatial and temporal patterns of global burned area in response to anthropogenic and environmental factors: Reconstructing global fire history for the 20th and early 21st centuries. Journal of Geophysical Research: Biogeosciences, **119**, 249-263.
Yang J, Tian H, Tao B, Ren W, Pan S, Liu Y, Wang Y (2015) A growing importance of large fires in the Conterminous United States during 1984 – 2012. Journal of Geophysical Research: Biogeosciences, **under review**.
Yang Q, Tian H, Li X *et al.* (2014b) Spatiotemporal patterns of evapotrans piration along the North American east coast as influenced by multiple environmental changes. Ecohydrology.
Yang Q, Tian H, Li X *et al.* (2014c) Spatiotemporal patterns of evapotranspiration along the North American east coast as influenced by multiple environmental changes. Ecohydrology.
Yu Z, Loisel J, Brosseau DP, Beilman DW, Hunt SJ (2010) Global peatland dynamics since the Last Glacial Maximum. Geophysical Research Letters, **37**.
Yue C, Ciais P, Cadule P *et al.* (2014a) Modelling the role of fires in the terrestrial carbon balance by incorporating SPITFIRE into the global vegetation model ORCHIDEE – Part 1: simulating historical global burned area and fire regimes. Geosci. Model Dev., **7**, 2747-2767.
Yue C, Ciais P, Cadule P, Thonicke K, Van Leeuwen T (2014b) Modelling the role of fires in the terrestrial carbon balance by incorporating SPITFIRE into the global vegetation model ORCHIDEE–Part 2: Carbon emissions and the role of fires in the global carbon balance. Geoscientific Model Development Discussions, **7**, 9017-9062.
Yue C, Ciais P, Cadule P, Thonicke K, Van Leeuwen TT (2015) Modelling the role of fires in the terrestrial carbon balance by incorporating SPITFIRE into the global vegetation

model ORCHIDEE – Part 2: Carbon emissions and the role of fires in the global carbon balance. Geosci. Model Dev., **8**, 1321-1338.
Zhang X, Kondragunta S, Roy DP (2014) Interannual variation in biomass burning and fire seasonality derived from Geostationary satellite data across the contiguous United States from 1995 to 2011. Journal of Geophysical Research: Biogeosciences.
Zhao M, Heinsch FA, Nemani RR, Running SW (2005) Improvements of the MODIS terrestrial gross and net primary production global data set. Remote Sensing of Environment, **95**, 164-176.
Zhao M, Running SW (2010) Drought-induced reduction in global terrestrial net primary production from 2000 through 2009. science, **329**, 940-943.

Appendix I

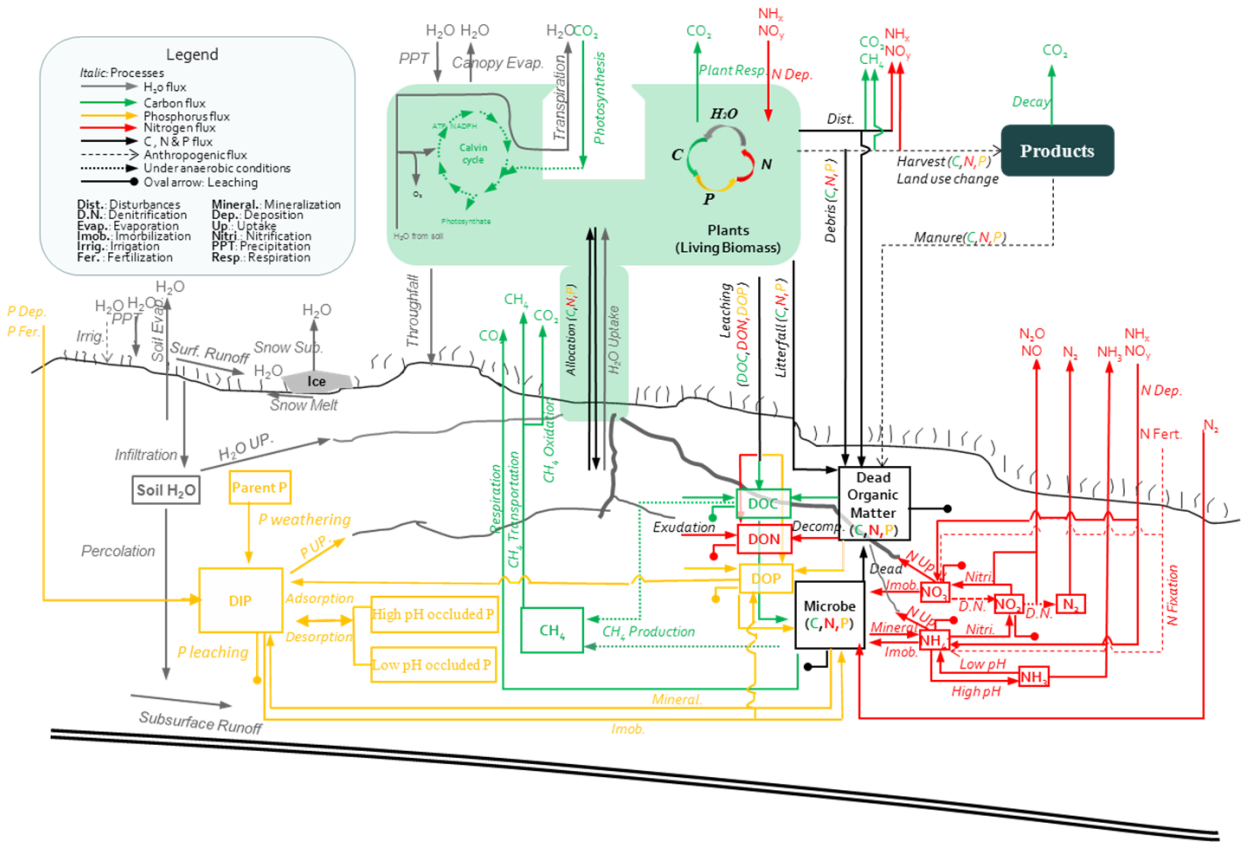

Figure S1. The detailed structure of the DLEM

Appendix II

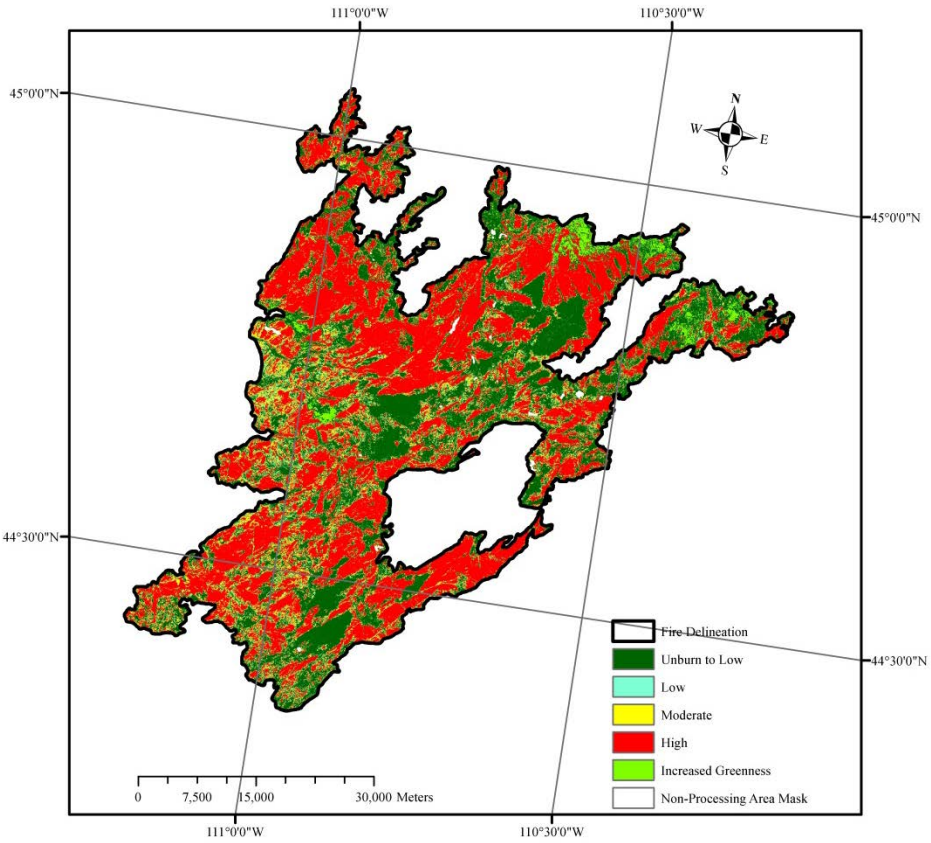

Figure S2. An example to illustrate the format of MTBS fire perimeter and burn severity. The example selected is “North Fork fire”, which started in July 1988.

Appendix III

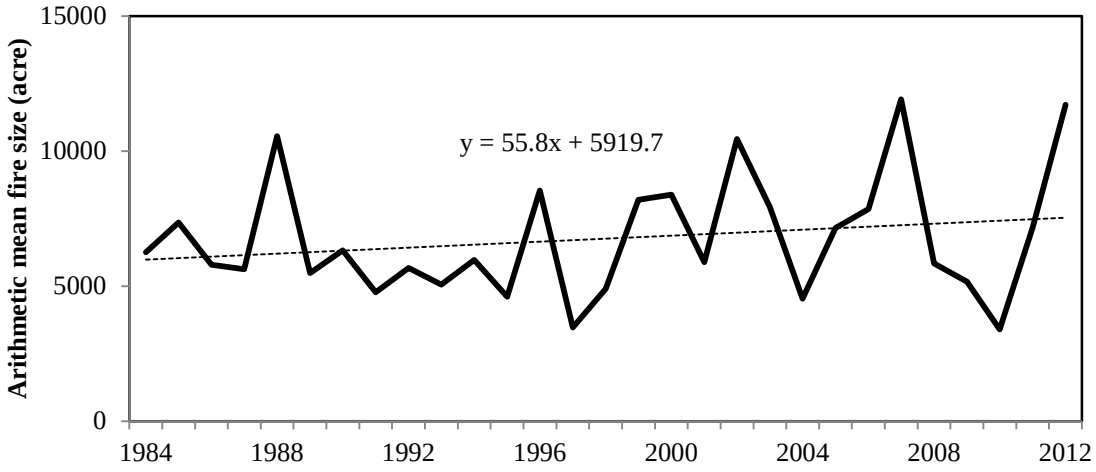

Figure S3. Inter-annual variations and changing trend in the arithmetic mean fire size from 1984 to 2012.

Appendix IV

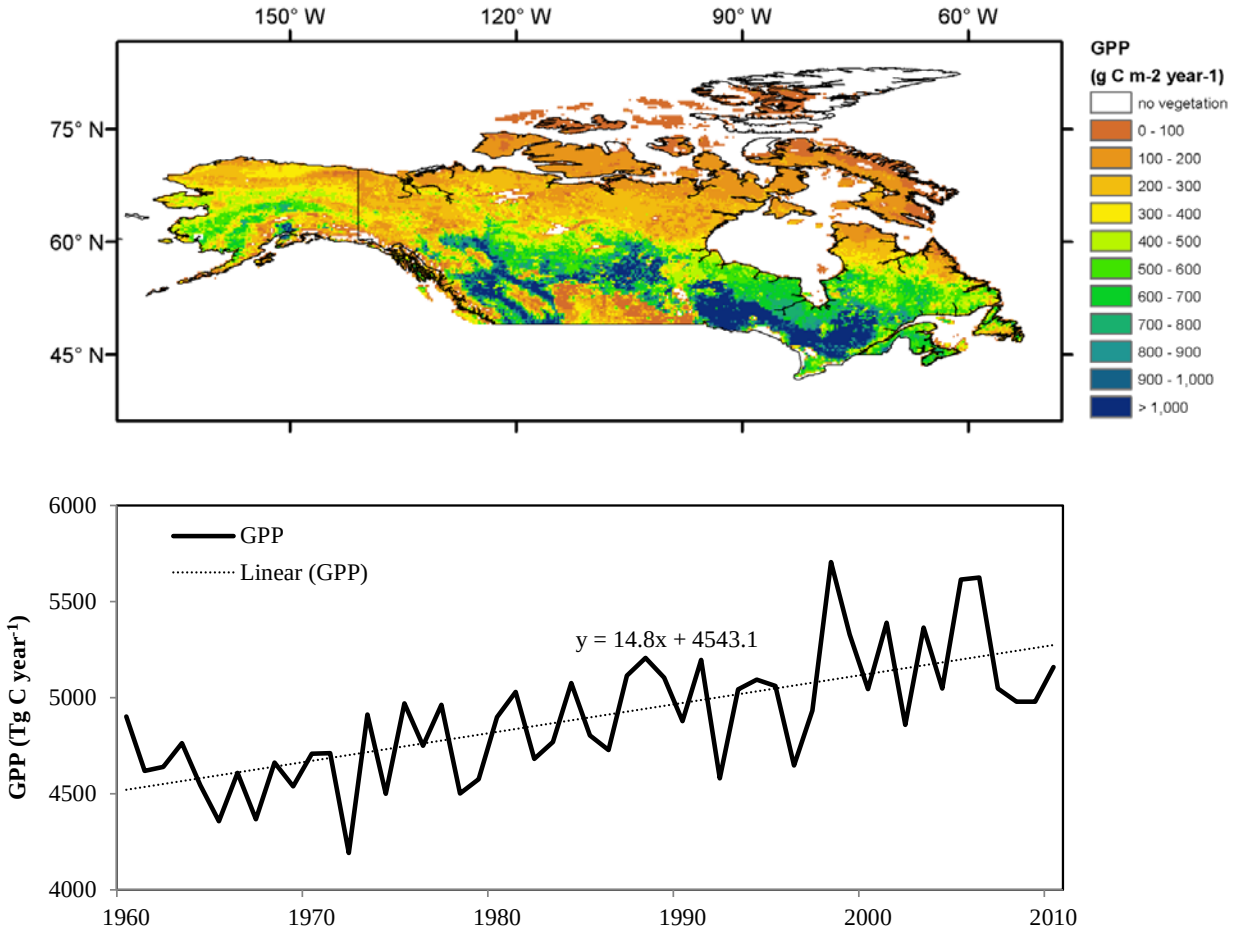

Figure S4. DLEM-simulated spatial distribution of average gross primary productivity (GPP), and inter-annual variations of GPP in the boreal North America from 1960 to 2010.

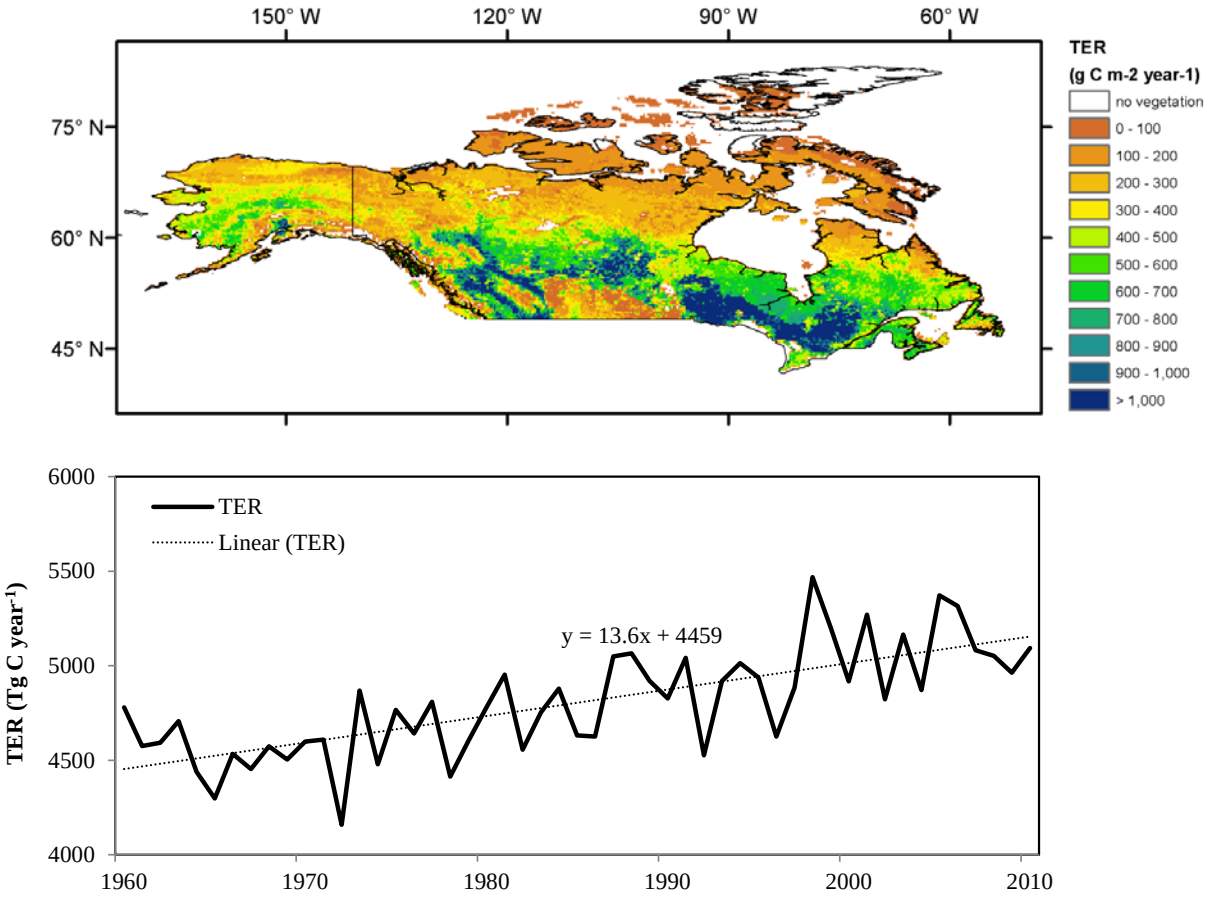

Figure S5. DLEM-simulated spatial distribution of average terrestrial ecosystem respiration (TER), and inter-annual variations of TER in the boreal North America from 1960 to 2010.

Appendix V

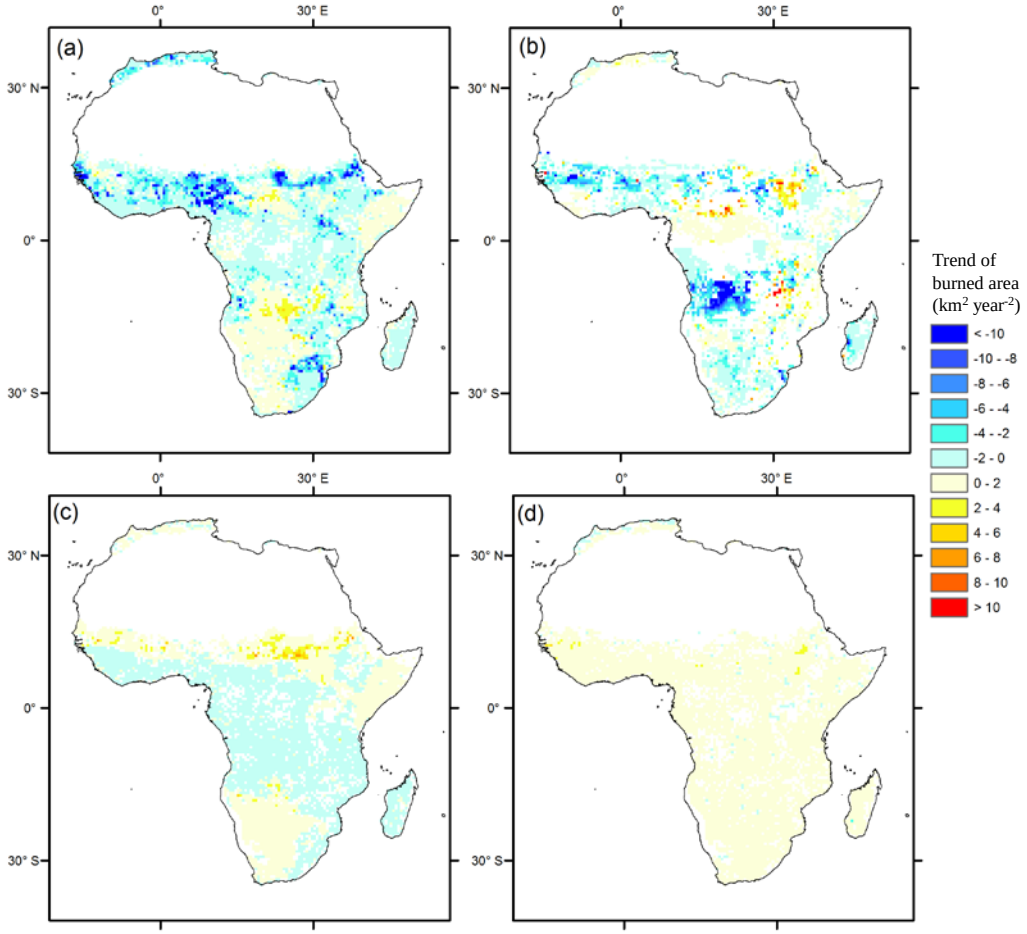

Figure S6. Changing trends of grid burned area during 1901-2010 under the impact of single factor: (a) human activities, (b) climate changes, (c) CO_2 concentration, and (d) nitrogen deposition. Grids without significant trend are masked white.

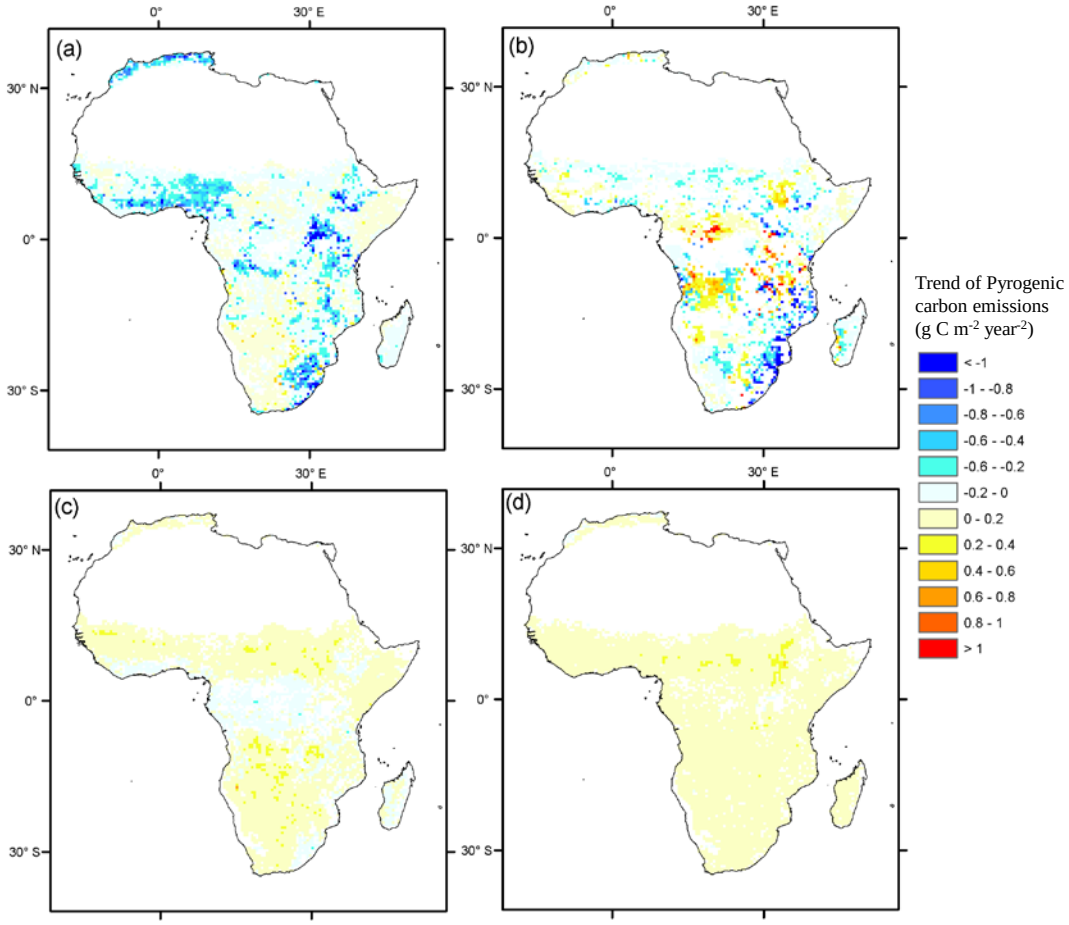

Figure S7. Changing trends of pyrogenic carbon emissions during 1901-2010 under the impact of single factor: (a) human activities, (b) climate changes, (c) CO_2 concentration, and (d) nitrogen deposition. The grids without significant trend are masked white.